Analysis and Optimization of Small Wind Turbines with Permanent Synchronous Machines

Análisis y Optimización de Miniturbinas Eólicas con Máquinas Síncronas de Imanes Permanentes

Alberto Arroyo Gutiérrez

Departamento de Ingeniería Eléctrica y Energética

Universidad de Cantabria

Ph.D. THESIS

Director Mario Mañana Canteli

2012

This thesis has been typeset using LaTeX and LEd editor.

RESUMEN

El creciente desarrollo de las energías renovables y más concretamente el de la energía minieólica hace que el sector sea cada vez más competitivo y que las miniturbinas eólicas (SWGs) presenten características cada vez más similares. La tendencia actual es buscar equipos lo más robustos posible, maximizando su produciendo energética y minimizando su coste de fabricación. Es por esto que, hoy en día, el principal objetivo de los fabricantes sea obtener incrementos en el rendimiento del sistema, conservando la robustez del mismo y no encareciendo, y si es posible disminuyendo, el coste de fabricación del mismo. Algunos de los estudios para conseguir dicha mejora se han centrado en:

- Mejorar el sistema de almacenamiento de la energía.
- El diseño de nuevas máquinas síncronas de imanes permanentes (PMSMs).
- El estudio aerodinámico de los SWGs.
- El control de la velocidad de giro del SWG.
- El estudio del comportamiento del convertidor.

En este trabajo se pretende desarrollar una metodología que aumente el rendimiento de los SWGs, no solo actuando individualmente sobre cada uno de los elementos que lo componen, si no que también teniendo en cuenta la interacción entre los mismos, como son: molino, PMSM, rectificador e inversor.

Para conseguir la optimización del sistema se trabaja principalmente sobre dos aspectos:

1. Factor aerodinámico: Calcular la curva de optimización del rotor eólico (MPPT y MTPT) que permite extraer la máxima energía del viento

trabajando con el máximo coeficiente de potencia C_p. Utilizando la MTPT y las curvas de trabajo del SWG (obtenidas mediante la simulación de los modelos) se podrá conseguir la relación tensión de continua v_{dc} a la entrada del inversor frente a la potencia de red P_{grid} a la salida del mismo. Dicha relación se debe introducir en el inversor y se conoce como la curva de carga óptima (MPCC).

2. Efecto de la batería de condensadores: Se conectarán diferentes baterías de condensadores entre el PMSM y el rectificador, de manera que la reacción de inducido produce un efecto magnetizante en el seno de la máquina eléctrica que se añade al campo magnético generado por los imanes, produciéndose de esta manera una mayor tensión en bornes de la máquina. Todo esto se traduce en que para generar una misma potencia se necesite una menor corriente circulando por los devanados de la máquina eléctrica. En definitiva, con esto se consigue un mayor rendimiento.

   De este modo se calculará para cada velocidad de viento u_h las baterías de condensadores que maximizan la potencia inyectada en la red P_{grid}. Pero se deberá tener en cuenta que la introducción de condensadores en el conjunto modificará las condiciones internas del mismo. Es por esto que para cada capacidad se debe recalcular la nueva MPCC que maximiza el coeficiente de potencia C_p.

Para poder estudiar los dos factores anteriormente mencionados, se necesitará realizar unos modelos del sistema que nos permitan visualizar su comportamiento ante posibles variaciones que se introduzcan.

Para realizar el primer modelo se utilizará Matlab-Simulink. Dicho modelo nos permitirá analizar el comportamiento del sistema ante variaciones en el mismo, como pueden ser la capacidad, la resistencia de carga o la velocidad de rotación.

El modelo Simulink se hará con el objetivo de estudiar el comportamiento del sistema en conjunto, viendo la influencia de unos elementos sobre otros. Es por esto que en este modelo se introducirán todos los elementos concernientes al SWG, tales como PMSM, rectificador e inversor.

Para el análisis del PMSM se usará un modelo basado en unas sencillas ecuaciones teóricas las cuales suministrarán resultados muy fiables.

A continuación, para la modelización del rectificador nos apoyaremos en su hoja de especificaciones.

Por último, para simular el inversor se realizarán numerosos ensayos sobre él y se obtendrá una expresión que relacione la corriente proveniente del rectificador i_{dc} con las pérdidas en el inversor ΔP_{inv}. De este modo se puede hacer un balance energético aproximado del conjunto, sin necesidad de hacer un modelo complejo del mismo.

El segundo modelo se realizará con el objetivo de poder estudiar el PMSM en detalle, debido a que el modelo simulink no lo permite. Para ello se usará un software de elementos finitos (FEM), denominado "Flux". Dicho software permite introducir todos los parámetros internos de la máquina eléctrica como pueden ser: número de ranuras, número de espiras, resistencia de los devanados, esquema eléctrico, etc. Además también permite introducir ciertos componentes electrónicos, como puede ser el rectificador.

Una vez definida la geometría, el mallado, los materiales, el circuito eléctrico y las propiedades dinámicas se estará en disposición de resolver el problema y analizar los resultados. Los resultados más representativos que se pueden obtener mediante esta herramienta son:

- Pérdidas en las diferentes partes de la máquina eléctrica: P_{fe}, P_{Cu}, $P_{magnets}$ y $P_{additional}$.
- Distribución de la densidad del flujo magnético en el seno de la máquina eléctrica.
- Distribución de las líneas de campo en el PMSM.
- Formas de onda de corriente y tensión en las diferentes fases de la máquina eléctrica y en el rectificador.

Una vez diseñados ambos modelos se desarrollará una metodología que permitirá aumentar la eficiencia de las miniturbinas eólicas que poseen un PMSM, mediante el uso de baterías de condensadores conectadas entre el PMSM y el rectificador. Dicha metodología constará de los siguientes pasos:

1. Realizar diferentes ensayos sobre el SWG que nos permitan conocer en detalle su comportamiento.
2. Definir los diferentes parámetros de los modelos. Ajustar dichos parámetros comparando los resultados obtenidos mediante Simulink con los obtenidos en los ensayos sobre el SWG del paso 1.
3. Cálculo de la curva de optimización del rotor eólico (MTPT) que extraiga la máxima potencia del viento.
4. Cálculo de un rango inicial de capacidades a ensayar.
5. Obtención de las curvas de carga óptimas (MPCCs) y comparativa para las diferentes capacidades.
6. Analizar los resultados y realizar un estudio económico.
7. Obtención de la curva de carga óptima final (FMPCC).

Posteriormente se implementará dicha metodología en un SWG comercial de 3.5 kW, calculándose la curva de optimización del rotor eólico (MTPT) y la batería de condensadores óptima para cada velocidad de giro.

Para contrastar los resultados obtenidos con dicha metodología se fabricará una bancada de ensayos la cual nos permitirá probar la fiabilidad del procedimiento expuesto.

Para finalizar, si se comparan los resultados reales con los simulados se puede concluir que:

- Ambos modelos, simulink y FEM, se ajustan perfectamente al sistema, y los resultados que con ellos se obtienen pueden considerase como correctos.
- La mejora en la eficiencia, que se predijo con las simulaciones, queda demostrada al conseguir ese mismo incremento de potencia al realizar los ensayos con baterías de condensadores sobre la máquina real.
- El modelo FEM permite analizar el balance energético que se produce en el PMSM, pudiendo con ello saber cuan de sobredimensionada o de subdimensionada se encuentra la misma.

Por otro lado, de la aplicación de la metodología en una máquina comercial de 3.5 kW se desprenden las siguientes conclusiones:

- A la hora de conectar diferentes elementos a un SWG se debe tener en cuenta que dichos elementos pueden variar el comportamiento del mismo y hacer que su curva de carga óptima (MPCC) varíe.
- La conexión de las baterías de condensadores aumenta el rendimiento que se puede obtener del sistema. Dicho incremento se ha visto en nuestro caso limitado, debido a la máxima intensidad que puede circular por los devanados del PMSM.
- En el caso de realizar un control automatizado de la capacidad de la batería de condensadores el incremento de la eficiencia sería máximo.
- Para obtener una misma potencia, se podría definir una nueva máquina eléctrica con batería de condensadores que posea una menor cantidad de hierro, cobre e imán; con el ahorro económico que ello conllevaría.

ABSTRACT

The increasing use of small-wind energy has made it necessary to develop new methods that improve the efficiency of this technology. This is best done by considering the interaction between the various components, such as wind rotors, electrical generators, rectifiers and inverters, as opposed to studying the individual components in isolation.

Nowadays, the electrical generator most widely used by manufacturers is the Permanent Magnet Synchronous Machine (PMSM). Its main advantages are: low maintenance, absence of rotor copper losses, less cooling and higher efficiency.

Hence, this paper describes a methodology to increase the efficiency of Small Wind Turbines (SWTs) equipped with a PMSM. To achieve this objective, capacitor banks will be connected between the PMSM and the rectifier.

This methodology is motivated by two clear aims. The first one is to operate the SWT with its maximum power coefficient C_p. The second one is to select the most suitable capacitor bank for each wind speed in order to optimize the energy supplied to the grid.

Finally, the methodology will be tested in a commercial 3.5 kW SWT, and the results will be studied to determine its feasibility. In this way, it can be concluded that the value of the capacitor bank C that produces the highest efficiency increase is $C = 12\mu F$. Using that value of C an efficiency increase of 3.83 % is obtained.

AGRADECIMIENTOS

La realización de la presente tesis lleva consigo muchas horas de estudio y trabajo, además de convivencia con muchas personas que en una u otra manera han colaborado en su desarrollo. Sirvan estas líneas para mostrarles mi más profundo agradecimiento a todas ellas, deseando no olvidarme de demasiados.

En primer lugar, me gustaría dar las gracias a mi director de tesis Dr. Mario Mañana. Su experiencia, conocimiento y amistad no sólo han ayudado a la realización de este trabajo, si no que también a mi bienestar durante el tiempo de elaboración del mismo. Además, su vista crítica, pienso fue de gran ayuda.

También me gustaría agradecer a D. Claudio Gómez su gran labor. Gracias a su colaboración la realización de esta tesis pudo ir poco a poco avanzando, hasta llegar a la finalización de la misma.

Quisiera mostrar mi más sincero agradecimiento por su desinteresada hospitalidad y ayuda a todos los miembros del Departamento de Ingeniería Eléctrica y Energética de la Universidad de Cantabria.

Entre ellos querría destacar al Dr. M.Á. Rodríguez y a D. J. Villazán cuya colaboración en el desarrollo de la bancada de ensayos fue de gran ayuda.

También querría mencionar al Dr. C. Renedo, al Dr. A. Ortiz, a la Dra. I. Fernández, al Dr. P. Sánchez, a la Dra. M.A. Cavia, al Dr. J.C. Lavandero, al Dr. F. Delgado, al Dr. D. Silió y al Dr. S. F. Pérez. Dar las gracias a todos ellos por haberme hecho todo este tiempo tan agradable, sin el cual hubiera sido muy difícil trabajar confortablemente.

Y para finalizar con el departamento, me gustaría agradecer a Dña. M.I. Carriles su paciencia y su asesoramiento, no sólo con temas relativos a la tesis, si no con muchos otros.

Además agradecer a la empresa Sonkyo Energy S.A. su colaboración y la ayuda prestada.

No quisiera olvidarme a todos aquellos amigos que siempre me recuerdan que hay más cosas a parte del trabajo, como por ejemplo Rubén y Lorena, los cuales siempre me tranquilizan haciendo uso de su enorme paciencia.

Dar las gracias a mis padres Juan y Tensi, que no pocas veces me han preguntado acerca de la tesis, y tantas veces les he contestado. Gracias otra vez por ser como sois y aunque en nuestra familia no solemos expresar el cariño, saber que os quiero.

A mis abuelas, por que a pesar de vuestra edad siempre os preocupáis por mí.

Agradecer al resto de la familia, Germán, Carlos, Carmina, Manuela, etc. su ayuda y constantes ánimos.

Y no podría acabar estos agradecimientos sin citar a mi novia, Esther. Sin duda ha sido la persona que más ha sufrido mis ausencias y a pesar de su atareada agenda, siempre sacó tiempo para ir a visitarme y darme palabras de ánimo y cariño. A ella un beso y espero que después de leer esto sepa lo mucho que la necesito.

Estando seguro que olvido a alguien, pido disculpas por ello y espero no se moleste.

Santander, primavera 2012

A mi madre

"En general, las madres y las amas de casa son los únicos trabajadores que nunca tienen días libres. Las madres componen una clase a parte. Una clase sin derecho a vacaciones."

Contents

List of Figures

List of Tables

Glossary

α	Attack angle [°].
β	Pitch angle [°].
ΔP_{add}	PMSM additional losses [W].
ΔP_{Cu}	PMSM copper losses [W].
ΔP_{fe}	PMSM iron losses [W].
ΔP_{inv}	Inverter losses [W].
ΔP_{mag}	PMSM magnet losses [W].
ΔP_{pmsm}	PMSM losses [W].
ΔP_{rect}	Rectifier losses [W].
η_{inv}	Inverter efficiency.
η_{pmsm}	PMSM efficiency.
η_{rect}	Rectifier efficiency.
η_{SWT}	Total SWT efficiency.
λ	Tip speed ratio.
ω	SWT angular speed $[rad/s]$.
Φ	Phase magnetic flux of the PMSM [Wb].
Ψ	SWT orientation angle with respect to air [°].

ρ	Air density $[Kg/m^3]$.
θ	Angle between the rotation plane and $\mathbf{c}$ [°].
A	Area of tube in turbine $[m^2]$.
a	Induced axial velocity coefficient.
A_1	Area at inlet of tube $[m^2]$.
A_2	Area at outlet of tube $[m^2]$.
C	Capacity of the capacitor bank [F].
c	Apparent wind speed $[m/s]$.
C_{dc}	DC bus capacitor [F].
C_p	Power coefficient.
d	Swept diameter of the SWT blades [m].
E_{c1}	Kinetic energy at inlet of tube [J].
E_{c2}	Kinetic energy at outlet of tube [J].
E_c	Air kinetic energy [J].
E_{tot}	Annual total energy that can be extracted from the SWT [kWh].
F	Resultant force on SWT blade $[N]$.
F_{axial}	Axial force on SWT blade $[N]$.
F_{drag}	SWT drag force $[N]$.
F_{lift}	SWT lift force $[N]$.
F_{torque}	Force that causes the turn of SWT blade $[N]$.
h_e	Number of SWT operating equivalent hours [hour].
i_{dc}	Rectifier current [A].

i_{grid}	Grid current [A].
$i_{r,s,t}$	Phase RMS current of the PMSM [A].
K	Shape parameter of the Weibull distribution.
L_e	Equivalent inductance of the PMSM [H].
m	Air Mass [Kg].
N	Number of SWT blades.
n	SWT rotation speed [rpm].
n_r	SWT rotation rated speed [rpm].
p	Pairs of poles.
p_+	Air pressure before turbine [Pa].
p_-	Air pressure after turbine [Pa].
P_{dc}	Rectifier DC power [W].
$P_d(u_h)$	SWT power density [kWh].
P_{grid}	Grid power [W].
P_{pmsm}	Total active power of the PMSM [W].
$P_{r,s,t}$	Phase active power of the PMSM [W].
P_{rated}	SWT rated power [W].
P_w	Mechanical power extracted from wind [W].
Q_{pmsm}	Total reactive power of the PMSM [var].
$Q_{r,s,t}$	Phase reactive power of the PMSM [var].
R	Variable resistor [Ω].
R_e	Phase resistance of the PMSM [Ω].

S_{pmsm}	Total apparent power of the PMSM [VA].
$S_{r,s,t}$	Phase apparent power of the PMSM [VA].
T_v	Winding temperature [°C].
T_w	Torque in the shaft of the SWT [Nm].
u	Wind speed $[m/s]$.
u_1	Wind velocity at inlet of tube $[m/s]$.
u_2	Wind velocity at outlet of tube $[m/s]$.
u_a	Induced axial velocity $[m/s]$.
u_g	Wind velocity due to rotation of blades $[m/s]$.
u_h	Wind velocity in turbine $[m/s]$.
u_m	Wind average speed of the Weibull distribution [m/s].
u_w	Linear velocity of SWT blades $[m/s]$.
v_{dc}	Rectifier voltage [V].
v_{grid}	Grid voltage [V].
$v_{r,s,t}$	Phase RMS voltage of the PMSM [V].
$v_{rs,st,tr}$	Line RMS voltage of the PMSM [V].
X_{cap}	Reactance of capacitor banks [Ω].
W(u_h)	Weibull distribution.

Abbreviations

AEE *Spanish Wind Energy Association*. 7

APPA *Renewable Energy Producer Association*. 16

AWEA *American Wind Energy Association*. 10

CNE *National Commission of Energy*. 7

FEM *Finite Element Methods*. 17

FMPCC *Final Maximum Power Characteristic Curve*. 85

GWEC *Global Wind Energy Council*. 3

MPCC *Maximum Power Characteristic Curve*. 20, 21, 32, 52, 60

MPPT *Maximum Power Point Tracker*. 20, 70

MTPT *Maximum Torque Point Tracker*. 20

NREL *National Renewable Energy Laboratory*. 83

PANER *Renewable Energy Action Plans*. 16

PMSM *Permanent Magnet Synchronous Machine*. 17, 19, 45–47, 49, 52, 55

SVC *Static Var Compensator*. 131

SWT *Small Wind Turbine*. 8, 10, 61

WCs *Wind Classes*. 83

1

Introduction

1.1 State of the art

1.1.1 Background

The fact that everyday more wind power is used, demands the development of new technologies of electronic production and the improvement of existing ones. The humankind challenge will be, on the one hand, trying to satisfy the demands of the aforementioned energy and on the other, being respectful to the environment in order to stop the climate change that is taking place.

Thus, wind power is one of the energies that have been developed in order to satisfy this demand and be respectful to the environment. Recently this energy has become one of the main sustainable sources used in developing countries.

The wind can generate electric power without producing undesirable pollutants associated with fossil fuels and nuclear energy. In addition, wind power is a potentially unlimited resource unlike fossil fuels and the elements used in nuclear power plants. Furthermore, wind power promotes a clear and sustainable energy future without the use of fossil fuel resources.

The wind industry promotes a clean and sustainable energy future distinct from the fossil resources. It is for this reason that the wind sector is the one which has experienced the biggest growth in recent years.

The goal of the Kyoto Protocol in 1997 is to reduce worldwide greenhouse gas emissions by 5.2% in the period from 2008 to 2012, with respect to levels measured in 1990. In this way, the European Community goal is to achieve that at least 22% of the

required energy comes from renewable sources when the aforementioned period ends. In order to achieve this percentage, countries started from the existing 17% of 1997.

Historically, wind power was linked to windmills on land. However, nowadays this trend is changing due to the discovery of the big benefits that these windmills would produce on the coast. Some of the main advantages of the off-shore farm are: large usable wind power, the reduction of the visual impact and the reduction of mortality levels of birds.

Therefore, wind power is not new but one of the oldest energy together with the thermal energies. The wind, as a driving force is, was already used in olden days, for instance to move the huge millstones that grind the wheat to produce flour (Fig. 1.1). In the same way it moved ships driven by the wind.

Figure 1.1: Windmill used in olden times to produce flour.

However in the early 80's this type of renewable energy began to develop and still is nowadays. From 2000, the wind power industry has been spreading all over the world, but especially in Germany, USA, Denmark and Spain. It is not necessary to go deeply into the issue but the main factor that produces such a development is the good wind condition found in those countries.

The first windmills were built in Sistan, Afghanistan in the VIIth century. These were vertical shaft windmills with rectangular blades. Eight windmills were built with 6 to 8 sails. Those sails were covered with fabrics and the mills were used to grind wheat and get water.

The earliest European windmills appeared in France and England in the 12th century and quickly spread throughout Europe. These early wood structures, called post mills, were rotated by hand around a central post to bring the sails into the wind.

The tower windmill was developed in France during the 14th century. It consisted of a stone tower with a rotatable wooden structure. This rotatable structure supported the wind shaft and the upper machinery. Early windmills all shared certain features. On top they had a horizontal shaft. This shaft owned four to eight wind sails, each about 3 to 9 m in length. The wood frames of the sails were either covered with fabrics or fitted with wood sheets. The power of the turning shaft was transmitted, through a system of gears, to the machinery placed at the base of the windmill. The horizontal shaft windmills were widely used in Occidental Europe from 1180 onwards to grind wheat (Fig. 1.1).

In the US, the development of the water-pumping windmill was the major factor in allowing the farming and ranching of vast areas, otherwise devoid of readily accessible water. Wind pumps contributed to the expansion of rail transport systems throughout the world, by pumping water from water wells into the steam locomotives.

As it was mentioned before, the development of the modern turbines began from the 80's decade. Since then, the wind power sector has undergone a vertiginous increase; thus, nowadays wind power has become one of the main supports of the worldwide economy.

1.1.2 Wind power development

According to the Global Wind Report created by the *Global Wind Energy Council* (GWEC), from 1996 the development of the world wind power has undergone a substantial increase. In 2010 this development was slowed down because of the crisis.

In Fig. 1.2 it can be observed the variation of the global annual installed wind capacity in MW. In the aforementioned figure it can be also observed how the crisis, as in all sectors, slowed down the development of the world installed power.

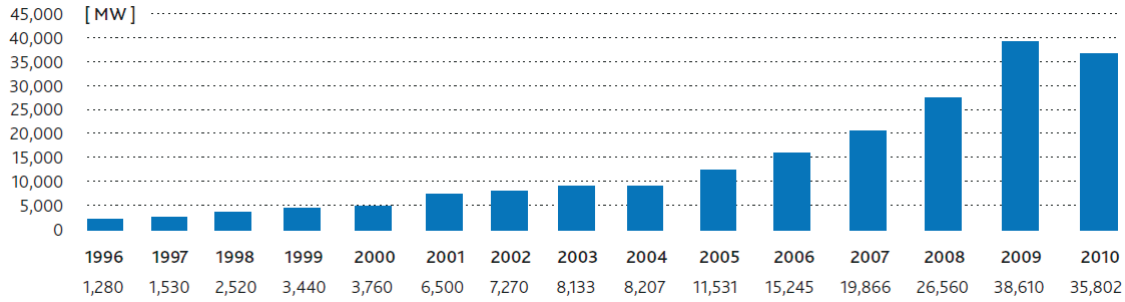

Figure 1.2: Global annual installed wind capacity 1996-2010. Adapted from (1).

In Fig. 1.3, it can be perceived the increase of the wind power that was produced worldwide, for several regions. It is important to take into account that the wind capacity development was different depending on the continent. It seems logical that in underdeveloped countries, there is a lower economic capacity to install this energy. Nevertheless, this does not imply that in the future a development will not be produced.

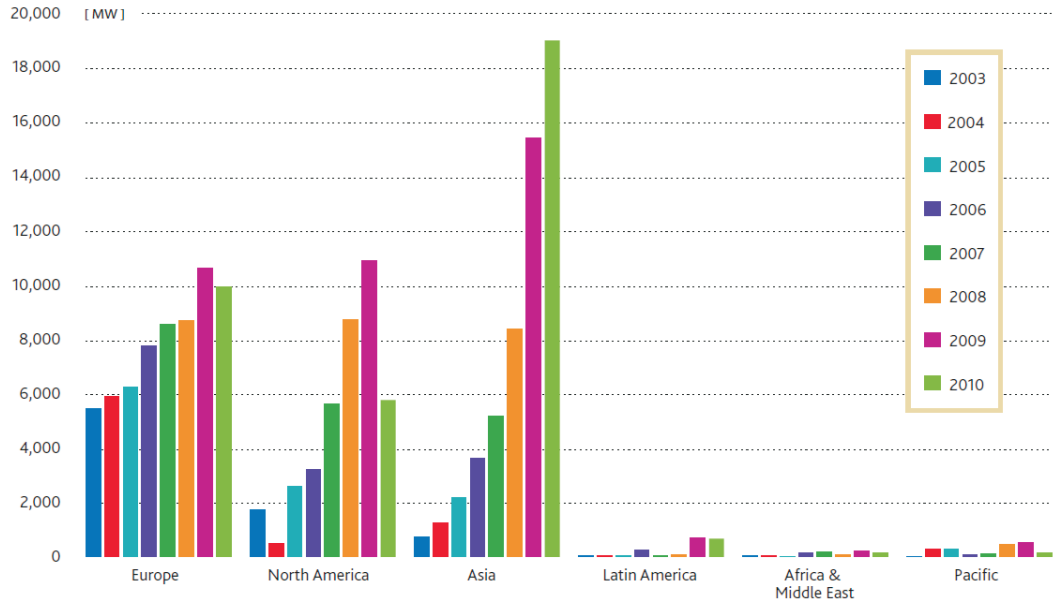

Figure 1.3: Annual installed wind capacity by region 2003-2010. Adapted from (1).

In the aforementioned figure various details can be observed:

- First, the current power installed in Europe and North America was gradually increased until 2010, when it is experienced the crisis influence.

- Second, the crisis has not influenced the wind power sector in Asia where the production even increased in 2010.

- Third, the installed power in Europe, Asia and North America is substantially higher than other regions such as Latin America, Africa, the Middle East and the Pacific.

- Finally, it can be observed that in Latin America, Africa, Middle East and Pacific production begins to increase gradually.

In addition, the predictions suggested by (1), assume an increase of the installed wind power, as can be observed in Fig. 1.4.

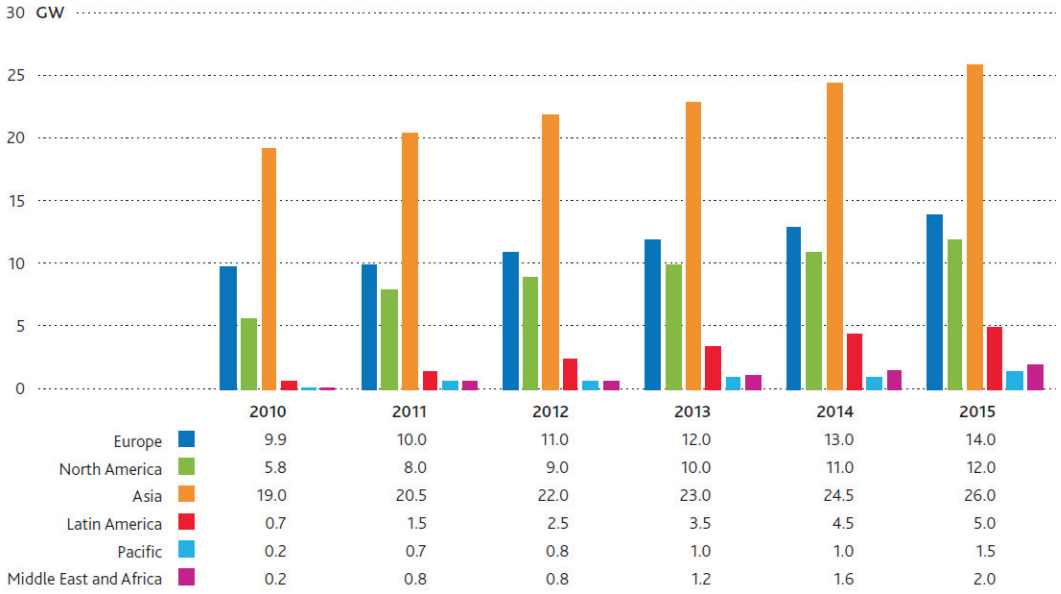

	2010	2011	2012	2013	2014	2015
Europe	9.9	10.0	11.0	12.0	13.0	14.0
North America	5.8	8.0	9.0	10.0	11.0	12.0
Asia	19.0	20.5	22.0	23.0	24.5	26.0
Latin America	0.7	1.5	2.5	3.5	4.5	5.0
Pacific	0.2	0.7	0.8	1.0	1.0	1.5
Middle East and Africa	0.2	0.8	0.8	1.2	1.6	2.0

Figure 1.4: Annual market forecast by region 2010-2015. Adapted from (1).

Finally, in Fig. 1.5 and in Table 1.1 it can be observed the difference between the ten countries with the highest installed wind power and the rest of the world. It can be easily appreciated how just China and the USA have almost half of the world production of wind power. This fact can be easily explained since they have a powerful economy and a vast extension.

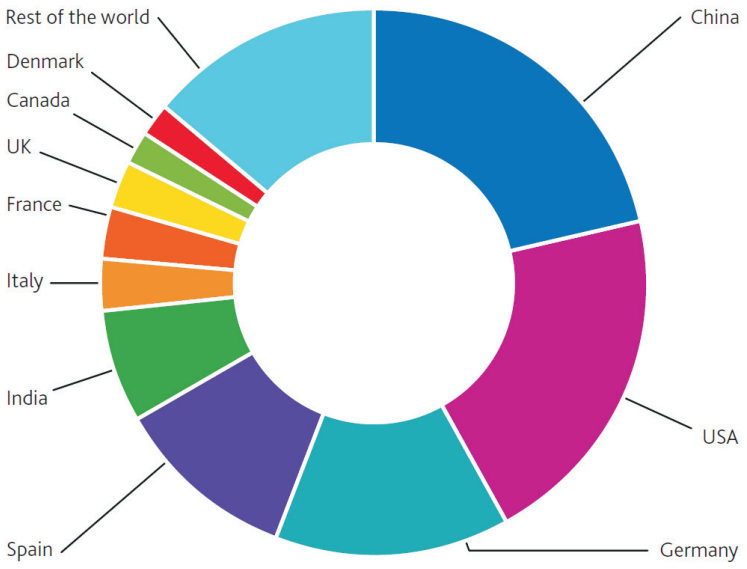

Figure 1.5: Top ten cumulative wind capacities, December 2010. Adapted from (1).

Table 1.1: Top ten cumulative wind capacities, December 2010. Adapted from (1).

Country	MW	%
China	42,287	21.8
USA	40,180	20.7
Germany	27,214	14.0
Spain	20,676	10.6
India	13,065	6.7
Italy	5,797	3.0
France	5,660	2.9
UK	5,204	2.7
Canada	4,009	2.1
Denmark	3,752	1.9
Rest of the world	26,546	13.7
Total Top 10	167,844	86.3
World Total	194,390	100

However, India, Spain and Germany have a wind production that also attracts attention. It is curious that these small countries (if they are compared with China and USA) have a joint production of 25% of the world.

Let us focus on one of those countries, for example Spain.

Despite the financial crisis, the Spanish wind market maintained a healthy pace of development and its cumulative installed wind capacity grew by 7.9% in 2010. According to the *Spanish Wind Energy Association* (AEE), 1,516 MW of new of capacity was added, bringing total installations up to 20,676 MW. Spain thereby remains Europe's largest annual market and home to the second highest total wind capacity after Germany. The leading region in Spain in terms of installed capacity is Castilla y León with almost 4,000 MW.

2010 was a windier year than average in Spain, and the country's wind farms generated 42.7 TWh of electricity, accounting for 16.6% of the national net power consumption. All renewable energy sources combined produced around 38% of Spain's electricity needs, with wind being the largest single contributor within the renewable energy mix.

The average size of the turbines installed during 2010 in Spain was above 2 MW, and the leading manufacturers supplying the Spanish market are Gamesa, Vestas and Alstom Wind. The majority of Spanish wind farms are operated by Iberdrola Renewables, Acciona and EDP Renewables.

This unusual increase of wind power in Spain was due to the policy environment for wind power in Spain.

The Spanish feed-in tariff system was first introduced in 1997, and then amended in 2004, 2006, 2007 and 2010. The 2007 modification (Royal Decree 661/2007) introduced two alternative remuneration options for wind power:

- A regulated tariff, which is a fixed amount paid for each kWh of wind generated electricity;
- A premium added to the market price

The power producer can choose between these two options for the duration of one year, after which they can keep the chosen formula or change to the other option. The electricity distributor has an obligation to buy electricity produced by renewable sources at a defined price and the *National Commission of Energy* (CNE) performs the settlement of costs incurred by distributors. The costs of renewable electricity generation are taken into account for the annual calculation of the electricity price, thereby ensuring that the additional cost to consumers is proportionate to their electricity consumption.

In Spain there was a Revision of the feed-in tariffs in 2010.

After a two month negotiation, the wind power sector and the Spanish Ministry of Industry reached an agreement in July 2010 on the revision of the feed-in tariffs from 1 January 2011 to 1 January 2013.

According to the agreement that was finally approved in December 2010 (Royal Decree 1614), the reference premium for those wind farms which chose the premium option will be temporarily reduced by 35% (from 30.98 to 20.13 €/ MWh). This reduction affects only installations covered by this option under the Royal Decree 661/2007. As a result, around 25% of the existing wind farms will receive a lower feed-in tariff if the sum of the market price plus the premium is above the threshold of 75.4 €/MWh. The cut in the tariff is motivated by the need of the Ministry of Industry to reign in the costs for the power sector, mainly following unexpectedly strong growth in the solar PV sector, which received a much higher feed-in tariff than wind.

The Royal Decree also includes a provision to limit the yearly hours of operation for wind power installations that can qualify for the feed-in tariff or premium. According to the legislation, when in a given year the average number of equivalent hours for the whole Spanish fleet of wind power installations is above 2,350 hours, those wind farms that have produced above 2,589 hours will only receive the market price for the hours above the limit. This has been repeatedly fought by the sector, as it creates an incentive for less efficient wind turbines.

In Table 1.2, it can be observed the increase of the wind power in Spain recently.

Table 1.2: Total installed wind capacity in Spain. Adapted from (1).

Year	2000	2001	2002	2003	2004	2005	2006	2007	2008	2009	2010
MW	32	73	105	198	380	708	817	824	1306	1712	1880

Together with the increase of the wind power in the world a study of the wind turbines was produced too. The aim of this study was to get better results and reduce prices with the final goal of being competitive. As a result, there were complex shape blades that were able to extract a bigger amount of wind energy, there were electric machines with better wind production, etc. Because of this, all the measures that can produce efficiency increases in the *Small Wind Turbine* (SWT), without increasing too much its cost or putting its robustness in danger, are always well received by manufacturers.

1.1.3 Development of small wind energy

Although it is foreseen that the conventional installed wind power will continue increasing (see Fig. 1.4), sooner or later this growth will stop. Due to the fact that this moment is close in certain countries, the study, development and implementation of the small wind energy will be a good point to continue working.

Although small wind turbines do not supply as much power as bigger ones, their implementation has a wide range of possibilities since they can be situated in other places such as roofs. In addition, they can work in isolated power systems and supply without any other mean of alternative energy when the average wind speed allows it.

Of course, this option does not imply the total retirement of other types of energies such as the nuclear or thermal ones. However, this may imply the reduction of the amount of thermal and nuclear power stations in those places. In this way, each citizen may self-supply part of his daily energy. If a whole country is considered, the produced energy will be substantially reduced, as well as the harmful effects to the environment. Both wind powers have been exhaustively studied, giving different kinds of settings.

USA is the country with the largest development of the small wind industry. USA had in 2009, an installed wind capacity of 100 MW and it has a prevision of exponential growth in the upcoming years. In the same continent, Canada has the aim of reaching 60 MW capacity.

In Europe, the country that has developed this energy the most is the UK due to the implementation of several strategies. These strategies establish that for 2050, 30-40% of the energy demand will be covered by microgeneration technologies.

In France and Italy, there is a trend for this type of energy with plans and decrees that enact the installation of small wind power. Portugal is strongly promoting this industry with the Decree 362/2oo7, where subsidies and bonuses for the small wind energy producers are established. This makes a total difference with the traditional wind energy, unlike countries such as Spain.

In Spain small wind energy, despite its numerous advantages, is not developed enough due to legislative, economic, technological and social barriers. Despite its low development, the people in charge of this industry state that this renewable energy has great potential. However to reach its potential, some barriers need to be overcome. This

can be done with the analysis of other successful markets such as the USA. Analysing these factors, Spain will be able to plan strategies for the development of this technology

DEVELOPMENT OF THE SMALL WIND ENERGY IN USA

The small wind turbine market (turbines whose rated power is below 100 kW) increased 15%, with 20.3 MW of new installed wind capacity and with 82.4 million in sales. This increase implies almost 10,000 new units and increases the installed wind capacity in the USA to 100 MW.

Table 1.3: Sales of small wind turbines in 2009.

Sales in USA 2009	World Sales 2009
20.3 MW	42.5 MW
A 15 % growth over 2008	A 10% growth over 2008
9,800 units	21,000 units
$83 USD million in sales	$189 USD million in sales

- 95% of the SWTs sold in the USA in the last year was made by American manufacturers.
- 2/3 of the SWTs sold in the world are from American manufacturers.
- Of the approximately 250 companies that manufactures these turbines in the world, 95 (1/3) are in the USA.
- It has been estimated that about 100,000 units have been sold in the USA since the 80's.

Predictions for the small wind industry show a continuity in the exponential growth in the USA market in the next five years. It is predicted that there will be 1 GW of installed wind power in 2015.

Based on the studies done by the *American Wind Energy Association* (AWEA) (2) on manufacturers all around the world, it was found that the USA market still grew in 2009 due to the subsidies and the tax credits, the private capital and the manufacturers ability to identify and take profit from the energy market.

The most important factor of the growth, in the last few years, may have been the improvement of the subsidies and administration credits. With these subsidies investments are reactivated and consumers can set up new installations more easily.

Although the installed power increased 15%, the number of units sold dropped 6%. This shows a change towards the energy connected to the grid. Since 2007 a prevailing market of turbines unconnected to the grid for domestic use, has appeared. But nowadays this market remains static.

Table 1.4: Global sales in 2009.

Connection	Units	kW
Off-grid	15,500	7,600
On-grid	5,200	34,400
Total	20,700	42,000

After the economic recession it was expected that there would be an increase in the sales of small wind turbines. A combination of various factors increases the consumer demand, so the economy and the environment are the main ones:

- Economic factors
  - Length of the repayment period (TIR).
  - Financial hedge against the increase of the electricity prices.
  - Financial stability.
- Practical sense.
  - Reliability of the electric supply.
  - Compatibility with photovoltaic systems.
  - Diversity of applications.
- Principles
  - Environment.
  - Freedom or independence.
  - Improvement of the image.

  - Consumer selection.
  - Self-confidence.

This kind of technology should especially be used in the property market. Therefore, there are different important factors to improve the development of small wind energy:

- Marketing of houses with clean energy.
- Feasibility of the integration of hybrid systems of sun and small wind energy.
- Discounts for consumers and for manufacturers.
- Prices of systems included in the value of housing.

MARKET AND DEVELOPMENT FACTORS

- Federal incentives in 2009 after the Recover and Reinvestment Law. This law allowed the consumers to install small wind turbines with subsidies up to 30% of the total installation price.
- Installation and certification of systems: the certification is the greatest achievement of the wind industry because for decades it has been self-regulated. The certification contributes to the industry maturity and it is a way to provide clear and reliable information to the consumers and members of the administration.
- External investment: the investment of $80 USD million of private capital in the foundation of new companies. This capital was invested in 20 new manufacturers; this increased the ability of companies to increment their production, reduce costs, achieve their demands and provide a quality service to their consumers.
- Licence: the current policy is too restrictive with this technology, with cumbersome rules; this slows down its development and installation and thus, it repels the companies. However, a small, but increasing tendency of the administration to establish laws that regulate the concession of licences, can reduce this barrier.

- Improvements of the resources for the assessment of technologies. A large number of private companies are developing technologies to identify geographical areas with higher average wind speeds. Data, which have been obtained in the wind power resources maps, usually assess the conditions at 50 metres high. Thus, these results will be extrapolated to 30 metres, since this is the usual height for the small wind turbines. There are not any useful tools for the conditions assessment in urban areas where the small wind energy has a bigger development. In addition the certification of these new technologies is looked for.

- Consolidations and policies. The government incentives make small wind energy a more attractive market for consumers, businessmen and external investments. Thus, with the administration support, the consolidation and maturity of this energy will be achieved. The increase in the number of manufacturers, installers and units means that the industry problems are a priority in the plans of the administrations.

- The economy: the economic recession meant that the consumers, especially the house owners, delayed their investment in these installations. Manufacturers predict that when the economy recovers, there will be a sales resurgence.

- Prices of the electricity. The high price of the traditional electricity means that the alternative energies become more competitive.

COSTS

Costs vary a lot depending on different factors that affect the installations. They tend to range between 0.15-0.20 [$/kWh]. Some of these factors may be:

- Availability and quality of the government incentives.

- Average annual wind speed.

- Costs of the traditional electricity.

- Equipment, installation and maintenance cost.

- Manufacturing raw materials.
- Insurances.
- Financial methods.
- Licence costs.
- Type of applications.

CO_2 EMISSIONS

One single turbine for a residential area saves the equivalent CO_2 of 1.5 average car emission. Therefore, 100 MW of SWT installed capacity in the USA implies:

- 17,000 cars are removed from the road.
- 12,000 housings are powered.
- 101,000 tons of CO_2 are saved per year.

PROFILE OF THE MANUFACTURER AND WORLD MARKET

Of the approximately 250 companies in the world:

- 95 (36%) have their central offices in the USA.
- 47 (12 in USA) have started to sell SWT.
- The number of USA manufacturers increased from 66 to 95 the last year.

Global distribution of manufacturers. Adapted from (3).							
USA	95	Spain	5	Israel	2	Iran	1
Japan	29	Sweden	5	Italy	2	Kenya	1
Canada	24	South Africa	4	Russia	2	Poland	1
UK	22	France	3	Argentina	1	New Zealand	1
China	19	India	3	Australia	1	Switzerland	1
Germany	16	Taiwan	3	Austria	1	Tanzania	1
Netherlands	6	Finland	2	Denmark	1		

Table 1.5: Global Distribution of Manufacturers

PRIORITIES IN THE DEVELOPMENT

The key to increase the production and to decrease the costs are the development of new materials and new manufacturing techniques. For the development of this technology some priorities are established:

- Efficiency
  1. Improve efficiency of blades from 32% to 45%.
  2. Improve the efficiency of electric generators from 65-80% to 90-92%.
  3. Inverters offer less improvement capacity. Many are adapted from those used in the photovoltaic sun industry.
- Design
  1. The area of blades is still increasing in order to capture more energy and reduce to the minimum design loads (use of new materials and processes).
  2. Reduce the number of components.
  3. Research about the reliability, lubrication, corrosion, isolation and electronic problems.
  4. Improve the SWT efficiency to slow wind speeds.
- Other

1. Keep the standards of efficiency, certification and placement of test equipment.
2. Use advanced materials for the towers and designs that reduce the time and cost of assembly.
3. Develop processes and tools that can predict the efficiency of the turbine in a specific location with a bigger precision.
4. Work with the administration to increase the public conscience about this type of energy.

The development of the power storage batteries is not one of the priorities of the industry since there is a bigger interest in the development of SWTs connected to the grid.

SMALL WIND DEVELOPMENT IN SPAIN

In order to reach the necessary development to be competitive, the Spanish small wind industry needs to follow different steps as the American market has done. Thus, it is necessary to invest in research, development and innovation, in order to get government support with protection plans and the announcement of the small wind energy as a reliable, competitive and efficient energy.

Nowadays in Spain, the estimated capacity is not higher than 7 MW. In this way, it was proposed to the government to include the development of this technology in the *Renewable Energy Action Plans* (PANER) 2011-2020.

Using the predictions included in PANER, la *Renewable Energy Producer Association* (APPA) estimates that about 100,000 small wind turbines could be installed in Spain before 2020. The PANER's draft establishes 370 MW as a goal for the small wind energy.

Spain has a great potential for the development of this energy since there are companies qualified for this. Nevertheless, till now the small wind turbines are off-grid, that is to say, the installations for the production of small wind energy are placed in difficult access locations where there is no electric grid. However, nowadays the development of SWTs connected to the grid is being researched. In order to get the market stimulation,

the APPA has proposed different subsidies and subventions for the installation of new SWTs. Thus, the investment is recovered in a period smaller than 10 years and with bonuses per kWh produced.

Due to the big number of small wind energy advantages, it is necessary a detailed study of the different elements that make it up. Therefore, in the last years numerous studies have been done to increase the SWT efficiency. The current trend is looking for equipment as robust as possible to maximize the energy production and minimize the manufacturing costs. Some of the studies to achieve that improvement have focused on:

- Improving the energy storage systems (4).
- Designing new Permanent Magnet Synchronous Machines (PMSMs) (5, 6).
- Improving the aerodynamic design of Small Wind Turbines (SWTs) (7).
- Controlling the SWT rotation speed (8).
- Enhancing the inverter operation (9).

1.2 Thesis structure

This thesis is divided in four sections:

1. Obtain the SWT electromagnetic models.

   This section tries to get two models that allow us to simulate a SWT with *Permanent Magnet Synchronous Machine* (PMSM). The aforementioned models will allow us to obtain relevant data about SWT, such as the efficiency of different elements, currents, voltages, etc.

   A SWT model will be developed using Simulink in order to analyse the system performance when some modifications are introduced. To get this model, the electric equations of the PMSM will be used. This model will also allow us to obtain all the electric parameters of the system (PMSM and back to back converter).

   Afterwards, it will be defined an electromagnetic model by means of *Finite Element Methods* (FEM) (see section 3.3). This method will provide us with all the magnetic and electric parameters of the assembly. This model will be more

comprehensive than the Simulink model but it has the disadvantage that the simulation time is bigger. The main results that you will get with this model will be: magnetic induction inside the PMSM, PMSM magnetic saturation and PMSM losses (in iron, copper, magnets and additional).

2. Definition and design of the set-up facilities.

   The final aim of this thesis is to improve the efficiency of SWTs with PMSM, by means of:

   - Extracting the maximum mechanical energy from the wind.
   - Connecting a capacitor bank between the PMSM and the rectifier.

   In order to get this, a methodology will be established that will be applied in a commercial SWT. Because of this, it will be necessary to define the SWT set-up facilities.

   This section will explain the technical characteristics of all elements that have been used in tests. Furthermore, the measuring elements will also be described.

3. Development of the methodology.

   In this part, it will be explained the different steps to follow, in order to carry out this methodology of SWT efficiency improvement. Once this all is understood, this methodology will be used in a commercial SWT. Then, it will be studied:

   - The power increment.
   - The profit increase.

4. Conclusions.

   Finally, the conclusions that are drawn from the results will be presented.

2

Aims of the Project

2.1 Final aim

Our ultimate goal is to increase the efficiency of a SWT by means of the connection of the necessary capacitor bank to extract the maximum energy from the wind, at every moment of operation. When a capacitor bank is connected at the output of the PMSM, the armature reaction generated by the current that flows through the stator windings, creates a magnetomotive force that is added to the magnetomotive force caused by the inductor.

In addition, it is also intended that the SWT works at all times with the maximum power coefficient C_p, extracting the maximum energy from the wind.

2.2 Preliminary aims

To achieve an improvement in the SWT efficiency, it will be necessary to set some preliminary objectives, such as:

1. Get a theoretical model of the PMSM to develop the Simulink model (10).
2. Study of the PMSM. All features about the PMSM should be known:
    - Dimensions of every element of the PMSM.
    - Materials of all elements of the PMSM.
    - Electrical winding diagram.

3. Study of the rectifier and the inverter.

4. Get the Simulink model of the SWT. Define: PMSM, rectifier and inverter. Using this model, the SWT operating surfaces can be easily obtained.

5. Get a model using finite element methods (FEM). This model allows us:

   - Make a detailed study of the internal PMSM performance.
   - Analyse the PMSM losses.
   - Obtain the waveforms of the various parameters.

6. Define, set up and connect all the instruments that will be used in the test platform:

   - Define a motor that is able to simulate the force of the wind and move the PMSM in all operating speed range.
   - Join mechanically the motor to the PMSM using a chain to transmit the movement.
   - Design a bedplate to provide the necessary rigidity to the system.
   - Put sensors in the shaft of the PMSM. These sensors allow us to measure the speed and torque of the SWT.
   - Connect the rectifier to the PMSM output.
   - Connect the inverter to the rectifier output.
   - Connect a wattmeter and a power quality analyser that allow us to obtain the waveforms and the values of all parameters.
   - Connect the temperature sensors in contact with the PMSM windings.
   - Connect a PC to control wattmeter, temperature sensors and inverter (to enter the *Maximum Power Characteristic Curve* (MPCC)).

7. Make SWT tests: no-load test, constant load tests and rated load test.

8. Adjust Simulink and FEM models to the real one.

9. Calculate the *Maximum Power Point Tracker* (MPPT) and the *Maximum Torque Point Tracker* (MTPT).

10. Calculate the initial range of capacities $[C_i - C_k]$.
11. Calculate the MPCC, for each case.
12. Study the system performance when a capacitor bank is connected.
13. Obtain the ideal capacitor bank.
14. Analyse the results and perform an economic study.
15. Conclusions.

3

Models of the Small Wind Turbine

3.1 Introduction

The aim of this thesis is to increase the efficiency of SWTs with PMSM. Therefore, it will be necessary to get simulation models that allow us to make a detailed study of each specific element of the SWT. That is the reason why two models have been made:

- Simulink model

  This model was made with the aim of studying the system performance as a whole and viewing the interaction between the different elements. That is the reason why this model contains all the elements concerning the SWT, such as PMSM, rectifier and inverter.

  To make the PMSM model, some theoretical equations were used. Those equations are shown in Section 3.2. Some necessary parameters were extracted from its datasheet (12).

  In the same way, the rectifier datasheet (13) helped us to create its model.

  Finally, to simulate the inverter numerous tests were carried out on it. In this way, you obtained the Eq. (5.31) that matched the rectifier current i_{dc} with the inverter losses ΔP_{inv}. Thus, you can do a rough energy balance of the SWT, without the need to create a complex inverter model.

- FEM model

  This model was made in order to study the PMSM in detail, because the Simulink model did not permit it. To create this model, the finite element software called

Flux (11) was used. This software allows you to enter all the PMSM internal parameters, such as: number of slots, number of turns, winding resistance, etc. Furthermore, you can also enter certain electronic components, such as the diodes of the rectifier.

Once the geometry, the meshing, the materials, the electrical circuit and the dynamic properties have been defining, you are ready to solve the problem and analyse the results. The main results that can be obtained by means of this tool are:

- Losses in several parts of the machine: ΔP_{fe} (14), ΔP_{Cu}, ΔP_{mag} and ΔP_{add}.
- Distribution of magnetic flux density inside the PMSM.
- Distribution of the magnetic field lines in the PMSM.
- Waveforms of current and voltage in the PMSM and in the rectifier.

3.2 System model using Simulink

A system model is needed in order to use the methodology presented here, and Simulink was used for this purpose (10). Such a model makes it possible to analyse the SWT in detail and to evaluate its performance under various operating conditions.

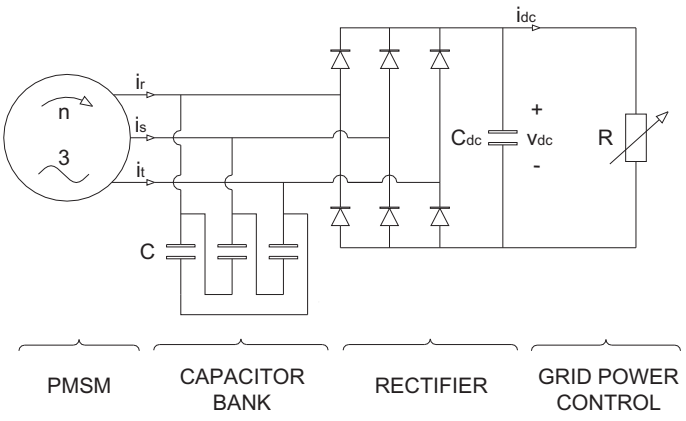

Figure 3.1: Wind power generation system.

The different parts of the SWT Simulink model are: PMSM, rectifier, grid power control (inverter and grid) and capacitor bank. See Fig. 3.1.

First of all, a PMSM model has to be created with the intention of including it in the system model. This has been done by using the electrical equations of synchronous machines. Eq. (3.1) defines the flux at the stator of the PMSM:

$$\begin{aligned}\psi_{ea}(t) =&(L_{\sigma_e} + M_{aa})i_{ea}(t) + M_{ea}i_{eb}(t) + M_{ea}i_{ec}(t)+ \\ &+ \psi_f cos(\theta_e(t))\end{aligned} \tag{3.1}$$

Where:

L_{σ_e}	Leakage inductance of a stator phase.
M_{aa}	Magnetization flux generated by the phase "a" on itself.
$M_{ea}(t)$	Magnetization flux generated by the other phases on the phase "a".

if $i_{ea}(t) = -(i_{eb}(t) + i_{ec}(t))$, then:

$$\psi_{ea}(t) =(L_{\sigma_e} + M_{aa} - M_{ea})i_{ea}(t) + \psi_f cos(\theta_e(t)) \tag{3.2}$$

Considering the geometry of the stator phases,

$$M_{ea} = M_{aa}cos(\frac{2\pi}{3}) = -\frac{M_{aa}}{2} \tag{3.3}$$

and incorporating it into Eq. (3.2),

$$\psi_{ea}(t) = (L_{\sigma_e} + \frac{3M_e}{2})i_{ea}(t) + \psi_f cos(\theta_e(t)) \tag{3.4}$$

the total flux at phase "a" can be expressed by the equation,

$$\psi_{ea}(t) = L_e i_{ea}(t) + \psi_f cos(\theta_e(t)) \tag{3.5}$$

where,

$\psi_{ea}(t)$	Total instantaneous flux in the stator phase.
L_e	Stator phase inductance $L_e = L_{\sigma_e} + \frac{3M_e}{2}$.
$i_{ea}(t)$	Instantaneous current flowing through the stator phase.
ψ_f	Flux generated by the rotor.
$\theta_e(t)$	Electrical angle between rotor and stator.

Extending Eq. (3.5) to the rest of the stator phases,

$$\psi_{eb}(t) = L_e i_{eb}(t) + \psi_f cos(\theta_e(t) - \frac{2\pi}{3}) \tag{3.6}$$

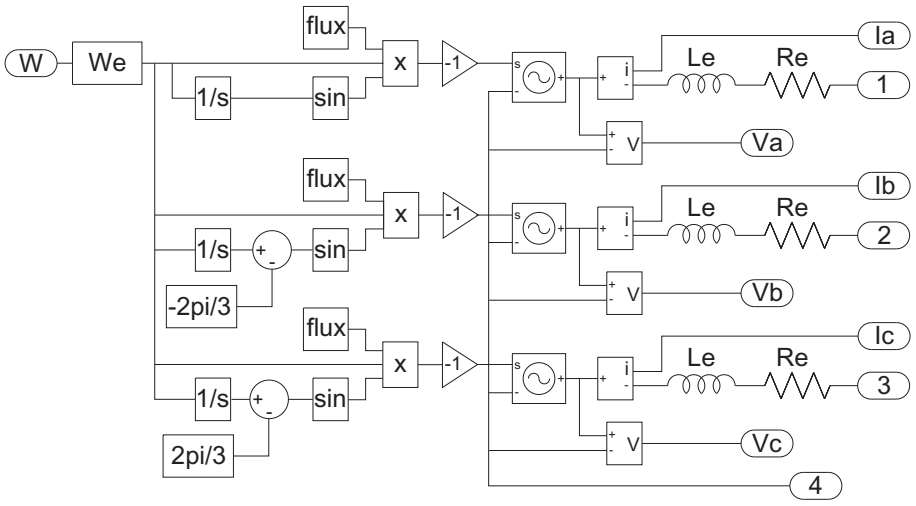

Figure 3.2: PMSM Simulink model.

$$\psi_{ec}(t) = L_e i_{ec}(t) + \psi_f cos(\theta_e(t) + \frac{2\pi}{3}) \tag{3.7}$$

The voltage at the stator windings is:

$$\begin{aligned} v_{ea}(t) &= R_e i_{ea}(t) + \frac{d\psi_{ea}(t)}{dt} \\ &= R_e i_{ea}(t) + L_e \frac{di_{ea}(t)}{dt} - \psi_f \omega_e sin(\theta_e(t)) \end{aligned} \tag{3.8}$$

R_e Equivalent resistance of one stator phase.
$\omega_e(t)$ Rotor electrical angular speed.
$\omega_g(t)$ Rotor mechanical angular speed.

Eq. (3.9) establishes the relationship between the electrical and the mechanical rotor speeds:

$$\frac{\theta_e(t)}{dt} = \omega_e(t) = p\omega_g \tag{3.9}$$

where p is the number of pole pairs.

Extending Eqs. (3.8) and (3.9) to the remaining phases, and using the vectorial notation, you obtain,

$$\begin{bmatrix} v_{ea}(t) \\ v_{eb}(t) \\ v_{ec}(t) \end{bmatrix} = (R_e + L_e \frac{d}{dt}) \begin{bmatrix} i_{ea}(t) \\ i_{eb}(t) \\ i_{ec}(t) \end{bmatrix} - \psi_f \omega_e(t) \begin{bmatrix} sin(\theta_e(t)) \\ sin(\theta_e(t) - \frac{2\pi}{3}) \\ sin(\theta_e(t) + \frac{2\pi}{3}) \end{bmatrix} \tag{3.10}$$

Fig. 3.2 shows the implementation of the Eq. (3.10), using Simulink.

The parameters R_e and L_e are required in Eq. (3.10).

The resistance value R_e is not a constant value, it depends on the winding temperature T_v. Thus, each operating condition has its own resistance value R_e.

It is for this reason that when a simulation model is required, it is necessary to know whether the resistance variation with temperature may influence the results or not.

A test will be done in order to obtain that relationship. The elements used in this test are:

1. Multimeter: To measure the winding resistances R_e.

2. Power source: To heat the windings.

3. Thermographic camera: If temperature probes were used, the temperature in certain points of the winding would be obtained. This type of device can lead to errors during measurements because the temperature of the whole winding is not known. If the winding has defects in the insulation or inter-turn short-circuits, the winding heating will not be uniform.

   That is why in this test, a thermographic camera will be used. This device will allow us to obtain the temperature distribution of the whole winding and verify if some defect exists.

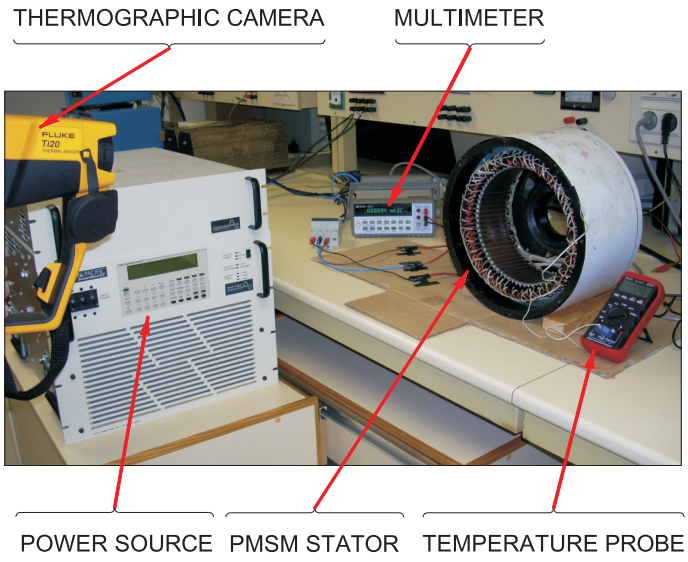

Figure 3.3: Set-up facility to determine the relationship R_e vs. T_v.

Fig. 3.3 shows the architecture of the set-up facility.

The test consists of feeding the PMSM stator with a constant current (using the power source) and when the winding temperature T_v is stabilized, the power supply will be stopped. Then, the power source will be disconnected and the multimeter will be connected in order to measure the winding resistance. Finally, using the thermographic camera, the winding temperature T_v will be measured.

In this way, you can obtain the relationship R_e vs. T_v (see Fig. 3.4).

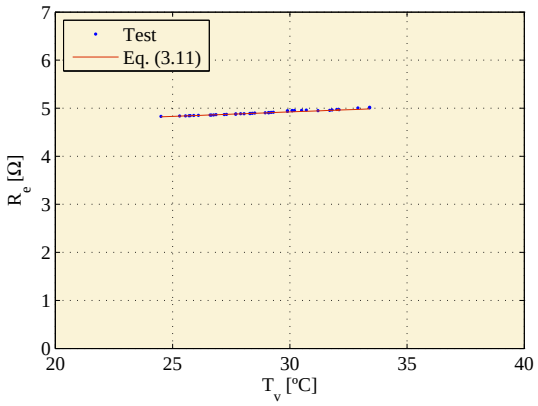

Figure 3.4: Real and theoretical relationships: R_e vs. T_v.

As can be seen in Fig. 3.4, results obtained during the test show a high degree of correlation with those obtained using the traditional formula that relates resistance with temperature (15), see Eq. (3.11).

$$R_{T_i} = R_{T_r} \frac{235 + T_i}{235 + T_r} \tag{3.11}$$

where,

R_{T_i}	Resistance at desired temperature [Ω].
R_{T_r}	Resistance at room temperature = 4.755 Ω.
T_r	Room temperature = 21 °C.
T_i	Desired temperature [°C].

As a result of this, the resistance for a specific temperature will now be obtained by means of Eq. (3.11).

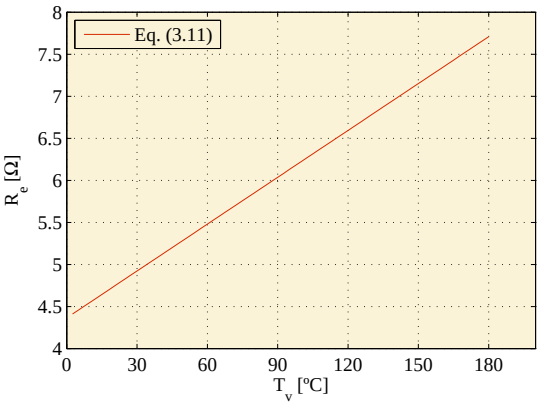

Figure 3.5: Resistance R_e vs. winding temperature T_v using Eq. (3.11).

If the PMSM winding insulation is class H (16) then the maximum temperature that may reach the winding is 180 °C. As shown in Fig. 3.5, the resistance value varies from 4.75 Ω at a temperature of 20 °C to 6.75 Ω at a temperature of 130 °C. Based on these data, the model of the PMSM machine should take into account that the resistance varies with the temperature.

However if you look at Fig. 3.4, the resistance variation with temperature, in a temperature range between 20 °C and 40 °C, is not significant. If you ensure that during the tests the winding temperature T_v is within that range, then the resistance value R_e could be considered constant and its value would be 4.755/2 Ω.

To verify the aforementioned, three temperature probes will be placed in the winding. Fig. 3.6 shows that the winding does not have any defects and the temperature distribution is uniform. In this way the use of temperature probes is justified.

Furthermore, tests will be done in short periods of time in order to ensure that the temperature reached by the windings does not exceed the limit set of 40 °C.

It can be concluded that if SWG tests are made fast enough so that the winding temperature T_v does not increase too much, then the resistance value R_e can be considered constant and can be used in the Simulink model.

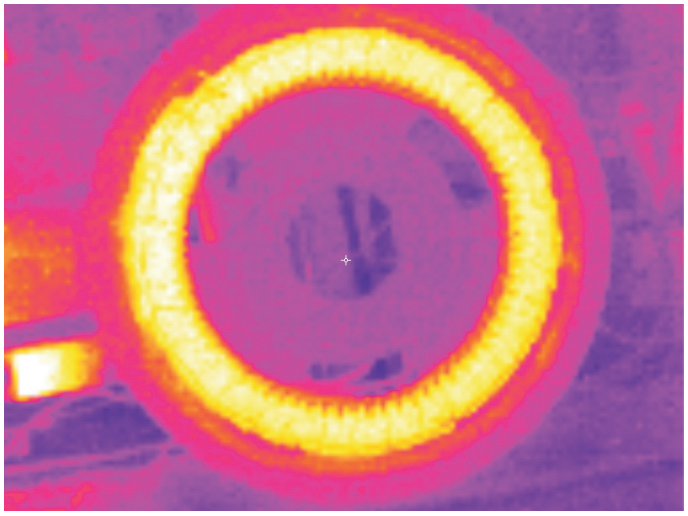

Figure 3.6: Temperature distribution viewed with a thermographic camera after disassembling the PMSM.

To obtain L_e, the formulation proposed in (17) is used.

Once the PMSM model is obtained, it is also necessary to define the rectifier model in Simulink (Fig. 3.1 and Fig. 3.7). This model consists of:

- Six diodes that rectify the AC signal to DC.
- Signal buffering capacity C_{dc}.
- Voltmeter and ammeter to measure v_{dc} and i_{dc}.

The next step will be to add the inverter and the grid effects into the system model. For this purpose, a variable resistor R will be defined (Fig. 3.1 and Fig. 3.7). This resistor R will control the power injected into the grid.

Following, if you place together the PMSM model (Fig. 3.2), the rectifier model (Fig. 3.7), the additional measuring elements and the capacitor bank at the output of the PMSM, you obtain the SWT complete model (Fig. 3.8).

In addition, to take into account the inverter efficiency, a study of the inverter losses ΔP_{inv} will have to be carried out (Fig. 5.71). Thus, the relationship between rectifier continuous current i_{dc} and inverter losses ΔP_{inv} will have to be obtained. Therefore, grid power P_{grid} will be calculated as:

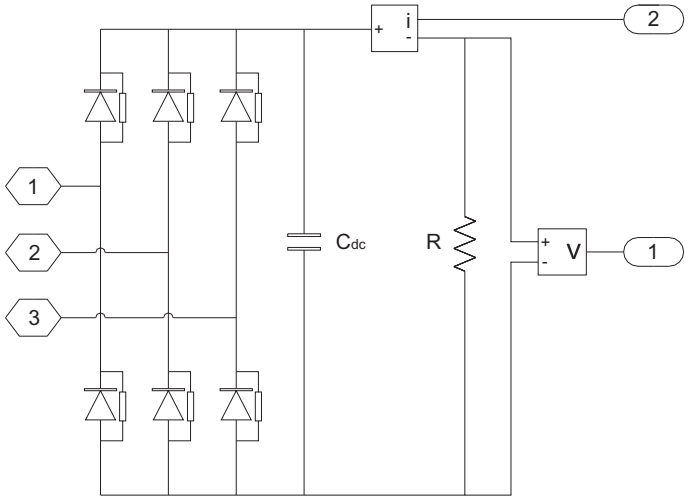

Figure 3.7: Simulink model of rectifier and grid power control.

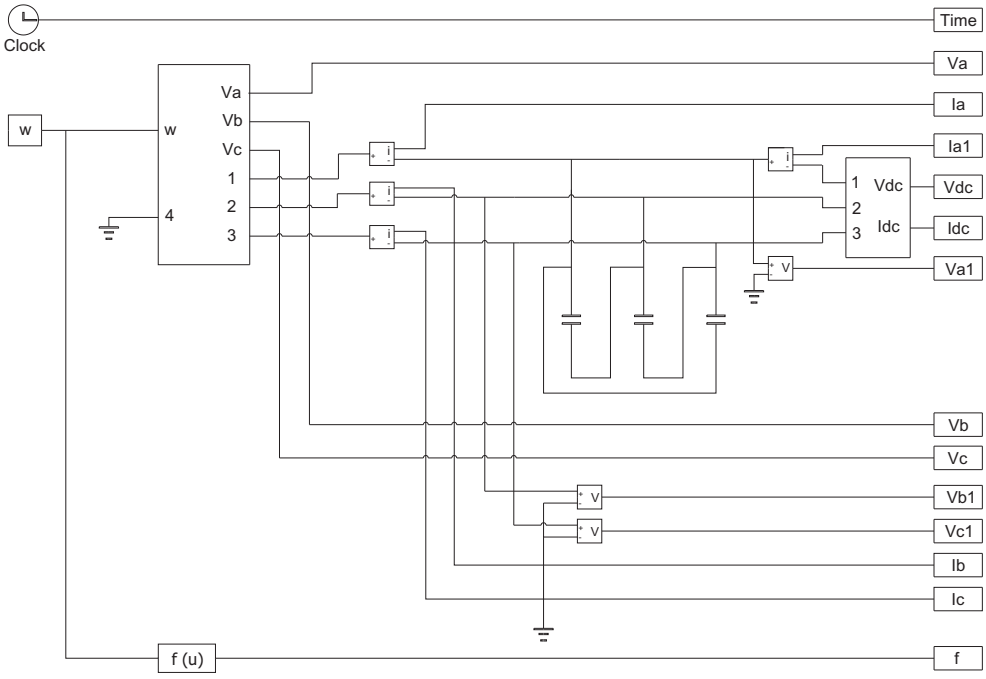

Figure 3.8: SWT Simulink model.

$$P_{grid} = P_{dc} - \Delta P_{inv}(i_{dc}) \tag{3.12}$$

where,

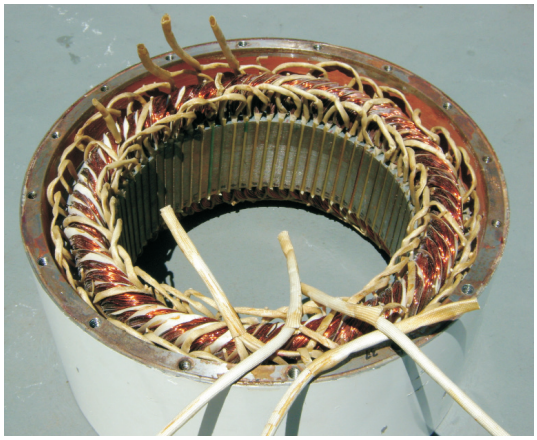

Figure 3.9: PMSM stator.

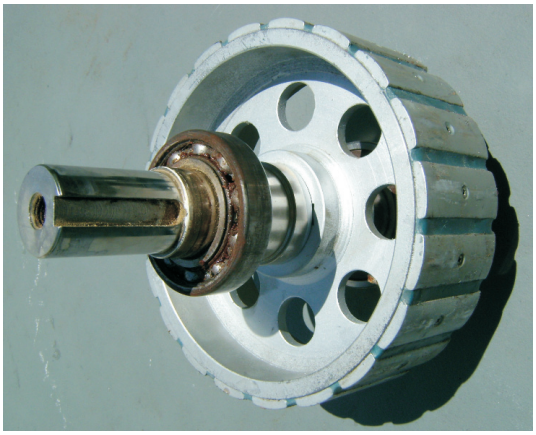

Figure 3.10: PMSM rotor.

P_{dc}	Rectifier DC power [W].
i_{dc}	Rectifier DC current [A].
P_{grid}	Grid power [W].
ΔP_{inv}	Inverter losses [W].

The final system model will be used to analyse the SWT performance when certain parameters are modified, such as rotation speed n, capacitor value C and variable resistor R. Thereby, the following can be obtained:

- The grid power P_{grid} and the rectifier DC voltage v_{dc} by combining different values of R, C and n.

- The MPCC for different operating conditions.

3.3 System model using FEM

In the other hand, the FEM model (11) allows us to analyse in more detail the PMSM performance. Thus, this model allows us to calculate the iron losses P_{fe}, the copper losses P_{cu}, the magnet losses P_{mag}, the additional losses P_{add}, the magnetic field distribution inside the PMSM and the voltage and current waveforms in the PMSM and in the rectifier.

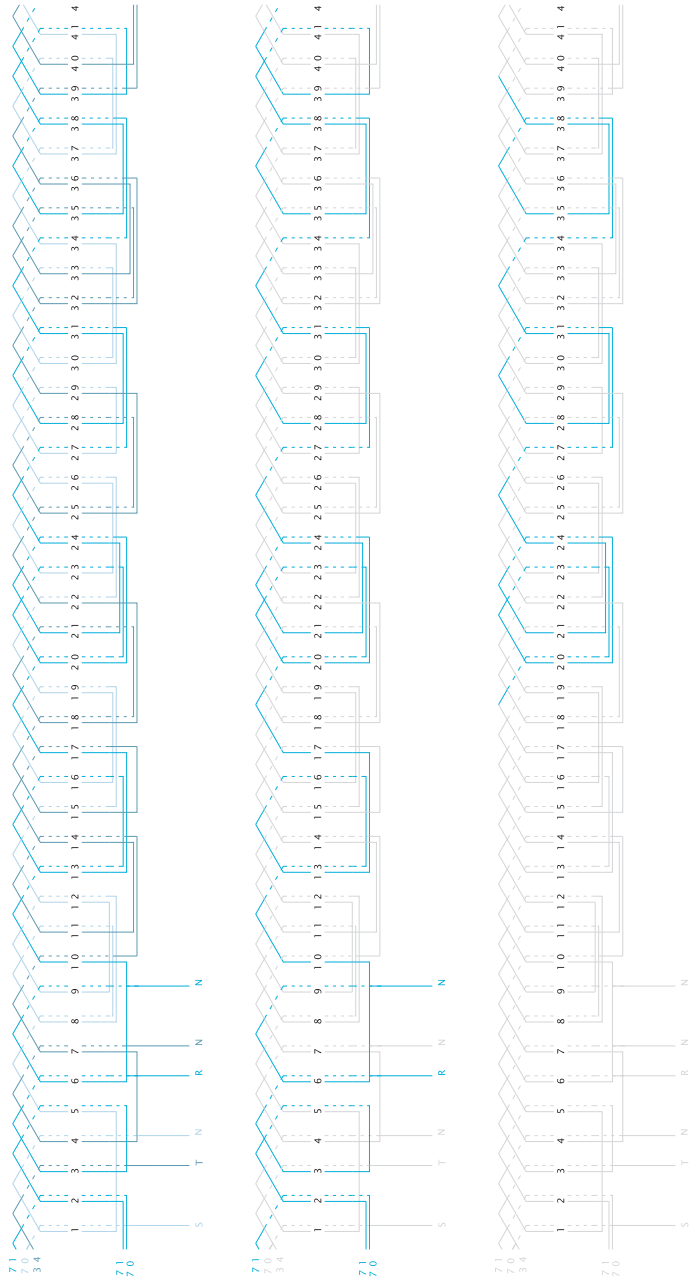

Figure 3.11: PMSM winding diagram.

To achieve this model it will be necessary to know all the PMSM geometry and its internal features. For this reason the PMSM had to be dismantled. Fig. 3.9 and Fig. 3.10 show the stator and the rotor of the PMSM. In this figures you can clearly see some specific characteristic of the PMSM, as for example: number of windings in

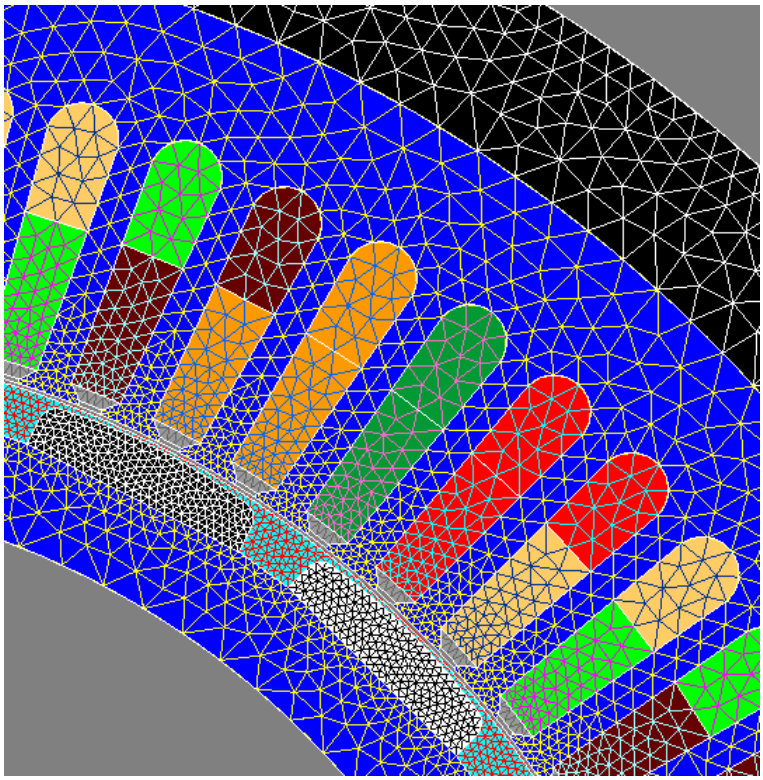

Figure 3.12: FEM model of the PMSM geometry.

parallel, number of slots, number of wires in parallel, number of turns per coil, wire diameter, slot angle, number of layers, type of bearings, shape of magnets, etc.

In addition, if the above parameters are used the PMSM winding diagram can also be obtained. That diagram can be seen in Fig. 3.11.

In Fig. 3.12 you can see the geometry of one tenth of the electric generator and its associated mesh. This mesh should have neither few nodes, because it would lead to erroneous results, nor many nodes because the computational cost and simulation time would be very high.

Fig. 3.13 shows the electric circuit diagram used in the FEM model. In this figure it can be seen all elements entered into the model, in order to obtain the desired waveforms. These elements are:

- R1, R2 and R3. High value resistors to measure the phase voltages: v_r, v_s and v_t.
- R4, R5 and R6. Low value resistors to measure the PMSM current: i_r, i_s and i_t.

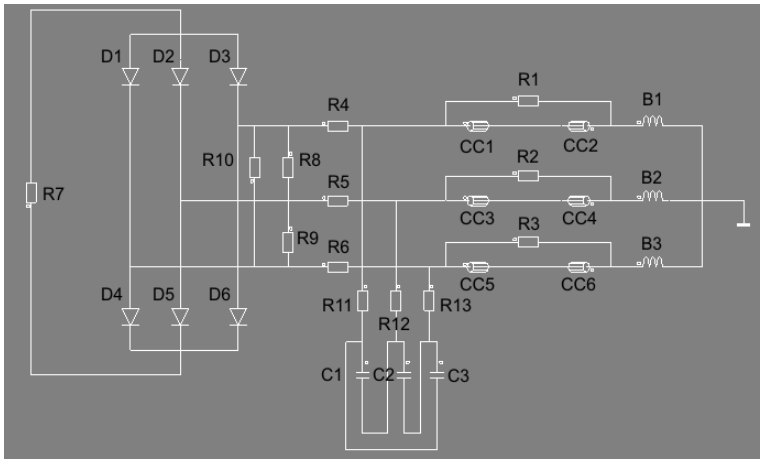

Figure 3.13: Electric circuit diagram using FEM model.

- R7. Variable resistor to measure the current and voltage after the rectifier: v_{dc} and i_{dc}.
- R8, R9 and R10. High value resistors to measure the line voltages: v_{rs}, v_{st} and v_{tr}.
- R11, R12 and R13: Low value resistors to measure the capacitor bank currents: i_{c1}, i_{c2} and i_{c3}.
- C1, C2 and C3: Value of the capacitor banks.
- B1, B2 and B3: Inductances of each phase.
- CC1 and CC3: Coil conductors of phase R.
- CC2 and CC4: Coil conductors of phase S.
- CC5 and CC6: Coil conductors of phase T.
- D1, D2, D3, D4, D5 and D6: Diodes of rectifier bridge.

In addition, to complete the model it has to be known:

- Some characteristics of the PMSM geometry, as for example: its length and its internal diameter.
- The materials and properties of: magnetic plates, copper, magnets, housing, etc.

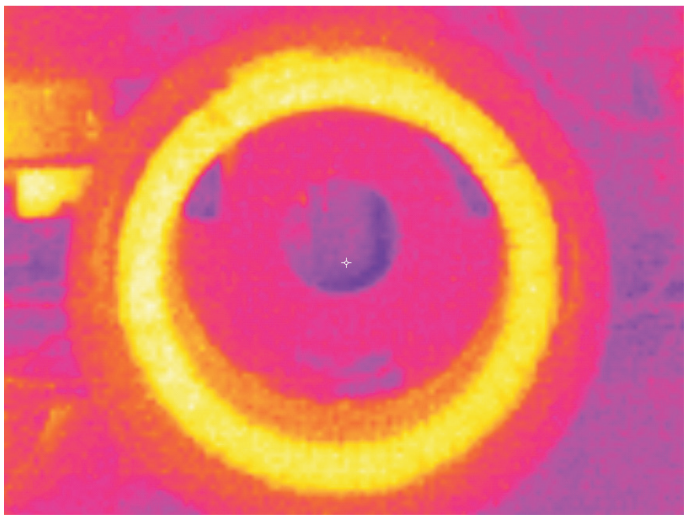

Figure 3.14: Temperature distribution viewed with a thermographic camera before assembling the PMSM.

- Some parameters related to the winding diagram, such as: number of slots, number of layers, number of coils, number of circuits in parallel, number of turns per coil, number of conductors in parallel per turn, etc.
- Other electrical parameters, such as: resistance and inductance of each phase.

Finally, to verify that during assembly and disassembly of the PMSM, the winding was not damaged, a thermographic camera could be used. Using this camera you can detect temperature variations in the windings due to insulation defects and inter-turn short-circuits (see Fig. 3.14).

Fig. 3.14 shows that there is not defect in the windings and the PMSM can be assembled again.

4

Set-Up Facility

4.1 SWT Block diagram

Fig. 4.1 shows the devices that were used during the tests of the SWT, as well as their connections.

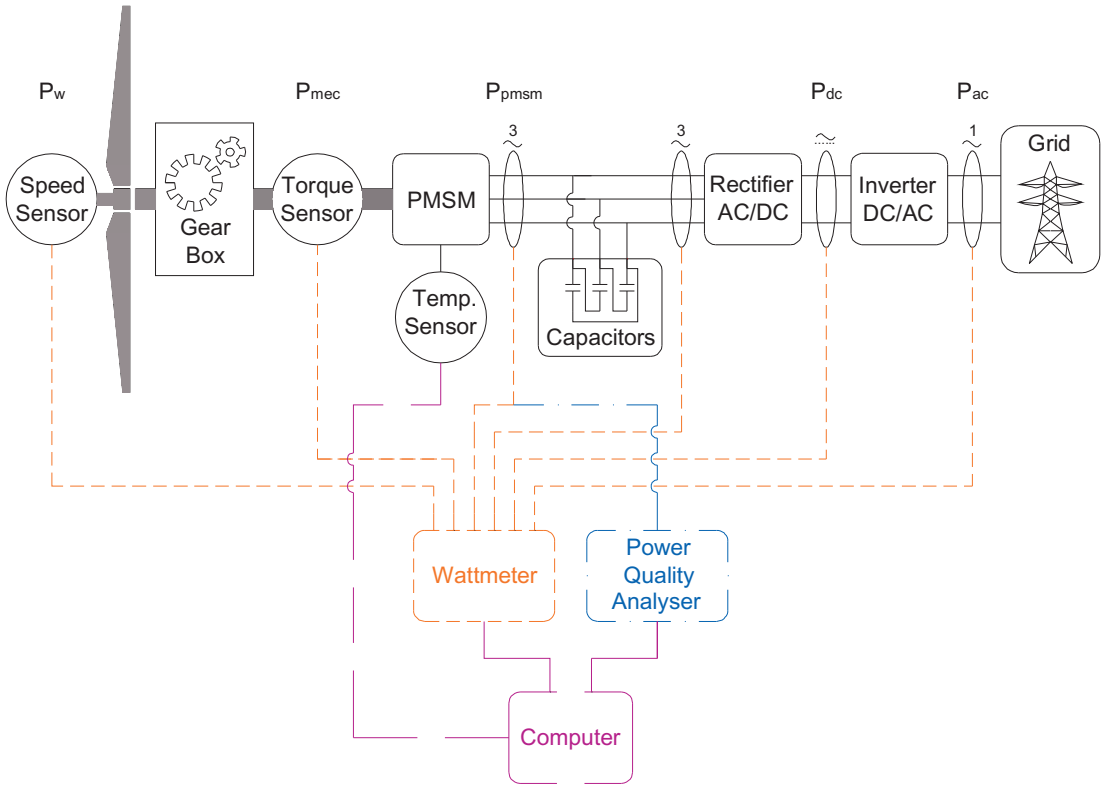

Figure 4.1: SWT block diagram.

Moreover, Fig. 4.2 shows the architecture of the set-up facility.

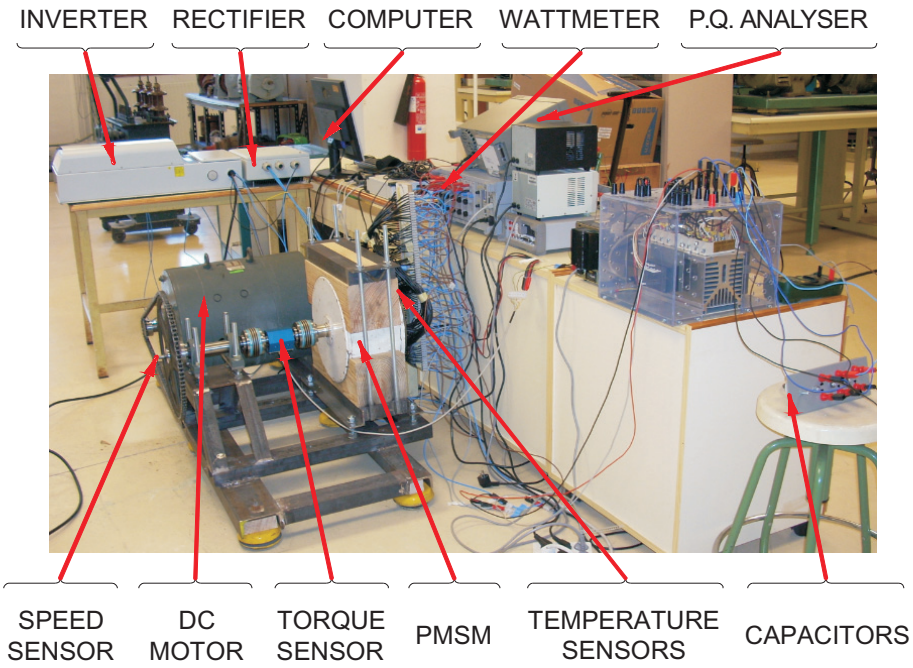

Figure 4.2: System: PMSM + Rectifier + Inverter + Capacitor bank.

4.2 Features of equipment

1. Oscilloscope HP54600B
   - 2 input channels.
   - Resolution of 8 bits.
2. Power quality analyser:
   - 4 differential inputs, 1-600 Vrms, AC/DC.
   - 4 inputs with CTs 0.1-6000 Arms CT-dependent, AC/DC.
   - 1 MHz High Speed Sampling.
3. Wattmeter: WT-1600
   - Input voltage range: 1.5 V - 1000 V.
   - Input current range: 10 mA - 5 A or 1 A - 50 A.

- Frequency range: 0.5 Hz - 1 MHz.
- 6 input channels.
- Precision ±0.1%

4. Multimeter
    - 6.5 digits of resolution.
    - 1000 readings per second.
    - Precision: 0.0035% V_{dc}.
    - Precision: 0.06% V_{ac}.
5. Inverter: Aurora 6 KW
    - AC power range: 6000 W.
    - Maximum voltage DC: 600 V.
    - Maximum current DC: 18 A per channel (2 channels in parallel).
    - Rated single-phase rms voltages (AC): 208, 240 and 277 V.
    - Rated frequency: 60 Hz.
    - Maximum line rms current: 30 A.
    - Current distortion $< 2\%$.
    - Maximum efficiency: 97% (96.5% C.E.C.).
6. Rectifier: GINLONG
7. Lorenz torque sensor DR-2477
    - Measuring range: 0.2 - 200 Nm.
    - Precision class: 0.25.
    - Output signal: ±5V.
    - DC input voltage: 12 - 28 V.
    - Tolerance sensitivity: ±0.1%.
    - Maximum torque: 250 Nm.
8. Hohner speed sensor

- DC input voltage: 11 - 30 V.
- 10000 pulses per revolution.
- Frequency 200 kHz.

9. Small wind turbine
   - Rated power: 3500 W.
   - Rated speed: 250 RPM.
   - Rated DC current: 11 A.
   - Rated torque at rated power: 150 Nm.
   - Insulation class H.
   - Star-connected three-phase generator (PMSM).
   - PMSM phase resistance at 20°C: 2.7 Ohm.
   - Total weight: 78 Kg.
10. DC motor
    - 220 V / 2.3 A and 5 kW.
    - 1500 RPM.
11. Temperature sensors: HOBO
    - Range of measures: from -20°C to 70°C.
    - Precision: ±0.54°C from 0°C to 50°C.
    - Resolution: From 0.1°C to 25°C.
12. Data Logger Topas 1000 LEM
    - 8 input channels.
    - AC Voltage range: 83 - 264 V and 45 - 65 Hz.
    - DC Voltage range: 100 - 375 V.
    - Maximum power consumption: 30 VA.
    - IP 65.
    - Ethernet connection.

4.3 Software

In this section, software used by each device of measurement will be explained.

1. Software used to set up the 6.0 KW Aurora inverter. This software is useful to measure some parameters and to enter the Maximum Power Characteristic Curve (MPCC).

    - MPCC setting by means of the software. Fig. 4.3 shows the screen where the MPCC must be defined. This MPCC will be sent later to the inverter. It can be seen that there are two ways to enter these curves: grid power vs. DC voltage and grid power vs. frequency. In this case, the first way will be used.

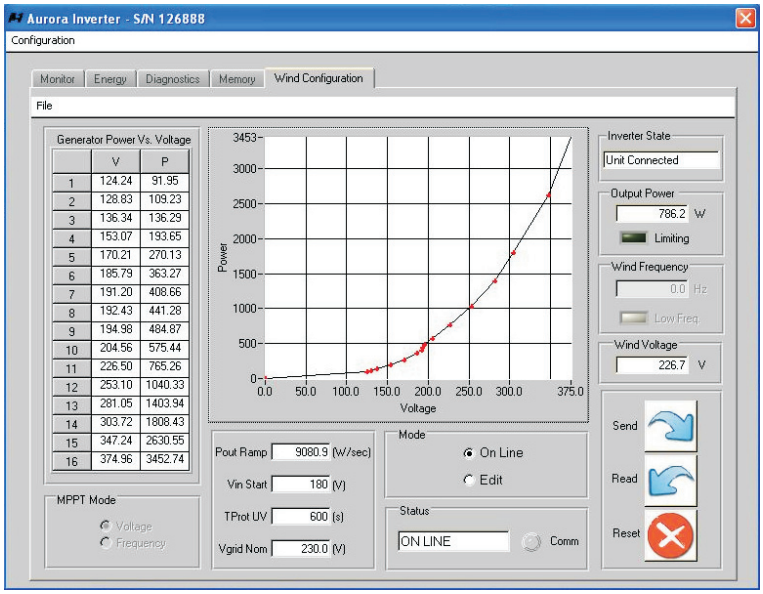

Figure 4.3: Software of Inverter: Aurora 6.0 KW. MPCC definition.

2. Data Acquisition Software for WT-1150

    - Software setting to take measurements. Fig. 4.4 shows the screen of data acquisition and the options to take the measurements (manual and automatic).

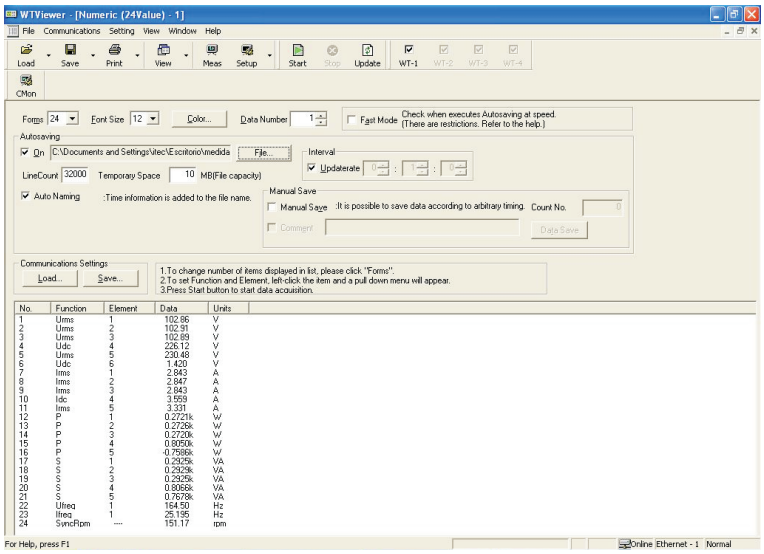

Figure 4.4: Software of wattmeter WT-1150 to acquire data.

3. Data Acquisition software for HOBO temperature sensors

- Software setting to take measurements. In Fig. 4.5 you can see a screen of that software. This figure corresponds to a heating test and its subsequent cooling.

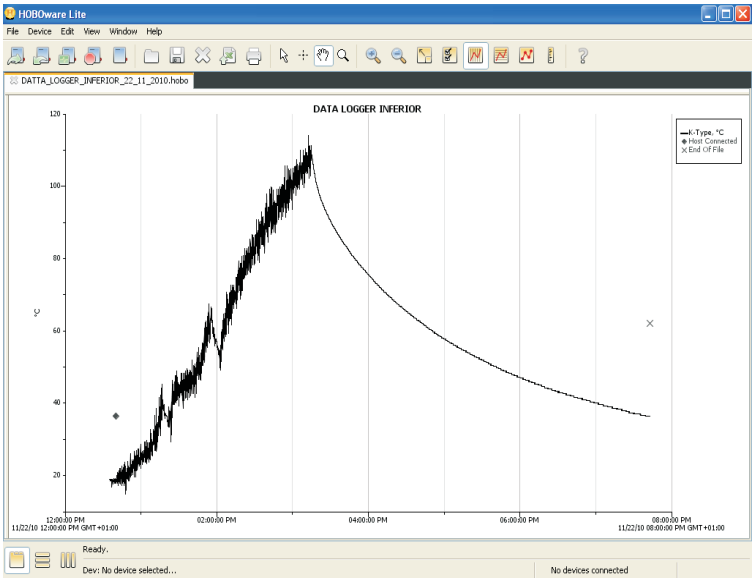

Figure 4.5: Software of HOBO temperature sensors to acquire data.

4.4 Description of mechanical assembly

As a preliminary step before any test, it will be described how all devices are assembled. First of all, it should be noticed that to simulate the torque generated by the wind, a DC motor will be coupled to the PMSM shaft.

A model with CAD software was developed. This model made it possible to define and design all the elements that make up the bedplate. These elements are:

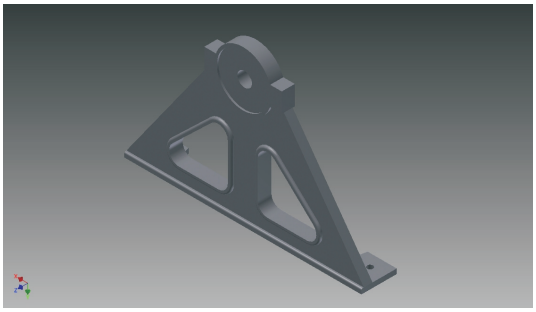

Figure 4.6: Machine support I.

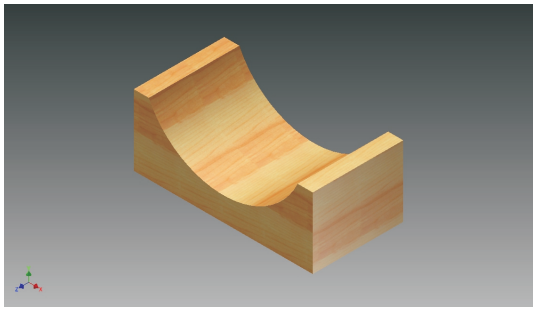

Figure 4.7: Machine support II.

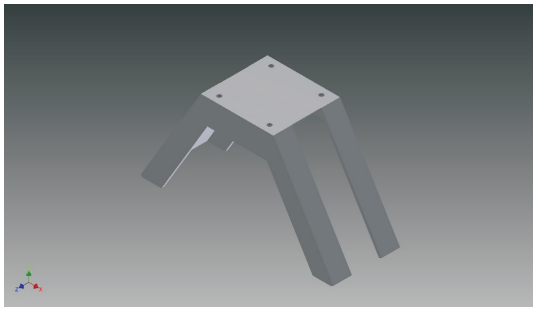

Figure 4.8: Machine Support III.

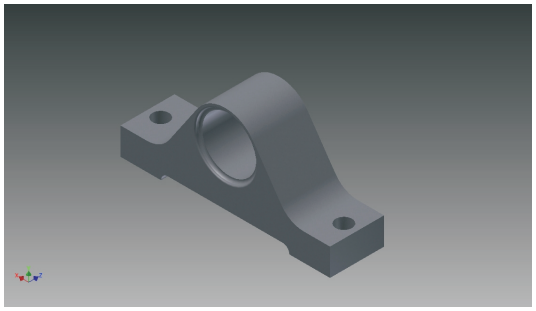

Figure 4.9: Shaft support.

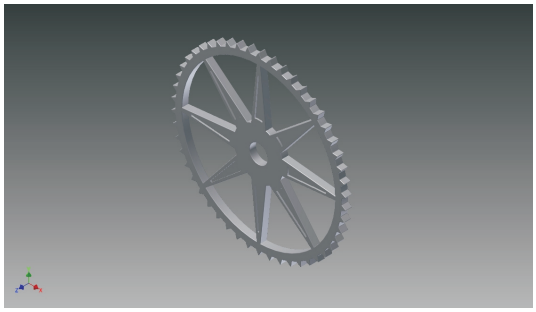

Figure 4.10: Big wheel.

Figure 4.11: Small wheel.

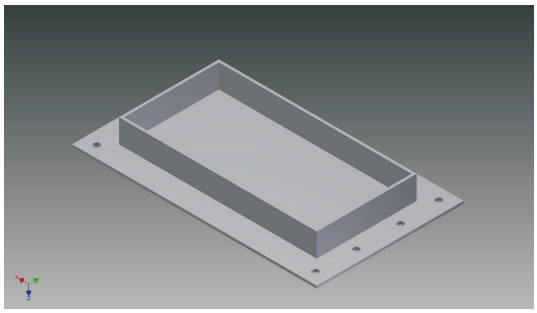

Figure 4.12: Bottom bar support.

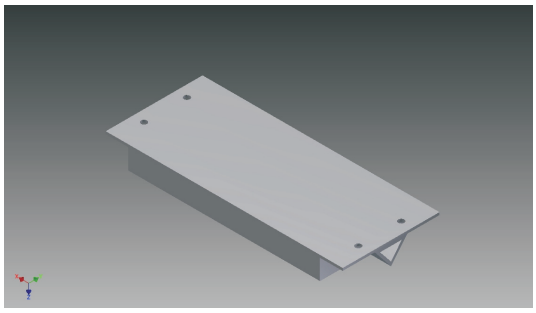

Figure 4.13: Top bar support.

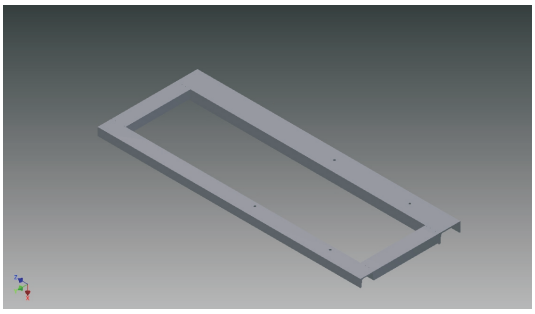

Figure 4.14: Bottom support.

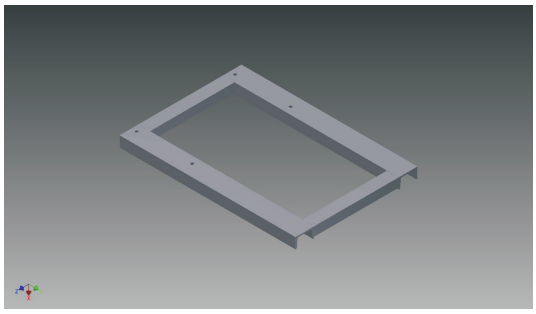

Figure 4.15: Top support.

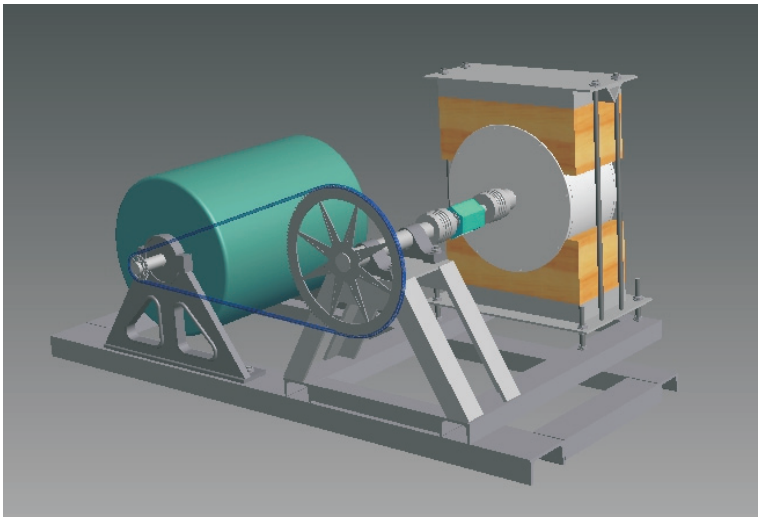

Figure 4.16: CAD design of the assembly.

All these devices were designed by means a CAD software and finally you can see the complete system in Fig. 4.16. Taking all this in practice, the test bedplate was

manufactured (see Fig. 4.17).

On the one hand, the rated speed of the commercial SWT is 250 rpm and it can even reach speeds of 300 rpm. On the other hand, the DC machine has a rated speed of 1500 rpm. Then, a gear wheel was used to match the speeds (Fig. 4.10 and Fig. 4.11). The gear ratio used was 1:6 (with respect to the DC machine pinion).

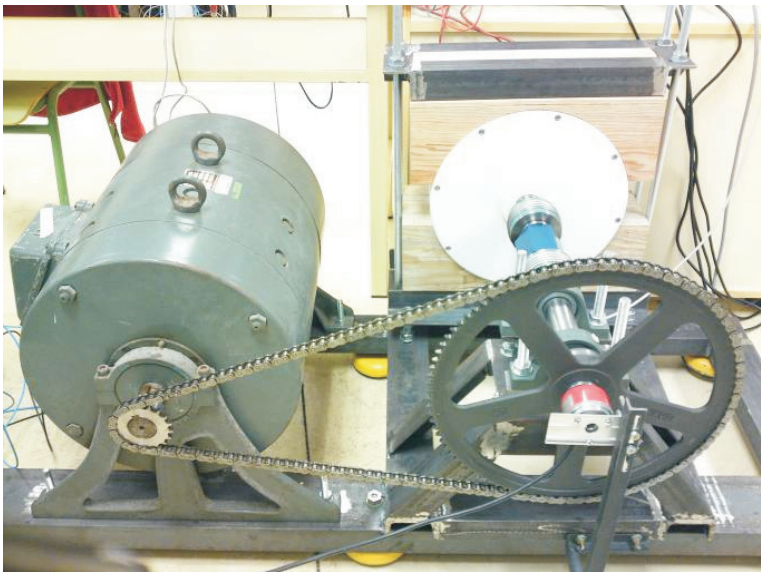

Figure 4.17: Coupling between DC motor and PMSM.

After placing the gear wheel, the next step was to proceed with the alignment of the shafts of both machines. This was done to avoid mistakes during measurements and unnecessary damages on mechanical elements (bearings, chain, etc..) and on measuring devices. Both machines were fixed to the test bedplate, in order to give greater rigidity to the structure and reduce vibrations on the system (PMSM-DC machine). In addition, six elastic supports (also called Silemblock) were placed under the test bedplate to absorb part of vibrations.

As shown in Fig. 4.18, the PMSM shaft has five elements:

1. Speed sensor.

2. Gear wheel to transmit the torque.

3. Support to absorb possible loads to the PMSM.

4. Torque sensor.

5. Flexible couplings.

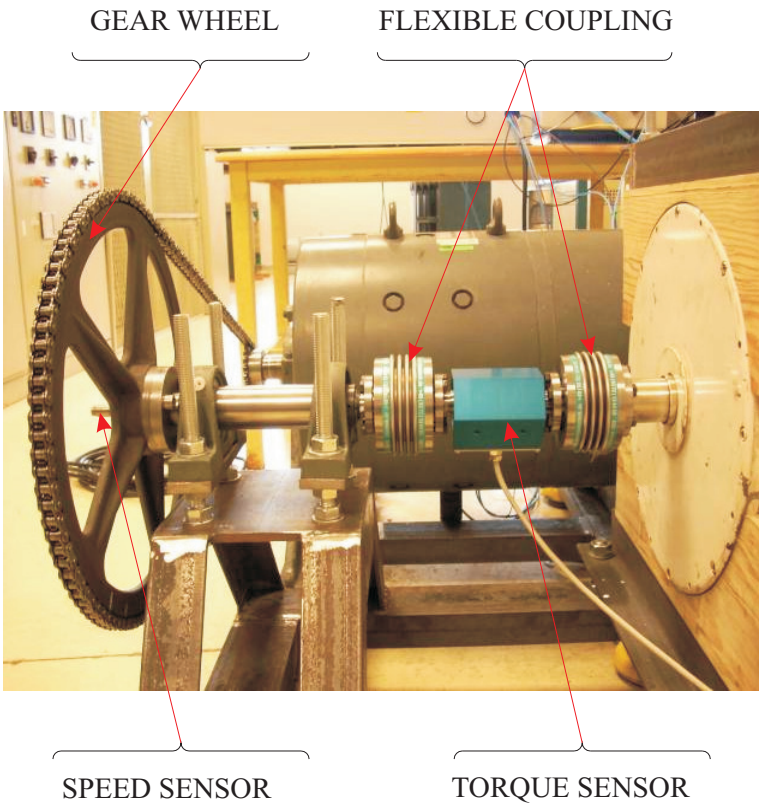

Figure 4.18: PMSM shaft.

4.5 Description of electrical assembly

After this, the rectifier (Fig. 4.19) was connected to the output of PMSM to convert the AC signal into a DC signal and then send that DC signal to the inverter Aurora 6.0 KW (Fig. 4.20). The output of the inverter was connected directly to the grid.

Once we have discussed the steps that were followed and the preventive measures taken during the assembly (mechanical and electrical), we will proceed to explain how to connect all the measuring elements to obtain the desired measurements (Section 4.7).

Figure 4.19: Rectifier.

Figure 4.20: Inverter.

- **Wattmeter WT-1150 (Fig. 4.21)**

  The wattmeter WT-1150 has six measuring channels which will be used to extract the following data:

  1. Channel 1, 2 and 3:
     - Waveforms of phase voltage and phase current in each of three phases of the PMSM.
     - Active, reactive and power factor in PMSM.
     - Phase voltage and phase current harmonics in PMSM.
  2. Channel 4:
     - Waveforms of DC voltage and DC current after the rectifier.
     - DC power after the rectifier.
  3. Channel 5:
     - Waveforms of phase voltage and phase current after inverter.
     - Active, reactive and power factor after inverter.
     - Voltage and current harmonics after inverter.
  4. Channel 6:
     - Torque in the SWT shaft measured by means of sensor torque.
     - Rotation speed measured by means of sensor speed.

In addition, the wattmeter can also calculate other parameters using data previously obtained. Some of these parameters are: PMSM efficiency, rectifier efficiency and inverter efficiency.

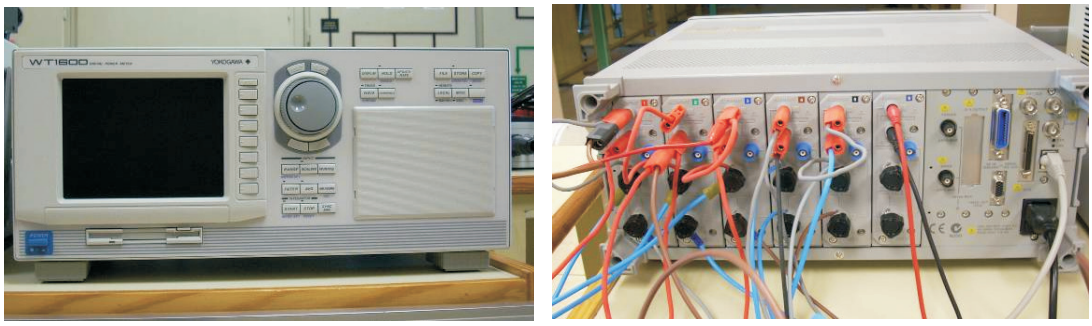

(a) Front. (b) Rear.

Figure 4.21: Wattmeter.

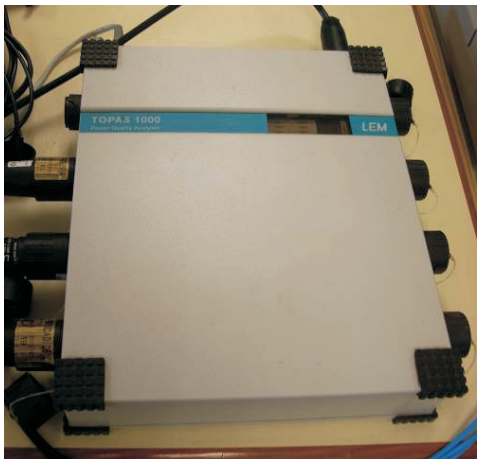

Figure 4.22: Data Logger.

Figure 4.23: Oscilloscope.

- **Data Logger (Fig. 4.22)**

  This element of data acquisition is redundant with the wattmeter and it is used due to its higher capacity to acquire data in comparison with the wattmeter. It measures:

  1. SWT mechanical torque.
  2. PMSM line voltage.

3. PMSM rotation speed.

4. It also has five additional channels although they are not currently used. These channels could become useful for the measurement of other parameters, such as vibrations caused by different elements.

- **Oscilloscope (Fig. 4.23)**

  This element allows us to see in real time the line and phase voltage of the PMSM and its frequency. In addition, it also allows us to display the torque waveform as well as the torque fluctuations.

- **Speed sensor (Fig. 4.24)**

  This element allows us to measure the SWT rotation speed ω. Fig. 4.29 and Fig. 4.30 show how this element is placed in the PMSM shaft.

- **Torque sensor (Fig. 4.25)**

  With the help of flexible couplings, the torque sensor allows us to calculate the mechanical torque value in the PMSM shaft. Moreover, it also allows us to obtain the PMSM internal losses ΔP_{pmsm}. These losses can be divided into three types: iron losses, copper losses and mechanical losses. If the torque T_w is known, it is easy to obtain the mechanical power P_w, by:

$$P_w = T_w \cdot \omega \tag{4.1}$$

  Thus, the PMSM losses can be got by means of,

$$\Delta P_{pmsm} = P_w - P_{pmsm} \tag{4.2}$$

  In Fig. 4.29 and Fig. 4.30 it can be seen where the torque sensor is connected.

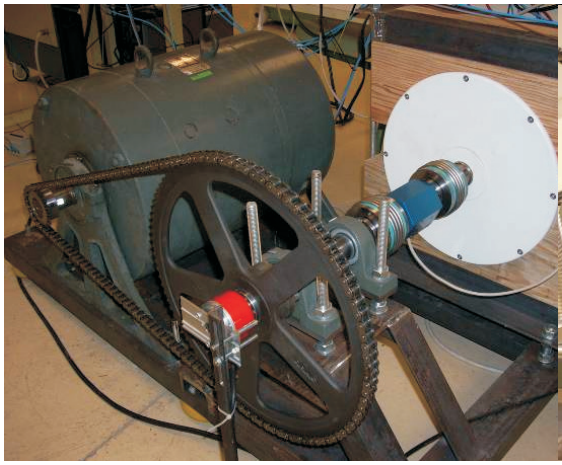

Figure 4.24: Speed sensor.

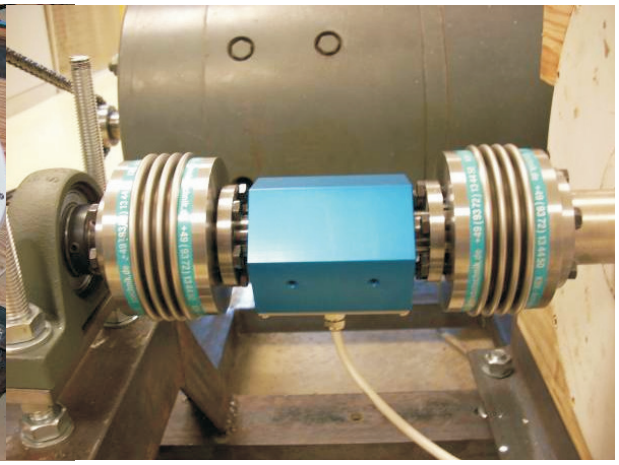

Figure 4.25: Torque sensor.

- **Temperature sensor (Fig. 4.26)**

  Two temperature sensors were placed inside the PMSM windings. These probes allow us to determine how the temperature varies inside the machine and see how this variation modifies the value of the winding resistance. This value will be quite important when the PMSM copper losses are measured.

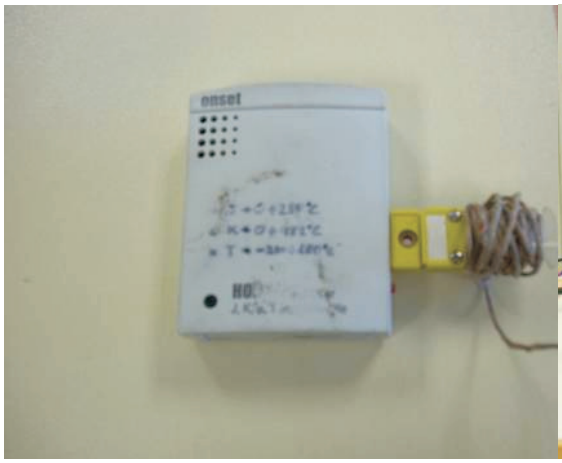

Figure 4.26: Temperature sensor.

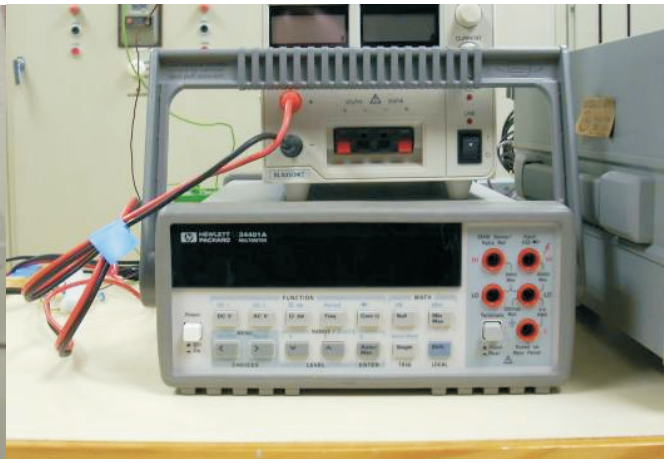

Figure 4.27: Multimeter.

- **Multimeter (Fig. 4.27)**

  It allows us to obtain, with high precision, the winding resistance values. It should be noticed that when the winding temperature increases, the winding resistance

value also does. This is the reason why this parameter has to be accurately measured.

- **Power quality analyser (Fig. 4.28)**
  This element allows us to study some power quality parameters, such us: the flicker P_{st} and the Total Harmonic Distortion (THD).

Figure 4.28: Power quality analyser.

4.6 Description of the No-Load and Load Test

Before starting the tests, all devices must be connected at the correct voltage.

1. DC motor: Before powering this element it is important to make sure that inductor and armature windings are without voltage. In case the armature winding is with voltage and the inductor winding is without it, an overspeed could be produced.

2. Torque and speed sensor: These elements will be connected to an external power source of 24 V_{dc}.

3. Wattmeter, oscilloscope, data logger and PC. Typical connection to the grid, 230 V_{ac}.

4. Inverter:

If the No-load test is going to be made, it is necessary that the inverter is disconnected.

But if the load test is going to be carried out, it is necessary that the inverter is connected to the grid. However, before connecting the inverter to the grid, it must be checked that the phase and neutral of the inverter match the phase and neutral of the grid. Otherwise, the system could be damaged.

Once verified that all elements work properly, the current flowing through the DC motor inductor has to be increased until its rated value. After reaching this value, the current flowing through the DC motor armature has to be gradually increased. In this way, the DC motor should start to turn the PMSM.

If the system turns properly, then the PMSM speed will be increased. Thus, the inverter voltage will also rise. When this voltage reaches a threshold value, the inverter will begin to work. In this moment the inverter will be able to power itself and we will be able to set up its software, as described above (Section 4.3). Using this software, some inverter internal parameters can be defined. Some of them are:

1. Connection type: COM or USB.
2. Inverter type: three phase or single phase.
3. Rated voltage and frequency of the grid.
4. Operating input voltage of the inverter.
5. Inverter MPCC. Entering an accurate MPCC is essential to obtain the SWT maximum efficiency (for each wind speed).

Once all the parameters of the software have been entered, it is time to perform the SWT No-load test and the SWT load test.

- **No-load Test**

  As defined above, this test should be done keeping the inverter disconnected from the grid, so that the SWT does not have connected any load.

  After taking this into account, the DC motor speed will be progressively increased, by means of rising the current flowing through the DC motor armature. In the

same way, the PMSM input torque will also increase. Each speed will be maintained the necessary time so that the wattmeter measurements stabilize. Once these measurements are steady, the data acquisition will be made by means of the wattmeter software. Finally, this process will be repeated for every speed, until the SWT rated speed is reached. In this way, the SWT No-load curve is obtained.

NOTE: This process could be automated. In this way, the software would automatically save the measurements, each certain interval of time. But this method has a big disadvantage. Many of the measurements are taken during the time intervals in which the parameters have not stabilized yet. Therefore, to obtain reliable data, all the inaccurate measurements will have to be deleted. On the other hand, the manual method ensures that data are accurate.

- **Load Test**

  The first step to perform this test is to connect the inverter to the grid, paying special attention to the phase-neutral sequence.

  Then, the rotation speed has to be increased (increasing the DC motor current) until the inverter starts to work and provide power to the grid. Once the inverter is working, it should be checked that the MPCC, which is entered in the inverter software, is correct. Otherwise, the MPCC must be modified, using the Aurora 6.0 KW software.

  Having checked these details, the DC motor speed must be reduced until the power injected by the inverter to the grid is close to zero watts. Thus, we will make sure that we cover all the range of powers (from zero watts to rated power).

  From here the test is identical to the No-Load test. The DC motor speed will be progressively increased, by means of rising the current flowing through the armature of the DC motor. In the same way, the PMSM input torque will also increase. Each speed will be maintained the necessary time so that the wattmeter measurements stabilize. Once these measurements are steady, the data acquisition will be made by means of the wattmeter software. Finally, this process will be repeated for every speed, until the SWT rated speed is reached. In this way, the SWT load curve is obtained.

  The location of the different elements can be seen in Fig. 4.29.

- **Additional tests**

  After the SWT basic tests have been performed, other tests will have to be made. These tests will be able to improve the SWT efficiency. In this way, several capacitor banks will be connected between the PMSM and the rectifier (Fig. 4.30).

  Once the capacitor bank is properly connected, the steps to follow will be the same as in the load test.

  It should be noted that MPCCs used in load tests without capacitors and the MPCCs used in load tests with capacitors are different. Therefore, each test will have its own MPCC that will have to be entered into the inverter software.

4.7 Electric diagram I

In this section you can see how the different elements were connected. In this case, the wattmeter measures the three-phase currents and voltages of the PMSM. Thus, their symmetry can be verified. Fig. 4.29 shows the setting used for tests with and without load.

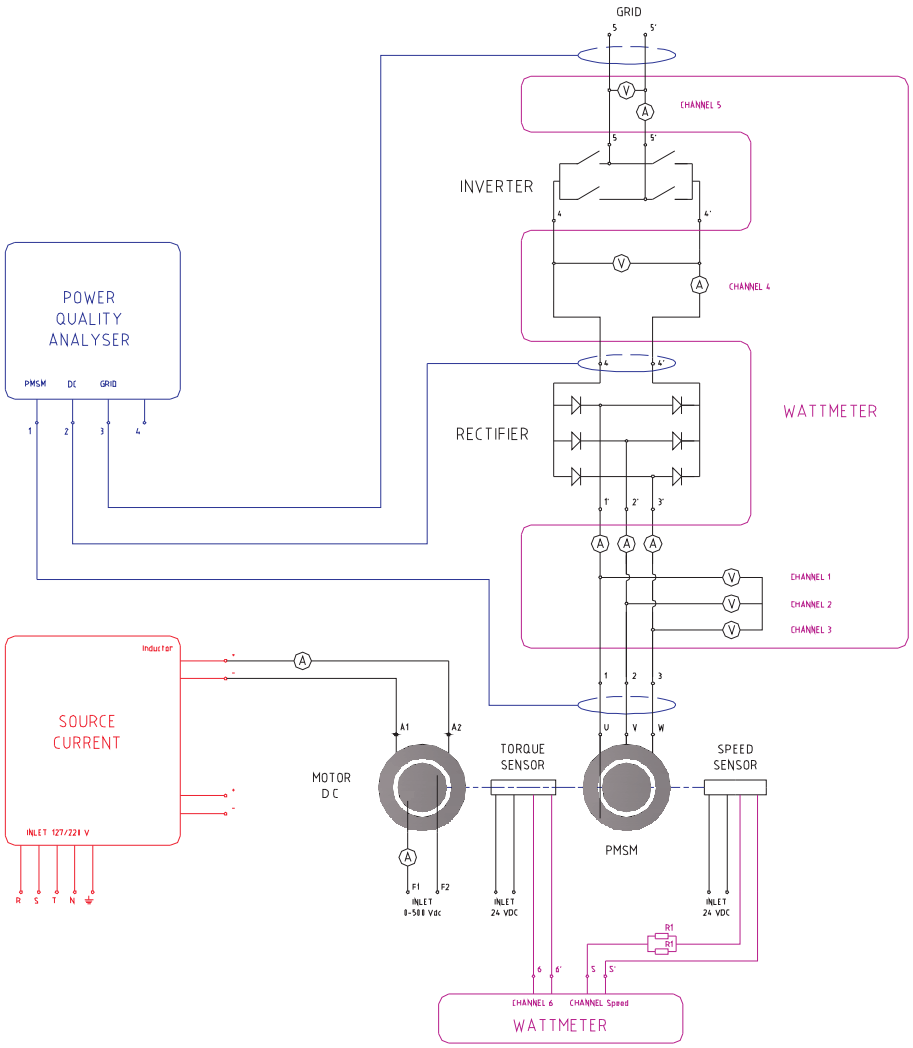

Figure 4.29: Block electric diagram I.

4.8 Electric diagram II

If a capacitor bank is connected, it is necessary to change the previous block diagram. The new one will be able to measure:

- Current and voltage in one phase of the PMSM.
- Current through the capacitor bank.
- Current through the rectifier.

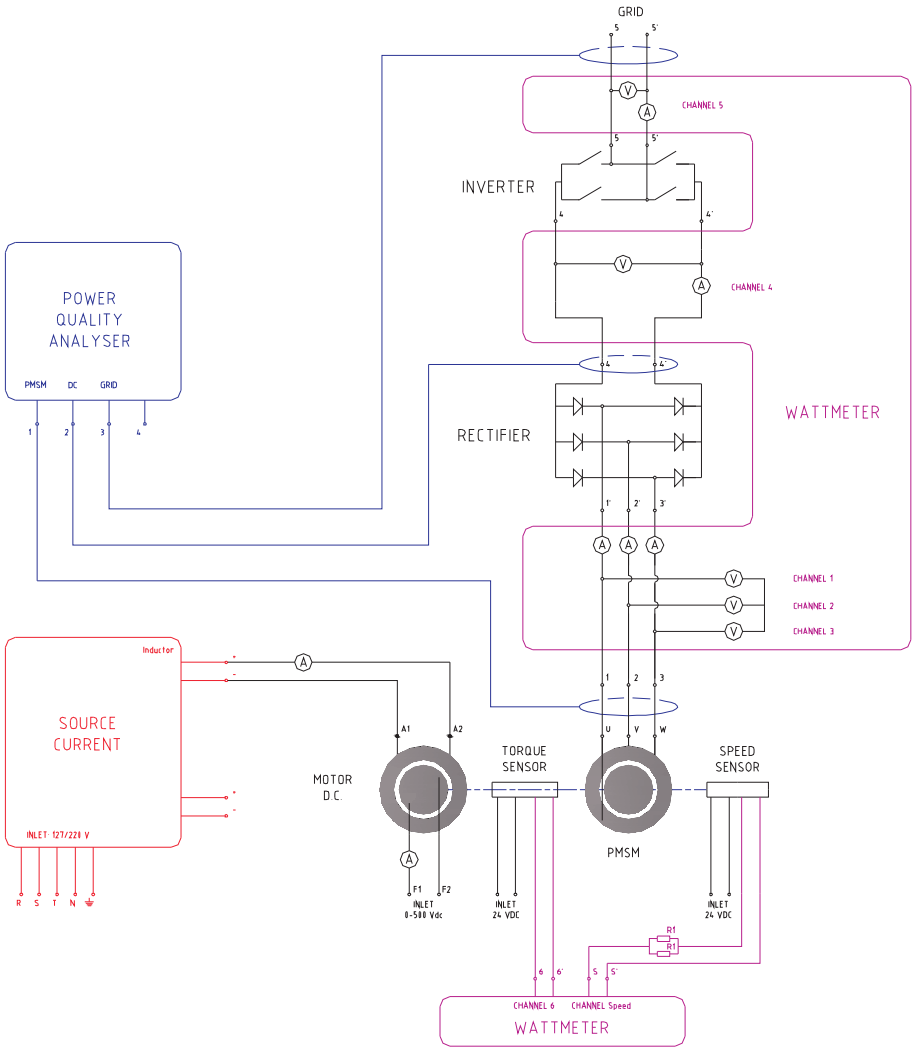

Figure 4.30: Block electric diagram II.

Note that for an accuracy measurement of the wattmeter, the PMSM winding neutral has to be used as reference. Fig. 4.30 shows the setting used for load tests with capacitors.

5

Discussion

5.1 Introduction

This section presents a methodology to optimize the efficiency of SWTs based on a PMSM. To test this methodology, it is necessary to create a model of the whole system (Sections 3.2 and 3.3). The Simulink software package was used for this purpose (10).

To achieve optimization of the system, two aspects are considered:

1. The aerodynamic factor: the Maximum Power Point Tracker (MPPT) (18) is calculated in order to extract the maximum energy from the wind (19). Using the MPPT and the SWT operating surfaces (obtained by means of Simulink model), the optimal relationship between the rectifier continuous voltage v_{dc} and the grid power P_{grid} can be determined. This relationship must be set in the inverter and it is known as the Maximum Power Characteristic Curve (MPCC).

2. The capacitor bank effect: when a capacitor bank is connected (Fig. 3.1) the armature reaction produces a magnetizing effect in the PMSM that is added to the magnetic field generated by the magnets. As a result, a higher voltage in the machine terminals is generated (20, 21).

   Then, before connecting a capacitor bank, some subjects have to be analysed. It must be verified that:

   - The current increment, that produces the capacitor bank, does not damage the PMSM windings. It should be noticed that if this methodology is used

in a commercial SWT, the winding wire diameter cannot be changed. Thus, this current increment must be limited.

- The magnetic saturation increment, that produces the capacitor bank, does not increase the iron losses too much.

In this way, for each wind speed u_h the capacitor bank that maximizes the power injected into the grid P_{grid}, will be calculated. But it should be noted that the placing of capacitors in the system changes its internal conditions. That is the reason why each capacitor bank value will have its own MPCC.

This methodology will be tested in a commercial 3.5 kW SWT with a PMSM, and the system improvements will be verified.

Finally, an economic study will be carried out in which the well-known Weibull Distribution (WD) will be employed (22).

5.2 Obtain MPPT and MTPT of a SWT

To be able to understand the calculation of MPCCs, you should firstly understand how the SWT operates. Thus, you will study the maximum power that can be extracted from the wind kinetic energy and the main characteristic parameters of the SWTs.

To perform this study it is necessary to start from the beginning, the wind. As it is known, the wind is made up of particles in motion. In this way, when these particles find in their path an element (SWT blades) that can rotate about a shaft (either horizontal or vertical), they make it rotate. And if this shaft has got an electrical machine, the electricity is generated.

The air mass before passing through the SWT has got a kinetic energy. This kinetic energy can be expressed according to Eq. (5.1).

$$E_c = \frac{1}{2} m\, u^2 \tag{5.1}$$

where E_c is the air kinetic energy [J], m is the air mass [kg] and u is the air velocity $[m/s]$.

The wind, in its path through SWT blades, suffers a decrease in its speed or what is the same a decrease in its kinetic energy. This lost kinetic energy is transformed, by means of the SWT blades, into mechanical energy. And the electrical generator transforms this mechanical energy in electrical energy (23).

To follow, a study of the air performance, when it passes through the SWT, will be made. This study let us obtain an expression to calculate the maximum mechanical power that can be extracted from the wind. For this analysis an air stream tube will be considered (see Fig. 5.1). This tube is formed by air lines in laminar regime, parallel to the wind and with an axial symmetry.

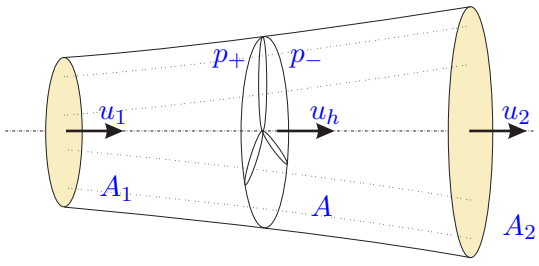

Figure 5.1: Airflow before and after wind turbine.

In the stream tube, it can be seen the following parameters:

u_1 Air velocity at inlet of tube [m/s].
u_2 Air velocity at outlet of tube [m/s].
u_h Air velocity in turbine $[m/s]$.
p_+ Air pressure before the turbine [Pa].
p_- Air pressure after the turbine [Pa].
A_1 Area at inlet of tube $[m^2]$.
A_2 Area at outlet of tube $[m^2]$.
A Area of tube in turbine $[m^2]$.

If it is considered the mechanical power P_w extracted from wind, as the loss of air kinetic energy due to its passage through the SWT, then it can be obtained:

$$P_w = \Delta E_c = E_{c1} - E_{c2} = \frac{1}{2} m u_1^2 - \frac{1}{2} m u_2^2 \tag{5.2}$$

$$P_w = \left(\rho u_h \frac{\pi d^2}{4}\right) \left(\frac{1}{2} u_1^2 - \frac{1}{2} u_2^2\right) \tag{5.3}$$

where,

E_{c1} Kinetic energy at inlet of tube [J].
E_{c2} Kinetic energy at outlet of tube [J].
ρ Air density $[Kg/m^3]$.
d Diameter of turbine blades [m].

Studying the Froudet's Theorem (23), it can be understood that the air average velocity in its passage through the stream tube is the arithmetic mean of u_1 and u_2. Thus:

$$u_h = \frac{u_1 + u_2}{2} \tag{5.4}$$

Eq. (5.4) can also be obtained, as follows:

- The air velocity at inlet of tube u_1.
- The air velocity, as it approaches the turbine, is modified. In this way, its value will be u_1 minus an axial induced velocity that it is known as u_a (see Fig. 5.1).

  $$u_a = a u_1 \tag{5.5}$$

  Consequently, it can be established that $u_h = u_1 - u_a$ or what is the same:

  $$u_h = u_1 (1 - a) \tag{5.6}$$

  Thus, the velocity u_2 will be:

  $$u_2 = u_1 (1 - 2a) \tag{5.7}$$

where a is the induced axial velocity coefficient, which is opposed to velocity u_1.

Thus, Eqs. (5.6), (5.7) and (5.3) yield the relation:

$$P_w = \left(\frac{1}{2}\frac{\pi\, d^2}{4}\rho\, u_1^3\right)(1-a)\left(1-(1-2\,a)^2\right) \tag{5.8}$$

The next step will be to derive Eq. (5.8) with respect to a and make it equal to zero. Then, the value of a, for which P_w is maximized, will be obtained.

$$\frac{\partial P_w}{\partial a} \Rightarrow a = \frac{1}{3} \tag{5.9}$$

Thus, if $a = \frac{1}{3}$ is replaced in Eq. (5.8), it is obtained:

$$P_{w_{max}} = \frac{16}{27}\left(\frac{1}{2}\frac{\pi\, d^2}{4}\rho\, u_1^3\right) \tag{5.10}$$

Eq. (5.10) is usually expressed in a dimensionless way as the power coefficient C_p:

$$C_p = \frac{P_w}{\left(\frac{1}{2}\frac{\pi\, d^2}{4}\rho\, u_1^3\right)} \tag{5.11}$$

Thus, C_p represents the percentage of power extracted from the wind kinetic energy. The maximum value that C_p might take is $\frac{16}{27} = 0.593$. This value is called *Betz limit* (24) and provides the maximum mechanical power P_w that can be extracted from wind kinetic energy, regardless of SWT type. In summary, no SWT will be able to extract more wind power than the Betz limit states.

The *Betz limit* is an upper limit. But it does not mean that all SWTs can extract that upper limit. In fact, the Betz limit does not take into account several parameters that reduce this upper limit. Some of these parameters are:

- Aerodynamic roughness of blades due to their aging.
- Lost energy due to wake generated by the rotation.
- Air properties.
- Interference of blades.
- Direction of SWT, Ψ.
- Pitch angle, β.

- SWT shape.

In this way, C_p will be function of the: SWT diameter, wind speed, air density, air viscosity, blade roughness, SWT shape, SWT rotation speed and SWT angles.

Of all these parameters, the viscosity and the roughness can be initially ignored due to their small influence on the final results. The SWT orientation can be also ignored because the SWT usually is orientated in the wind direction. Furthermore, if you have a SWT specific shape, it can also be assumed that C_p does not depend on it.

Thus, it is concluded that for this study C_p will be function of the: diameter d, wind speed u_h, SWT rotation speed ω and pitch angle β.

$$C_p = f(d, u_h, \omega, \beta) \tag{5.12}$$

Taking all this into account it seems logical to think in a coefficient that includes all these parameters. This coefficient is the *Tip Speed Ratio* λ, and it is defined as:

$$\lambda = \frac{Speed\,of\,rotor\,tip}{Wind\,speed} = \frac{\frac{\omega d}{2}}{u_h} \tag{5.13}$$

Fig. 5.2 shows an example of the relationship $C_p(\lambda)$, for different values of β. Paying close attention to this figure, it can be seen that the maximum value of C_p is close to 0.4 and not to 0.593, as predicted by the Betz limit. This difference is due to the parameters that were not taken into account when the Betz limit was calculated, such as: shape, interference of blades, etc.

In addition, that figure also shows that for each value of β there is a value of λ that maximizes C_p. It is important to understand this fact because MPCCs will be always defined in order to optimize the SWT electrical generation (working with the maximum value of C_p).

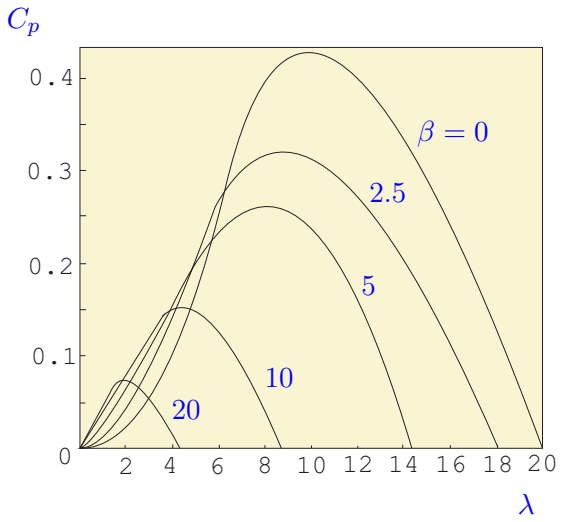

Figure 5.2: Typical family of curves $C_p(\lambda)$ for various values of β. Adapted from (23).

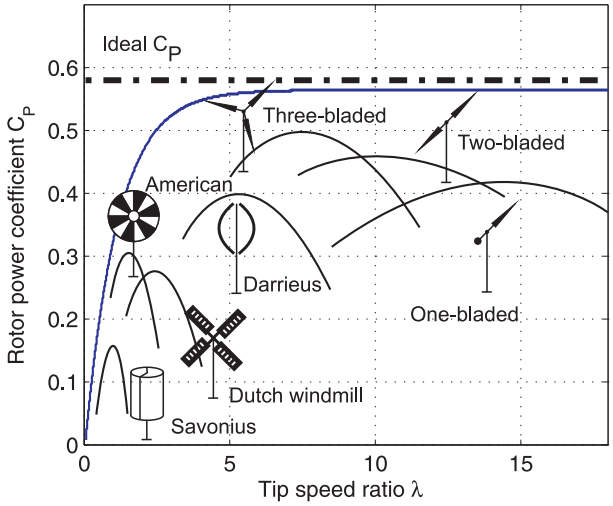

Figure 5.3: Typical family of curves $C_p(\lambda)$ for different SWT types.

Other point to consider might be the influence of the SWT type in the relationship $C_p(\lambda)$ (see Fig. 5.3). This figure lets us identify the families of turbines that produce a higher value of C_p and consequently a higher efficiency. These families are: one-bladed, two-bladed and three-blades. That is the reason why the worldwide major manufacturers usually produce those kinds of turbines.

Having explained all this, a simple study of forces occurring in SWT blades will be developed. In Fig. 5.4(a) you can see that when the wind $\mathbf{u_h}$ hits a blade, a compo-

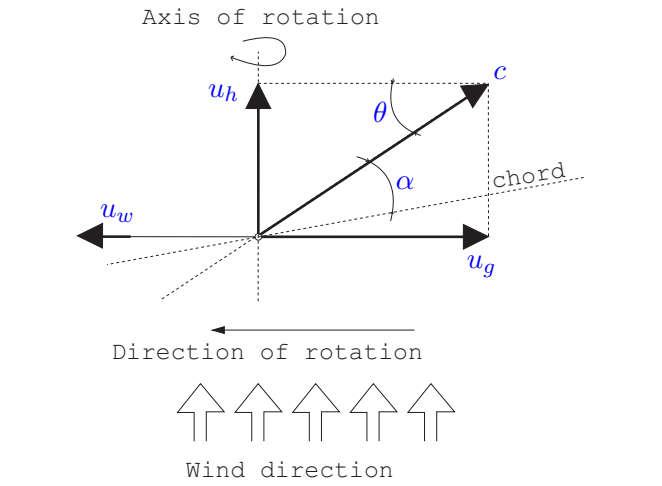

(a) Velocities

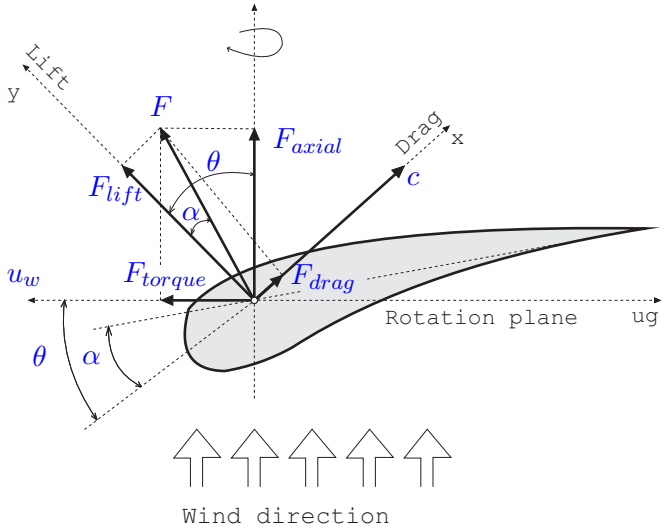

(b) Forces

Figure 5.4: Velocities and forces acting on a blade of a horizontal SWT.

nent $\mathbf{u_g}$ appears due to the displacement or blade rotation. The addition of these two components will result in the vector $\mathbf{c}$.

On one hand the wind component $\mathbf{u_h}$ will allow us to calculate the forces that arise on the blade at the turbine input. On the other hand, the component $\mathbf{c}$ will allow us to do the same, but in this case, at the turbine output. Moreover, three angles will be defined:

- α: Angle between the blade chord and $\mathbf{c}$, called *Attack angle*.

- θ: Angle between the rotation plane and $\mathbf{c}$.
- β: Angle between the blade chord and the rotation plane, called *Pitch angle*.

The resultant force $\mathbf{F}$ (in its aerodynamic center) will be used to calculate the SWT speed. That force will be obtained either with the SWT input wind $\mathbf{u_h}$ or with the SWT output wind $\mathbf{c}$:

- Forces at the SWT input (see Fig. 5.4(b)): In this case the wind, that hits the blade at the input $\mathbf{u_h}$, produces two kinds of forces. One in the direction of rotation axis $\mathbf{F_{axial}}$ and another in the perpendicular direction. This last one causes the SWT rotation $\mathbf{F_{torque}}$. Adding $\mathbf{F_{axial}}$ and $\mathbf{F_{torque}}$ the resultant force $\mathbf{F}$ will be obtained.

- Forces at the SWT output (see Fig. 5.4(b)): In this other case, if the vector $\mathbf{F}$ is decomposed according to the direction of the apparent velocity $\mathbf{c}$ and its perpendicular, the drag force $\mathbf{F_{drag}}$ and the lift force $\mathbf{F_{lift}}$ will be obtained. The latter two forces are usually associated in a parameter, called L/D. Where L is the lift force $\mathbf{F_{lift}}$ and D is the drag force $\mathbf{F_{drag}}$.

  This parameter gives an idea of whether the blades are well designed or not. On one hand, the lower the value of L/D is, the greater the influence of $\mathbf{F_{drag}}$ will be and the lower the blade speed $\mathbf{u_w}$ will be. And on the other hand, the higher the value of L/D is, the greater the influence of $\mathbf{F_{lift}}$ will be and the higher the blade speed $\mathbf{u_w}$ will be.

Eq. (5.14) allows us to calculate an initial value of C_p. This relation assumes that C_p is depending on λ, L/D and N (number of SWT blades). This equation is worldwide known as *Correlation of Wilson (1976)* (25).

$$C_p = \frac{16}{27}\frac{\lambda}{\lambda + \frac{1.32+(\frac{\lambda-8}{20})^2}{N^{2/3}}} - 0.57\frac{\lambda^2}{\frac{L}{D}(\lambda + \frac{1}{2N})} \tag{5.14}$$

Although the Eq. (5.14) is an expression that does not take into account many parameters, it will help us to achieve an initial power coefficient C_p. Once C_p is calculated, it will have to be reduced by means of a percentage. This reduction will help us to get a value of C_p which takes into account the rest of the parameters that were initially ignored. Thus, a value closer to the real one can be obtained.

Fig. 5.5 shows an example obtained using the Eq. (5.14), assuming $N = 3$. In the figure it can be clearly seen, as it had been previously deduced from the study of wind forces, that higher values of L/D produce higher power coefficients C_p and therefore, higher mechanical powers P_w.

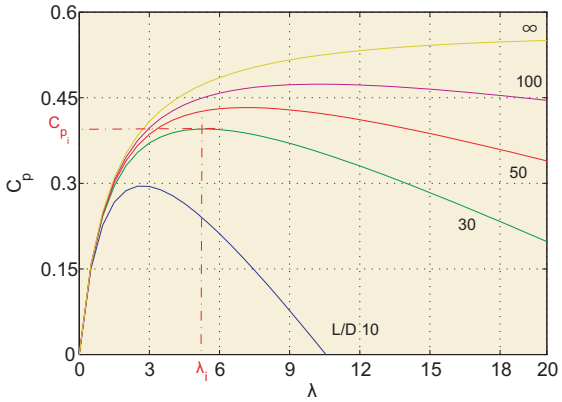

Figure 5.5: C_p vs. λ for several values of L/D.

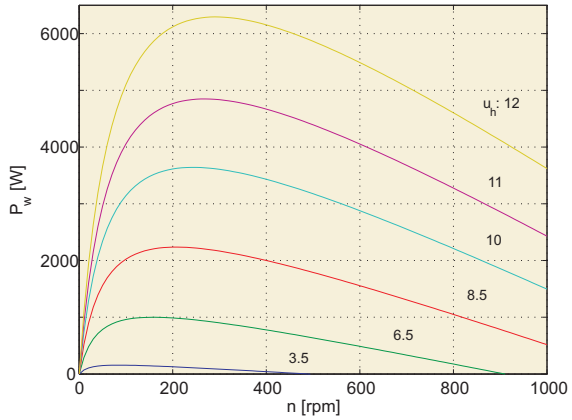

Figure 5.6: P_w vs. n for various wind speeds u_h and assuming $L/D = 30$.

During the design of the SWT blades, you will have to make sure that the combination of the parameters λ and L/D produces a maximum value of C_p. That is the reason why, a constant relation L/D along the whole blade is searched for. Therefore, it is easy to understand that each SWT will have its own relation L/D.

Eqs. (5.11) and (5.14) yield the relation,

$$P_w = \left(\frac{1}{2}\frac{\pi\, d^2}{4}\rho\, u_1^3\right)\left(\frac{16}{27}\frac{\lambda}{\lambda + \frac{1.32+(\frac{\lambda-8}{20})^2}{N^{2/3}}} - 0.57\frac{\lambda^2}{\frac{L}{D}(\lambda+\frac{1}{2N})}\right) \tag{5.15}$$

Using Eq. (5.15), it can be obtained the value of P_w, for:

- Constant values of: d, ρ and L/D.
- Different values of: n and u_h

In the example of Fig. 5.6 it can be seen the relationship $P_w(n)$, for various wind speeds u_h. Paying close attention to this figure and assuming a constant wind speed u_h, two conclusions can be drawn:

1. When the SWT rotation speed n increases, the mechanical power in the shaft P_w also does it.
2. P_w increases up to a maximum value from which decreases.

Having explained this, it is easy to understand that if any change was introduced in the SWT, it should be studied whether this modification varies the value of λ or not. Analysing Fig. 5.5 and assuming $L/D = 30$, you can observe that for a value of $\lambda = \lambda_i$, the corresponding value C_{p_i} is maximum. Thus, if some parameter of which are mentioned above is modified, it is very likely that the value of λ also varies, either by moving left or right. Therefore, the increase or decrease of λ causes a reduction of the power coefficient C_p and with it a drop in mechanical power P_w.

SWTs are designed in order to maximize the value of C_p. In this way, if any change is introduced into the system, it is important to verify that the tip speed ratio λ remains constant. For this reason, all MPCCs that will be entered in the inverter software (Section 4.3) are calculated in order to ensure a specific constant value of λ_i.

To get this value of λ_i it is required that for all wind speeds u_{h_i}, the SWT turns at a specific speed $n_{u_{h_i}}$. In other words, to get a maximum mechanical power P_{w_i}, it will be necessary that:

- The value of λ_i is constant.

- The value of λ_i provides the maximum power coefficient C_{p_i} (see example in Fig. 5.5). The example of Fig. 5.7(a) shows the maximums of P_w for every wind speed u_h (highlighted points). Therefore, if a maximum mechanical power P_{w_i} wants to be obtained for a specific wind speed u_{h_i}, it will be necessary to turn the SWT to a particular rotation speed n_i.

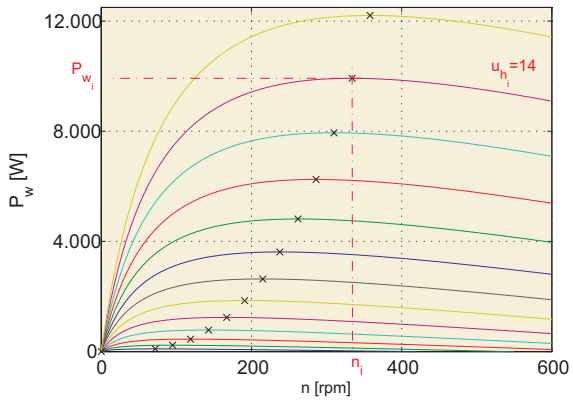

(a) P_w vs. n for several values of u_h.

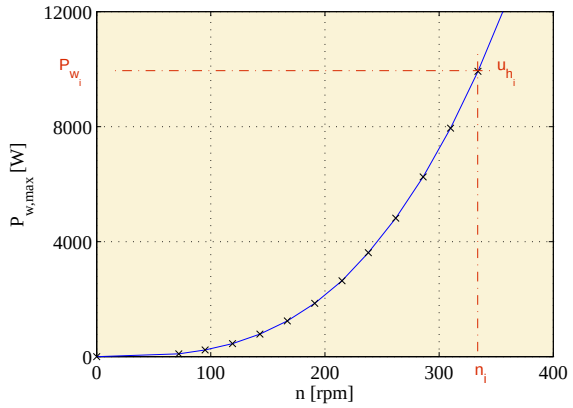

(b) Curve created with the maximums of P_w.

Figure 5.7: Maximum Power Point Tracker (MPPT), assuming a $L/D = 30$.

If all these maximums are plotted in a new curve, the relationship $P_{w_{max}}(n)$ is obtained (see Fig. 5.7(b)). This curve is known as the MPPT.

Fig. 5.7(b) has the special characteristic that all its points provide a maximum value of P_w and consequently a maximum value of C_p. That is the reason why, all the points have associated a constant value of λ.

Moreover considering the Eq. (4.1), the optimal relationship between T_w and n can be also obtained. It will be known as Maximum Torque Point Tracker (MTPT) (see example in Fig. 5.8).

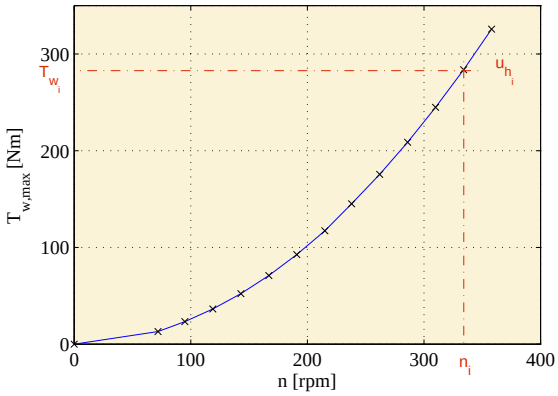

Figure 5.8: Maximum Torque Point Tracker (MTPT), assuming a $L/D = 30$.

5.3 Capacitor banks in a SWT

As it is known, if the electrical machine is working in the No-load test, it provides a rated voltage v_o at the output of the machine. Then, if an electrical load is connected at the machine output, the voltage v_o is reduced. This reduction is due to the emergence of a current in the armature winding that generates a voltage drop in that winding. Moreover, it also produces a magnetomotive force which reacts with the magnetomotive force generated by the inductor. In this way, the air-gap magnetic flux is modified (21).

Depending on the type of load that is connected to the output of PMSM, this effect may vary.

On one hand, if an inductive load is connected at the PMSM output, then the magnetomotive force caused by the armature reaction goes against the magnetomotive force caused by the inductor. This effect is known as the demagnetizing effect (see Fig. 5.9).

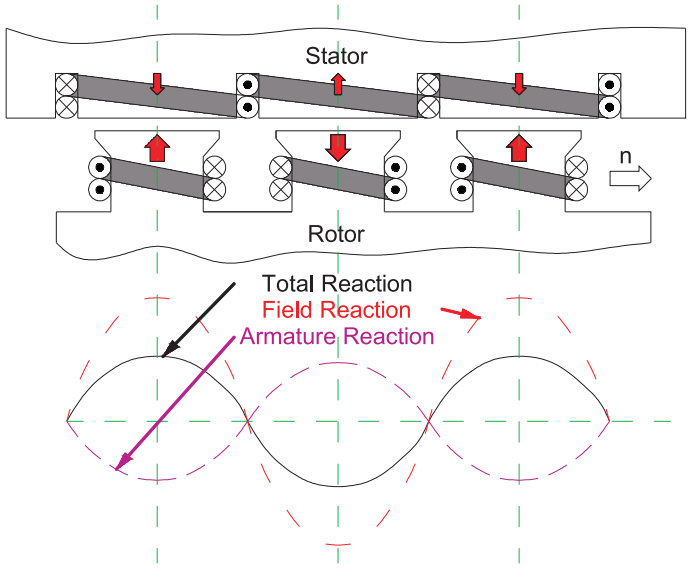

Figure 5.9: Magnetic field behaviour inside an electrical generator, connecting an inductive load.

On the other hand, if a capacitive load is connected to the PMSM output, the opposite happens. The magnetomotive force caused by the armature reaction is additive to the magnetomotive force caused by the inductor. This effect is known as magnetizing effect (see Fig. 5.10).

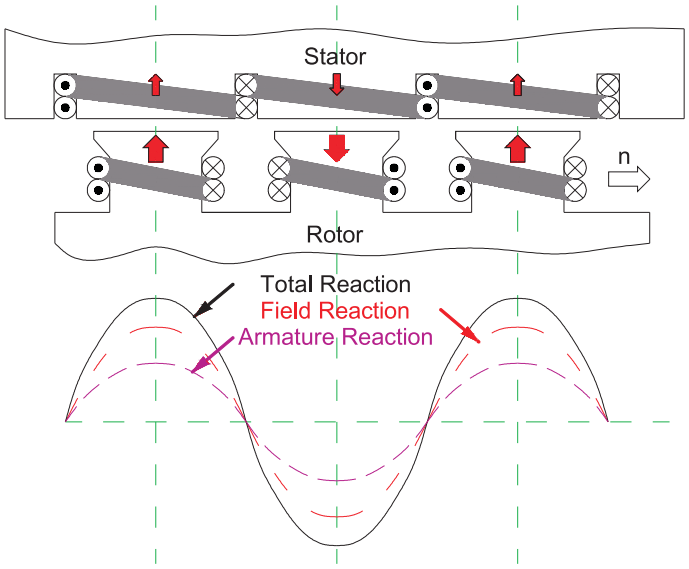

Figure 5.10: Magnetic field behaviour inside an electrical generator, connecting a capacity load.

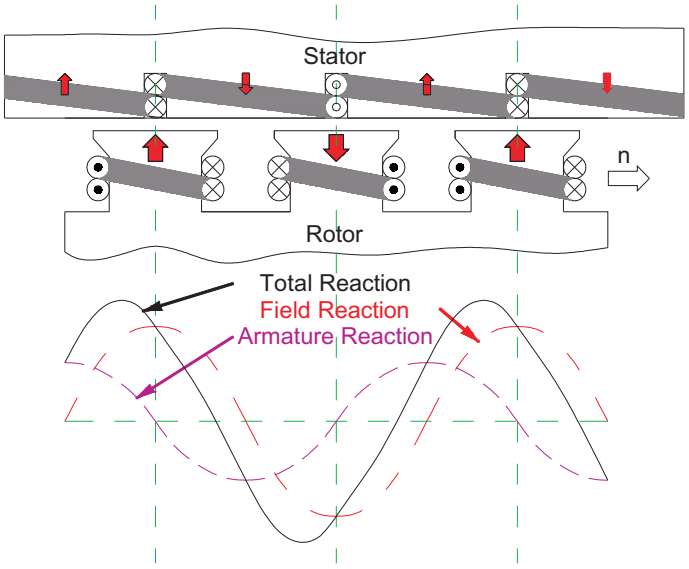

Figure 5.11: Magnetic field behaviour inside an electrical generator, connecting a resistive load.

In addition, if a resistive load is connected to the PMSM output, an intermediate effect will occur. In some moments, the magnetomotive force caused by the armature reaction is additive to the magnetomotive force caused by the inductor and in others, the

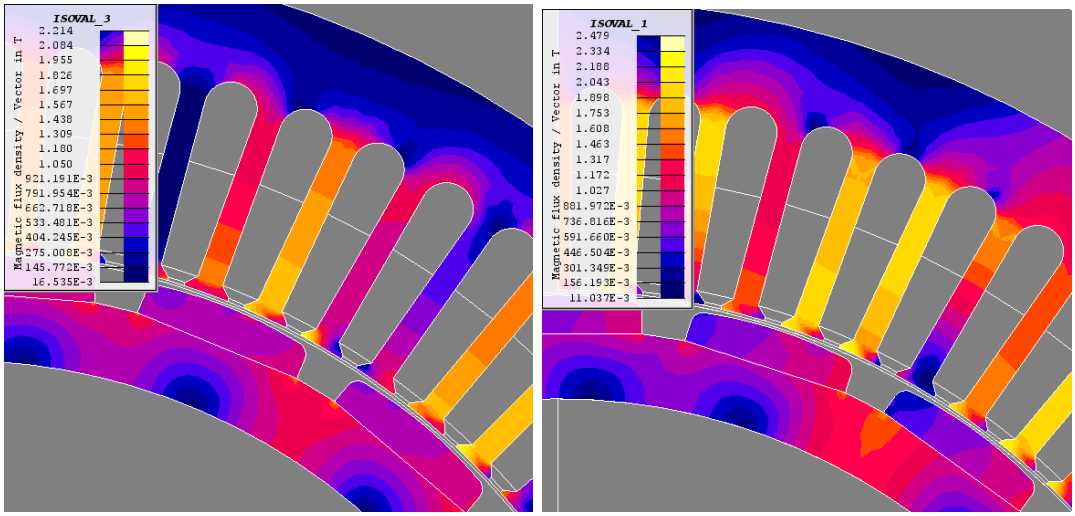

(a) Without capacitor banks.

(b) With capacitor banks of 110 μF (delta connection).

Figure 5.12: Comparison of magnetic flux density in the models: with and without capacitor bank.

magnetomotive force caused by the armature reaction goes against the magnetomotive force caused by the inductor. In this case, the variation of the magnetic field inside the electrical machine can be seen in Fig. 5.11.

Thus, taking all this into account, an increase in the PMSM magnetic field can be obtained by connecting a capacitor bank in the PMSM output.

The FEM model, described in Section 3.3, will help us to understand the magnetizing effect produced by the capacitor bank in the PMSM. Fig. 5.12(a) shows the PMSM magnetic flux when the capacitor bank is not connected and Fig. 5.12(b) shows the magnetic flux when a capacitor bank of 110 μF is connected. If both figures are compared, it can be seen the magnetizing effect.

The FEM model was also used to see the phase difference, that occurs on a PMSM, between the current $i_{r,s,t}$ and the voltage $v_{r,s,t}$ due to the connection of various capacitor banks. The values of the capacitor banks that were simulated are: 0, 16, 50, 80, 110 and 1000 μF, assuming a constant speed of 150 rpm.

In Fig. 5.13 can be observed that if the capacity value is increased, then the phase difference between the current and the voltage also increases. As explained previously, this phase difference generates a magnetizing effect on the PMSM and increases the

voltage v_o.

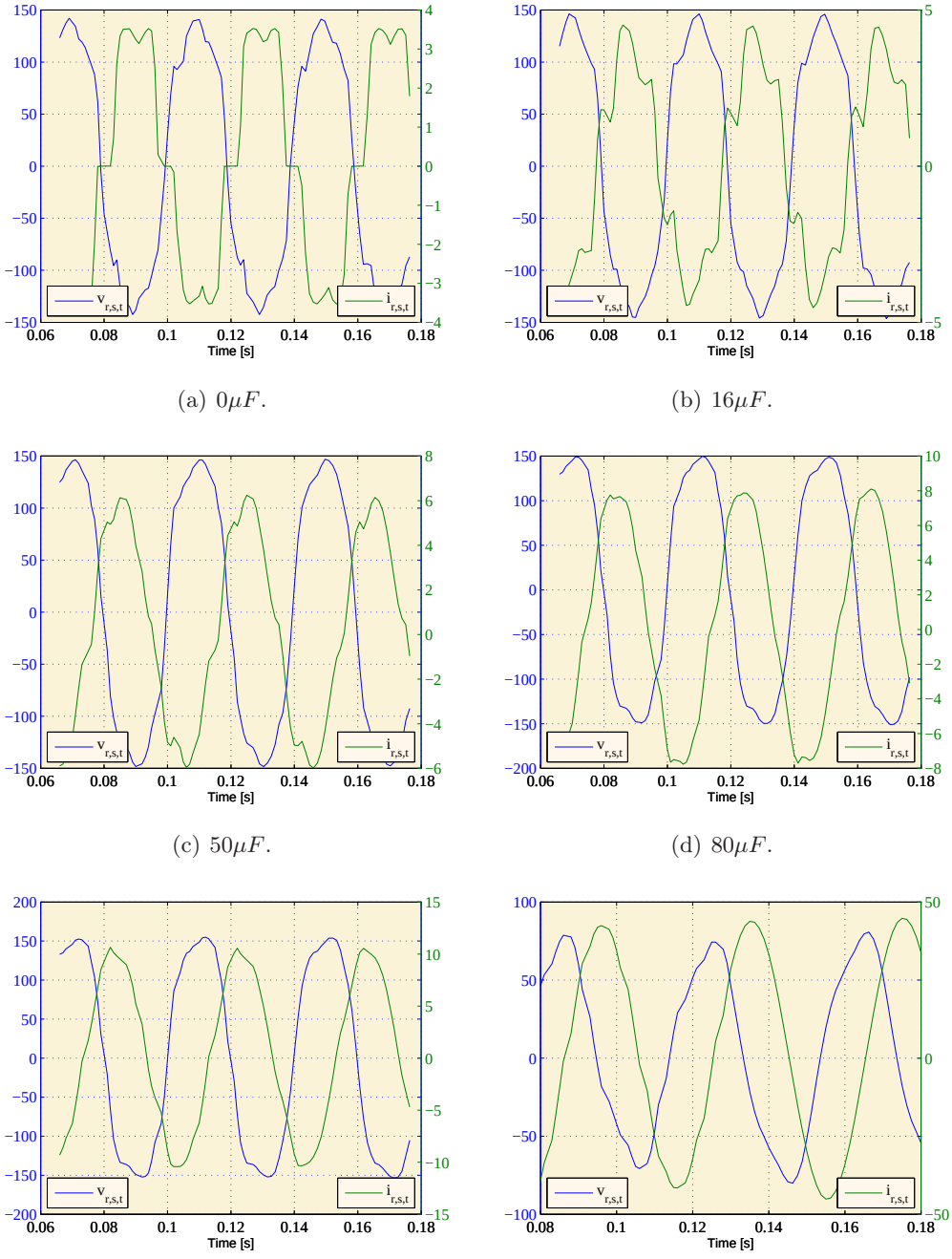

(a) $0\mu F$. (b) $16\mu F$.

(c) $50\mu F$. (d) $80\mu F$.

(e) $110\mu F$. (f) $1000\mu F$.

Figure 5.13: Phase difference between $v_{r,s,t}$ and $i_{r,s,t}$ for different capacities, assuming a speed of 150 rpm.

In addition, it can also be seen that if we increase the capacity values, then the waveforms of voltage and current are less distorted.

5.4 Methodology for calculation of the optimal capacitor bank and the MPCCs

Fig. 5.15 presents the flowchart for calculating the optimal capacitor bank and associated MPCC. The steps of the methodology are:

Step 1: Perform several tests on the SWT. At a minimum, a no-load test and a rated load test should be carried out.

Step 2: Define a system model.

Adjust model parameters (L_e and R_e) by comparing simulation results with those obtained in Step 1. Thus, a reliable model of the system can be defined.

Step 3: Calculate the MTPT to extract the maximum power of the wind (see Section 5.2).

Using the SWT rated parameters and Eqs. (4.1) and (5.11), the optimal relationships $P_w(n)$ and $T_w(n)$ can be obtained, see Fig. 5.7 and Fig. 5.8.

Note that the MTPT must remain unchanged for every value of the variable resistor R. Therefore, MTPT in 3D can be represented as a parallel surface to axis R, Fig. 5.14.

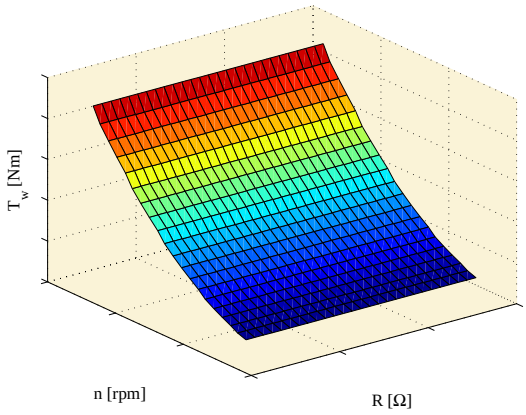

Figure 5.14: MTPT in 3D.

Step 4: Calculate a capacity range [C_i-C_k] which contains the optimal capacitor C.

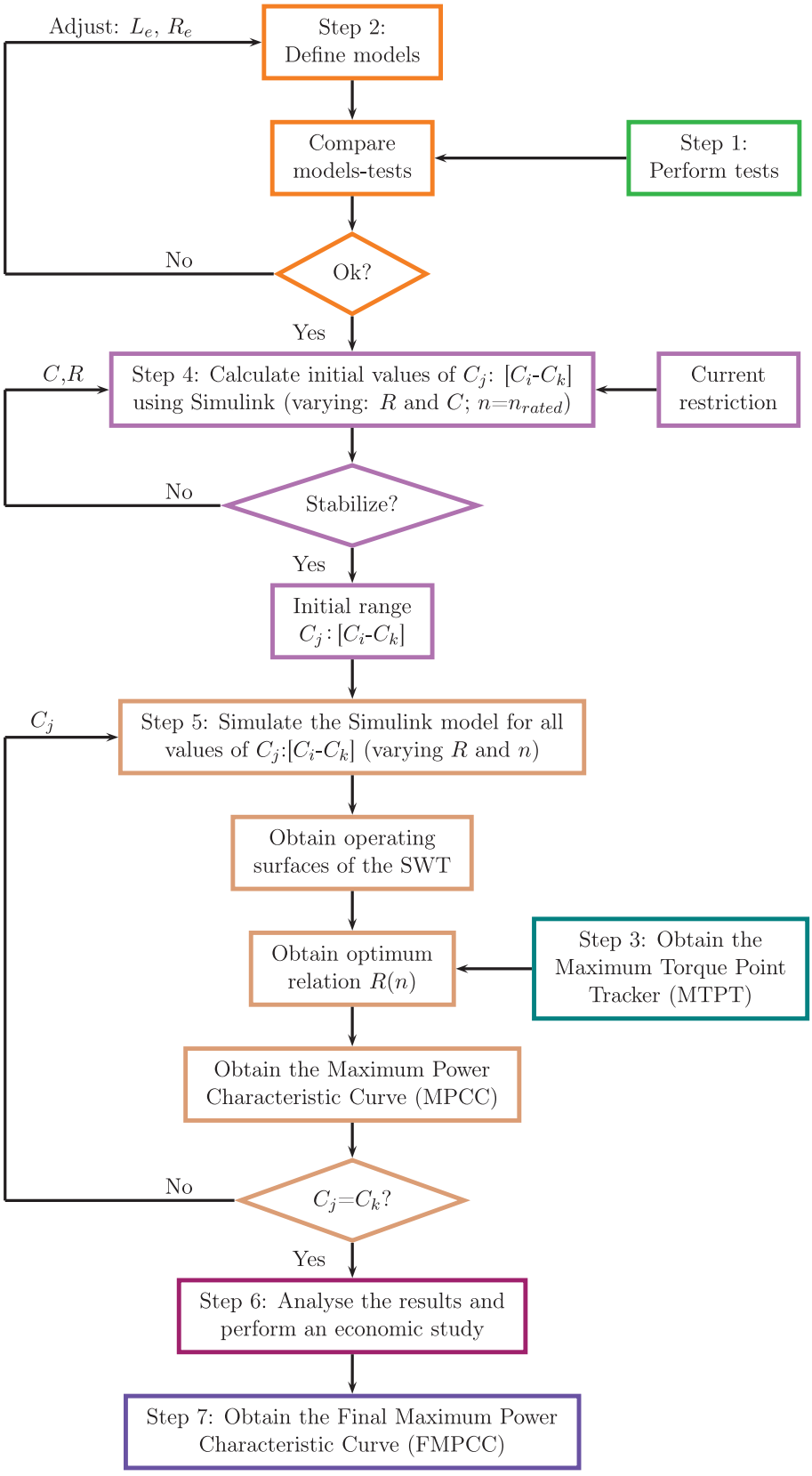

Figure 5.15: Flowchart of the methodology.

In order to find this range, a simulation will be performed varying R and C for the SWT rated speed using Simulink (see Section 3.2). The initial ranges of R and C must be wide enough to effectively analyse the SWT performance.

Fig. 5.16 indicates that by increasing the capacity C for each value of R, the power injected to the grid P_{grid} increases up to a maximum capacity value C_{max}, from which point P_{grid} decreases. Thus, the value C_{max} that maximizes the P_{grid} is obtained.

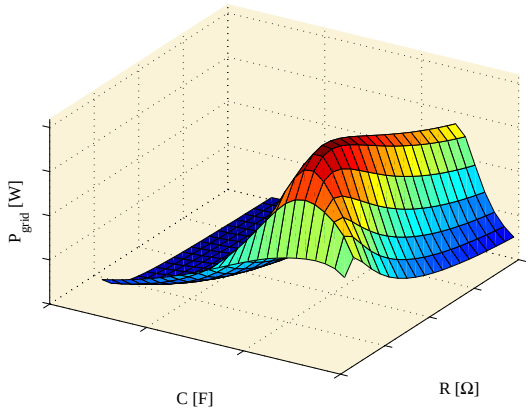

Figure 5.16: Grid Power P_{grid} vs. resistor R and capacity C for the rated speed n_r.

However, the value of C_{max} must be controlled because it could also increase the current $i_{r,s,t}$ flowing into the PMSM windings and thereby cause damage. Therefore, it is important to know the winding wire diameter to determine the maximum current $i_{r,max}$ that can flow through the winding.

Once the value of $i_{r,max}$ is known, the capacity range [C_i-C_k] can be obtained by means of drawing a perpendicular surface to the axis $i_{r,s,t}$ (see an example in Fig. 5.17(a)).

By representing the intersection of both surfaces on the plane C-R (Fig. 5.17(b)), the capacity values that might be connected, for different values of the resistor R, can be determined. In this way, the current value that could damage the PMSM will not be reached. So, the capacity range [C_i-C_k] is determined.

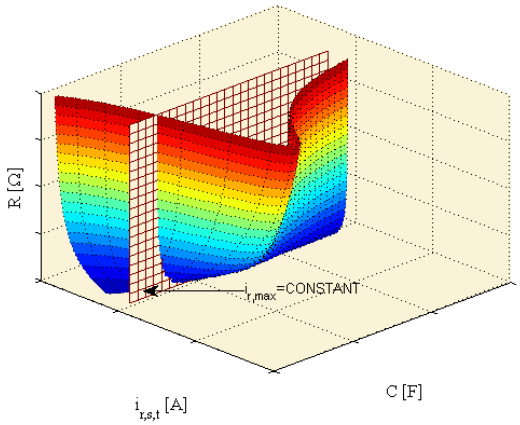

(a) Winding current i_r vs. resistor R and capacity C.

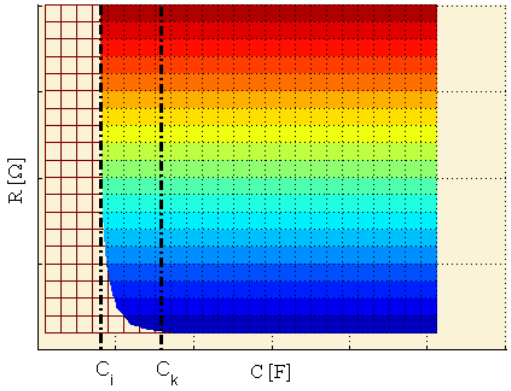

(b) Capacity C vs. variable resistor R.

Figure 5.17: Relationship $R(C)$ not exceeding the restriction of $i_{r,max}$ and for the SWT rated speed.

Step 5: Obtain MPCCs for several values of C.

Perform simulations, varying n and R, for constant values of C within the range [C_i-C_k]. It should be borne in mind that the more values of C you test, the more accurate the results will be. For each value of C, the following steps need to be performed:

- Step 5.1: Use the system model to determine the SWT operating surface $T_w(R, n)$. Then, obtain the intersection of that surface with the MTPT (see Fig. 5.18(a)). Thus, the relationship $R(n)$ for maximum mechanical power extraction from wind

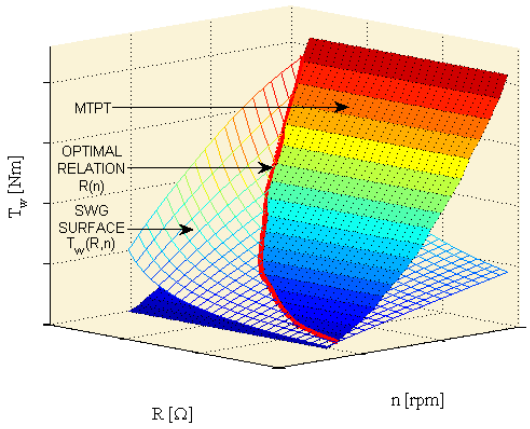

(a) 3D intersection.

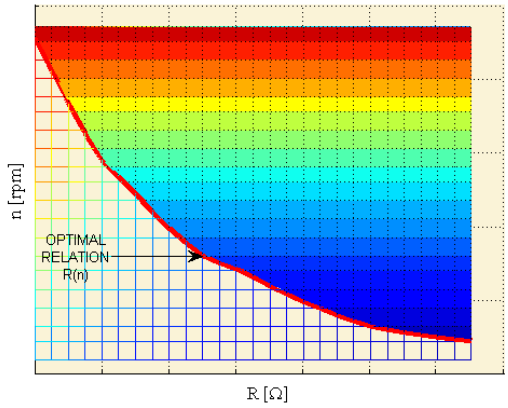

(b) Optimal relationship $R(n)$.

Figure 5.18: Intersection between the MTPT and the SWT operating surface $T_w(R, n)$.

is given (see Fig. 5.18(b)).

- Step 5.2: Project the optimal relationship $R(n)$ perpendicular to the R-n plane (Fig. 5.19).

- Step 5.3: Use the model to determine the SWT operating surfaces $P_{grid}(R, n)$ (see example in Fig. 5.19) and $v_{dc}(R, n)$ (see example in Fig. 5.20). After that, derive the intersection of those SWT surfaces with the surface obtained in Step 5.2. In this way, the optimal relationships $P_{grid}(n)$ and $v_{dc}(n)$ will be determined.

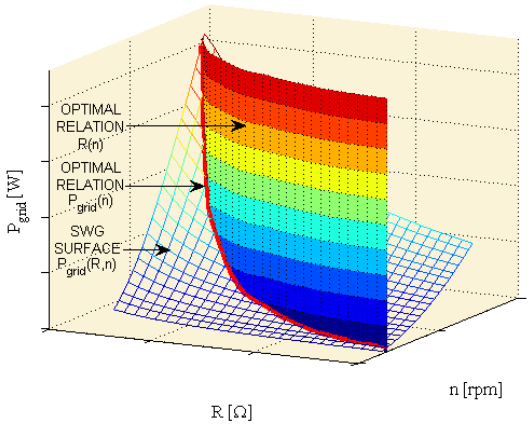

Figure 5.19: Intersection between the optimal relationship $R(n)$ and the SWT operating surface $P_{grid}(R, n)$.

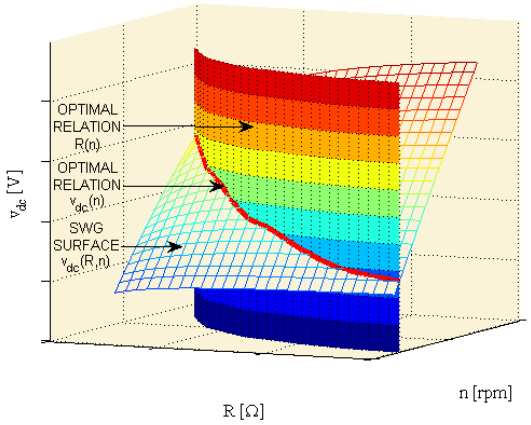

Figure 5.20: Intersection between the optimal relationship $R(n)$ and the SWT operating surface $v_{dc}(R, n)$.

- Step 5.4: Finally, joining the values of $P_{grid}(n)$ and v_{dc}(n), the optimal relationship $P_{grid}(v_{dc})$, also known as the MPCC, can be easily determined. See example in Fig. 5.21.

By repeating steps 5.1 to 5.4 for each value of C, the additional MPCCs can be obtained.

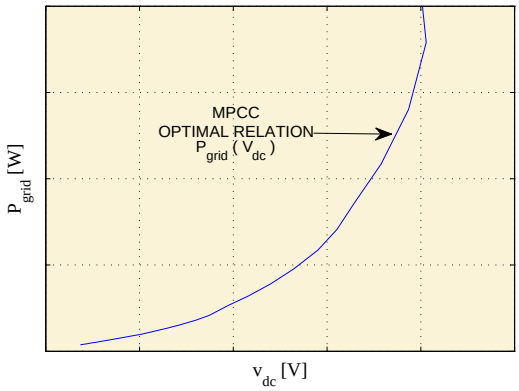

Figure 5.21: Maximum Power Characteristic Curve (MPCC): Grid power P_{grid} vs. rectifier DC voltage v_{dc}.

Step 6: Analyse the results and perform an economic study.

To perform the analysis, the well-known Weibull Distribution (WD) will be used (19, 22, 26). This distribution is defined as:

$$W(u_h) = \frac{K}{u_h}\left(\frac{u_h}{u_m}\right)^K e^{-\left(\frac{u_h}{u_m}\right)^K} \tag{5.16}$$

where K is the shape parameter of the WD, and u_m is the average wind speed.

Nevertheless, if this distribution is going to be used, certain features of the location where the SWT will be placed need to be known. The *National Renewable Energy Laboratory* (NREL) defines seven different *Wind Classes* (WCs). The WC is a function of the average wind speed u_m and the height at which the SWT will be located with respect to the ground (10 or 50 m) (27). These WCs can be seen in Table 5.1.

Fig. 5.22 represents the Weibull distribution (5.16) for a value of $K = 1.9$ and for average wind speeds listed in Table 5.1 (assuming a height of 10 m).

Table 5.1: Wind classification according to average speed. Adapted from (27).

Wind Class	u_m (10 m)	u_m (50 m)
1	0 - 4.4	0 - 5.6
2	4.4 - 5.1	5.6 - 6.4
3	5.1 - 5.6	6.4 - 7
4	5.6 - 6	7 - 7.5
5	6 - 6.4	7.5 - 8
6	6.4 - 7	8 - 8.8
7	7 - 9.4	8.8 - 11.9

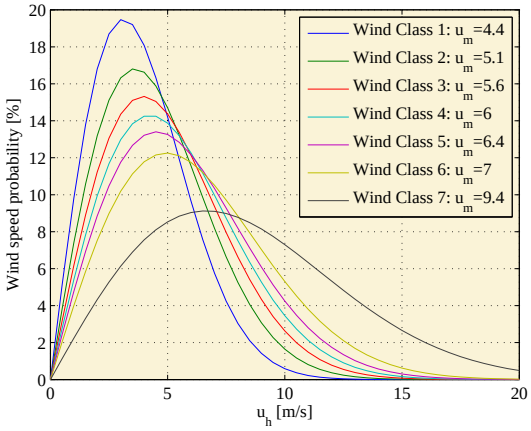

Figure 5.22: Weibull Distribution for different WCs and a height of 10 m.

To compare the results obtained with different values of C, five parameters will be used: $P_d(u_h)$, h_e, E_{tot}, $\Delta\eta$ and $\Delta€$.

1. $P_d(u_h)$ is the SWT power density and is defined as:

$$P_d(u_h) = W(u_h)\frac{P_{grid}(u_h)}{P_{rated}} \tag{5.17}$$

   where $P_{grid}(u_h)$ is the grid power for each wind speed u_h, and P_{rated} is the rated power of the SWT.

2. E_{tot} is the annual total energy that can be produced by the SWT. It is obtained

from the equation:

$$E_{tot} = 8760 \left[\frac{hours}{year}\right] \cdot \Sigma \left(W(u_h) P_{grid}(u_h)\right) \tag{5.18}$$

3. h_e is an indicative parameter which helps to determine the increment in hours per year for which the axis of the machine will supply power into the grid. This parameter is defined as:

$$h_e = \frac{E_{tot}}{P_{rated}} \tag{5.19}$$

4. $\Delta\eta$ represents the increment in annual total energy injected into the grid E_{tot} for different capacitor banks ($C = C_j$), as compared to the case without a capacitor bank ($C = 0$).

$$\Delta\eta = \frac{E_{tot,C=C_j} - E_{tot,C=0}}{E_{tot,C=0}} \tag{5.20}$$

5. $\Delta €$ represents the annual financial benefit obtained by using different capacitor banks ($C = C_j$), as compared to the case without a capacitor bank ($C = 0$). In the calculations, an energy cost of 0.17373 €/kWh is assumed (including electricity taxes).

$$\Delta € = \left(E_{tot,C=C_j} - E_{tot,C=0}\right) \cdot 0.17373 \left[\frac{€}{kWh}\right] \tag{5.21}$$

Step 7: Obtain the *Final Maximum Power Characteristic Curve* (FMPCC).

To determine the FMPCC it is necessary to calculate, for each wind speed u_h, the capacity C that supplies the maximum grid power P_{grid}. Thus, the optimal relationship $C(u_h)$ is calculated. The FMPCC will be made up of sections of the MPCCs that were obtained for different values of C.

5.5 Use of the methodology in a commercial SWT

The methodology and the test bedplate were used to optimize a commercial SWT whose rated parameters are:

- Number of blades: 3.
- Diameter: 4.2 m.
- PMSM Rated Power: 3500 W.
- Rated speed of the wind: 11 m/s.
- Power coefficient: 0.36.
- $L/D \simeq 30$.

Following the previously explained methodology, the results were as follows:

5.5.1 Step 1: SWT Tests

To adjust the models, several SWT tests were made. These tests were:

- SWT No-load test.
- SWT test, assuming a load of 31 Ω.
- SWT test, assuming a load of 75 Ω.
- SWT test, assuming a rated load.

5.5.1.1 SWT No-load test

To proceed with the performance of this test, the steps defined in Section 4.6 were followed. Once, all the electrical and the mechanical steps were made, the test was carried out. A brief summary of the results is presented below.

- Relationship $v_{dc}(n)$ (see Fig. 5.23).

- Relationship $v_{r,s,t}(n)$ (see Fig. 5.23).

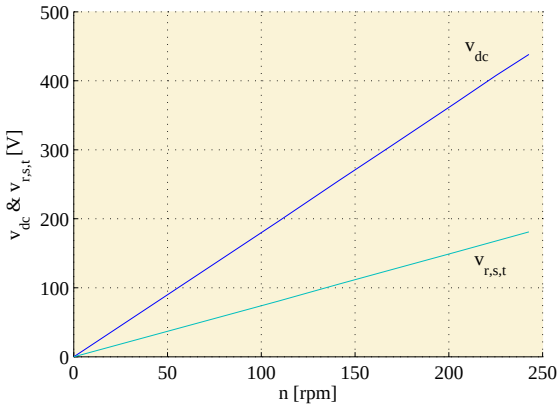

Figure 5.23: v_{dc} vs. n and $v_{r,s,t}$ vs. n, for a No-load test.

- Rectifier voltage waveform v_{dc}, assuming $n = 150\,rpm$ (see Fig. 5.24).
- PMSM voltage waveform $v_{r,s,t}$, assuming $n = 150\,rpm$ (see Fig. 5.24).

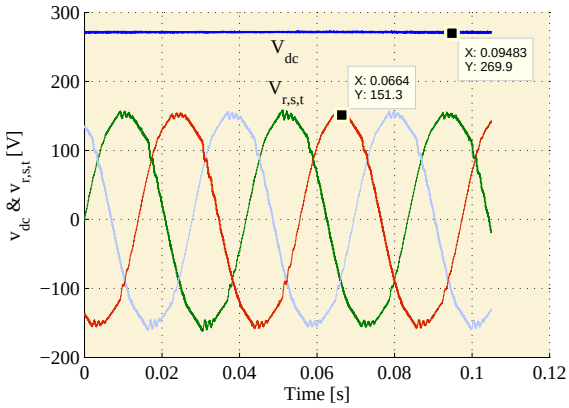

Figure 5.24: Voltage waveforms: v_{dc} and $v_{r,s,t}$, for a No-load test.

5.5.1.2 SWT test, assuming a load of 31 Ω

Below, some of the most characteristic curves of this test are shown.

- Relationship $v_{dc}(n)$ (see Fig. 5.25).
- Relationship $v_{r,s,t}(n)$ (see Fig. 5.25).

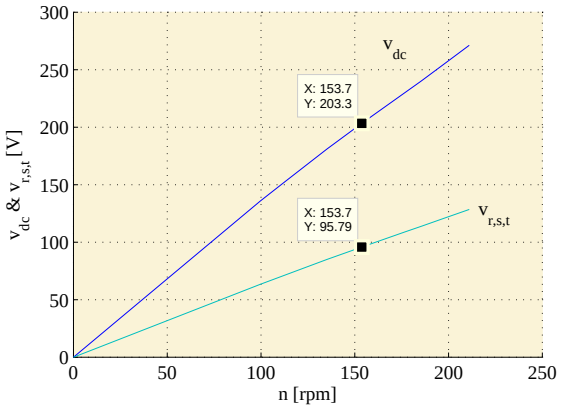

Figure 5.25: v_{dc} vs. n and $v_{r,s,t}$ vs. n, for $R = 31\ \Omega$.

- Relationship $i_{dc}(n)$ (see Fig. 5.26).

- Relationship $i_{r,s,t}(n)$ (see Fig. 5.26).

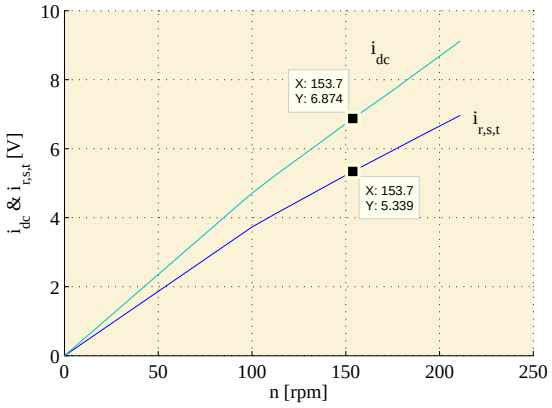

Figure 5.26: i_{dc} vs. n and $i_{r,s,t}$ vs. n, for $R = 31\ \Omega$.

- Rectifier voltage waveform v_{dc}, assuming $n = 150\,rpm$ (see Fig. 5.27).

- PMSM voltage waveform $v_{r,s,t}$, assuming $n = 150\,rpm$ (see Fig. 5.27).

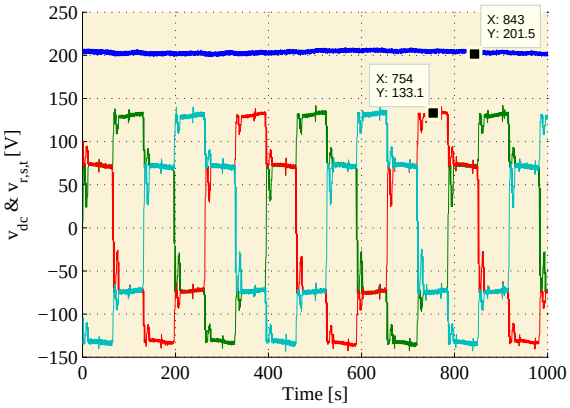

Figure 5.27: Voltage waveforms: v_{dc} and $v_{r,s,t}$, assuming a load $R = 31\ \Omega$ and $n = 150$ rpm.

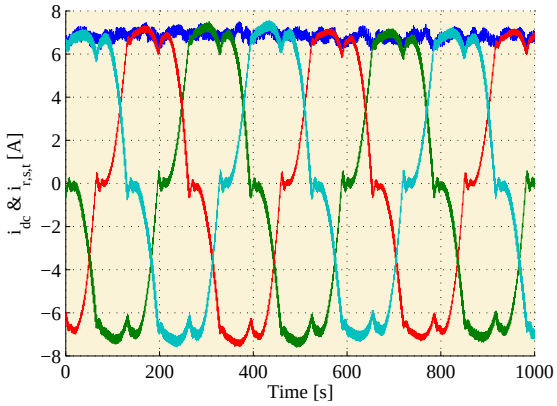

Figure 5.28: Current waveforms: i_{dc} and $i_{r,s,t}$, assuming a load $R = 31\ \Omega$ and $n = 150$ rpm.

- Rectifier current waveform i_{dc}, assuming $n = 150\,rpm$ (see Fig. 5.28).
- PMSM current waveform $i_{r,s,t}$, assuming $n = 150\,rpm$ (see Fig. 5.28).

Once voltage and current values are measured, a study of the efficiency of the whole system (PMSM, rectifier and inverter) will be carried out. To get these efficiencies the six channel wattmeter will be used (Fig. 4.21).

Fig. 5.29 shows active power in each element of the system.

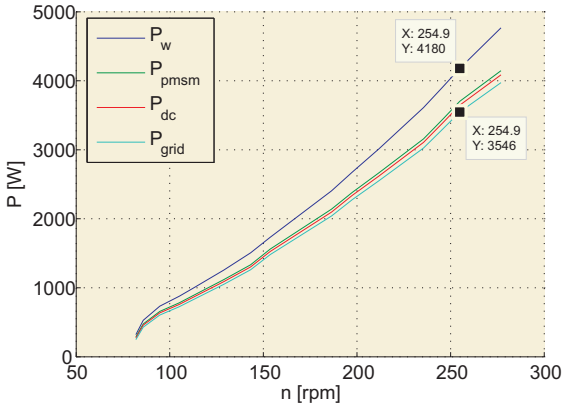

Figure 5.29: SWT efficiency study, assuming a load $R = 31\ \Omega$.

Table 5.2 illustrates the efficiency values for several rotation speeds.

Table 5.2: Efficiency comparison of all the SWT components, assuming a load $R = 31\ \Omega$.

$n[rpm]$	η [%]			
	η_{pmsm}	η_{rect}	η_{inv}	η_{SWT}
80	10.5	5.0	8.5	22.0
85	10.5	3.8	6.3	19.0
95	10.5	3.2	5.0	17.5
105	10.9	3.0	4.3	17.4
130	11.0	2.5	3.5	16.3
155	10.9	2.2	2.9	14.4
200	10.9	1.8	2.6	14.9
235	12.5	1.6	2.6	16.2
245	11.9	1.5	2.6	15.6
255	11.4	1.5	2.7	16.6

5.5.1.3 SWT test, assuming a load of 75 Ω

The results obtained with a variable resistor of 75 Ω can be observed below. The performance of this test is justified by the need to analyse the system operation at various load levels. As in the previous section, some of the most characteristic curves are shown.

- Relationship $v_{dc}(n)$ (see Fig. 5.30).

- Relationship $v_{r,s,t}(n)$ (see Fig. 5.30).

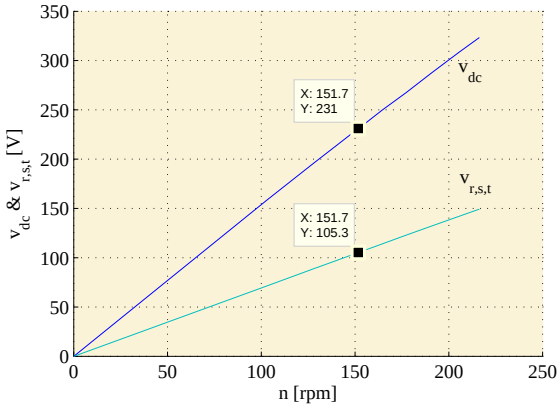

Figure 5.30: v_{dc} vs. n and $v_{r,s,t}$ vs. n, for $R = 75\ \Omega$.

- Relationship $i_{dc}(n)$, (see Fig. 5.31).

- Relationship $i_{r,s,t}(n)$, (see Fig. 5.31).

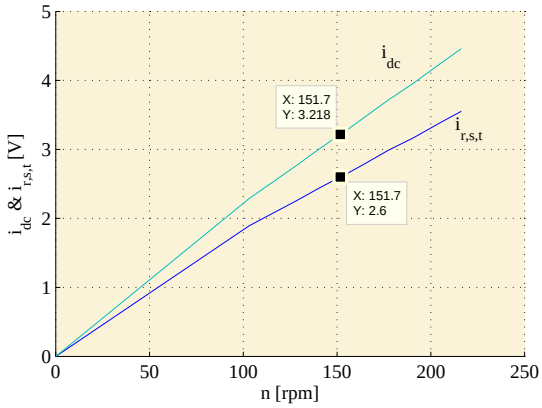

Figure 5.31: i_{dc} vs. n and $i_{r,s,t}$ vs. n, for $R = 75\ \Omega$.

- Rectifier voltage waveform v_{dc}, assuming $n = 150\,rpm$ (see Fig. 5.32).

- PMSM voltage waveform $v_{r,s,t}$, assuming $n = 150\,rpm$ (see Fig. 5.32).

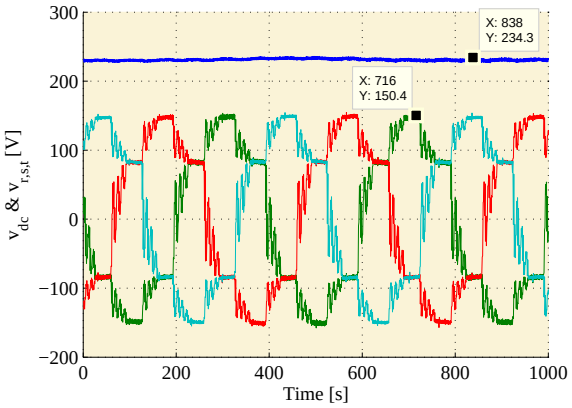

Figure 5.32: Voltage waveforms: v_{dc} and $v_{r,s,t}$, assuming a load $R = 75\ \Omega$ and $n = 150$ rpm.

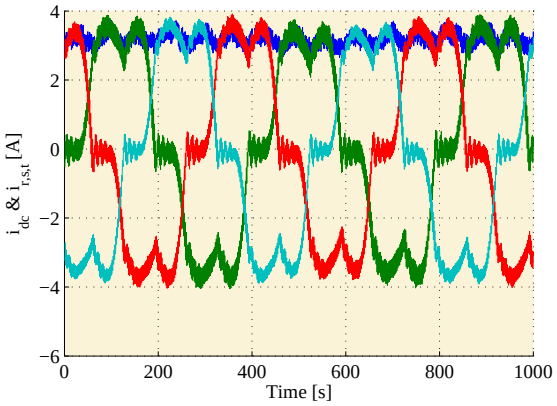

Figure 5.33: Current waveforms: i_{dc} and $i_{r,s,t}$, assuming a load $R = 75\ \Omega$ and $n = 150$ rpm.

- Rectifier current waveform i_{dc}, assuming $n = 150\,rpm$ (see Fig. 5.33).
- PMSM current waveform $i_{r,s,t}$, assuming $n = 150\,rpm$ (see Fig. 5.33).

Following, the efficiency of all SWT components will be studied. Fig. 5.34 shows active power of these components when the rotation speed n increases.

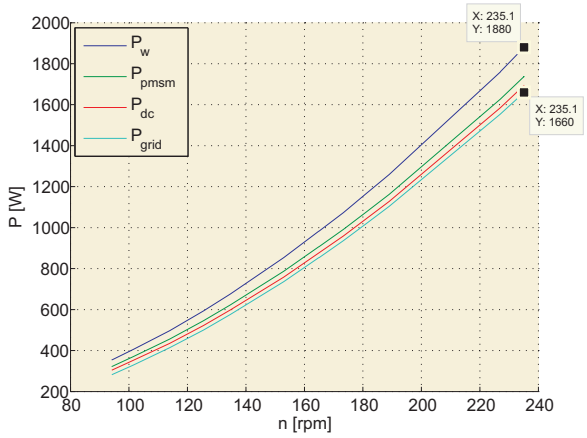

Figure 5.34: SWT efficiency study, assuming a load $R = 75\ \Omega$.

Table 5.3 illustrates the efficiencies of the SWT elements obtained during this test for different speed values.

Table 5.3: Efficiency comparison of the all SWT components, assuming a load $R = 75\ \Omega$.

$n[rpm]$	η [%]			
	η_{pmsm}	η_{rect}	η_{inv}	η_{SWT}
95	9.0	5.4	7.2	20.1
110	8.2	4.6	4.8	16.7
135	7.8	4.0	3.6	14.7
165	7.7	3.3	2.7	13.2
190	7.7	2.9	2.1	12.3
225	7.5	2.6	1.9	11.7
235	7.5	2.5	2.0	11.7

5.5.1.4 SWT test, assuming a rated load

This section studies the SWT performance under its rated load curve, given by the manufacturer. It is quite important that the results obtained with the models and those obtained in this test fit very well, because the real MPCC will be similar to this one.

In the case of not having the manufacturer's MPCC, you will have to fit the models with the tests presented above. Then, the MPCC will have to be obtained using the

methodology (see Section 5.4). Finally, it will have to be verified that the results obtained with the models match with the results obtained on the SWT.

Results obtained after entering the manufacturer's MPCC in the inverter software, can be observed below.

- Relationships: $v_{dc}(n)$ and $v_{r,s,t}(n)$ (see Fig. 5.35).

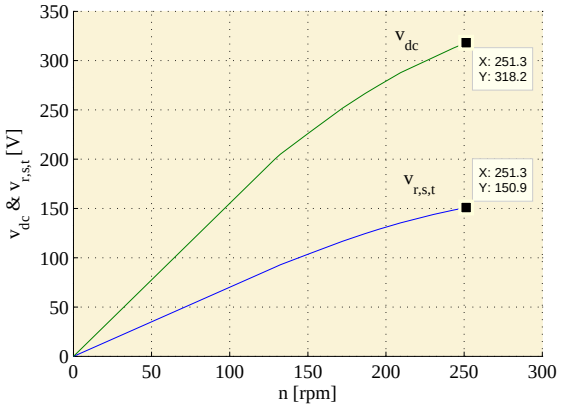

Figure 5.35: v_{dc} vs. n and $v_{r,s,t}$ vs. n, for the rated load test.

- Relationships: $i_{dc}(n)$ and $i_{r,s,t}(n)$ (see Fig. 5.36).

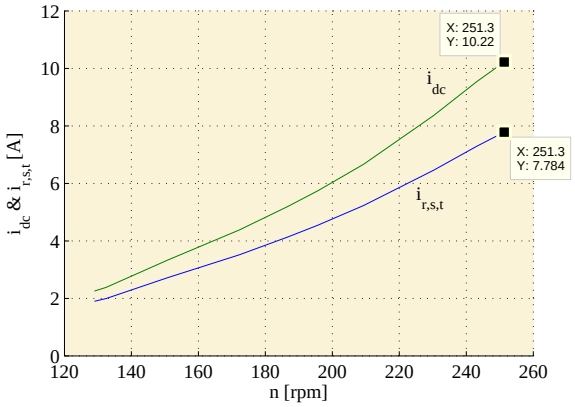

Figure 5.36: Relationships: i_{dc} vs. n and $i_{r,s,t}$ vs. n, for the rated load test.

- Rectifier voltage waveform v_{dc}, assuming $n = 150\,rpm$ (see Fig. 5.37).
- PMSM voltage waveform $v_{r,s,t}$, assuming $n = 150\,rpm$ (see Fig. 5.37).

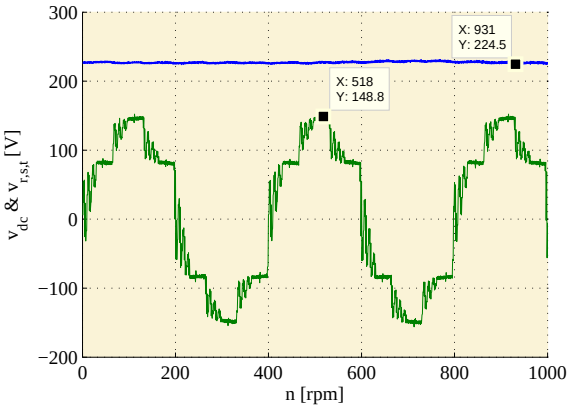

Figure 5.37: Voltage waveforms: v_{dc} and $v_{r,s,t}$ for the rated load test and $n = 150$ rpm.

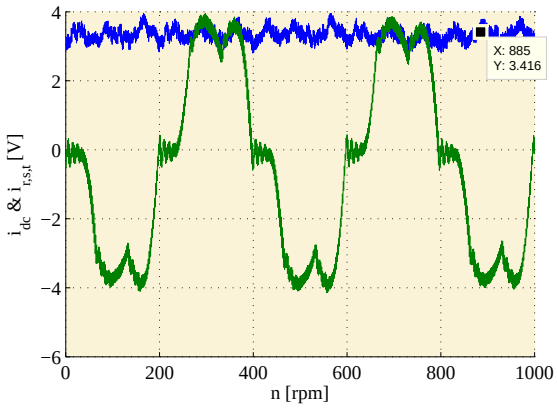

Figure 5.38: Current waveforms: i_{dc} and $i_{r,s,t}$ for the rated load test and $n = 150$ rpm.

- Rectifier current waveform i_{dc}, assuming $n = 150\,rpm$ (see Fig. 5.38).

- PMSM current waveform $i_{r,s,t}$, assuming $n = 150\,rpm$ (see Fig. 5.38).

- Active power of the SWT components for the rated load test (Fig. 5.39).

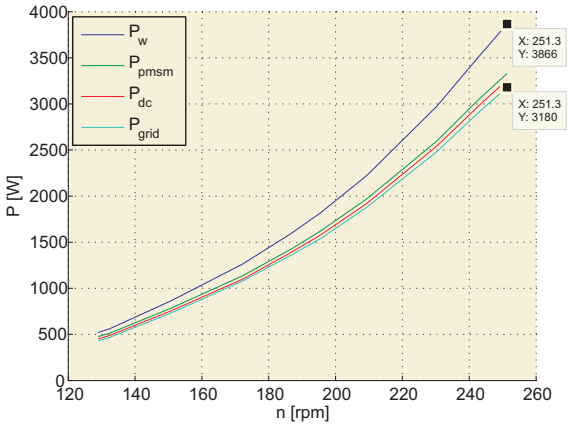

Figure 5.39: SWT efficiency study, assuming the rated load test.

5.5.2 Step 2: Verification of FEM and Simulink models

In this section the aim sought is to simulate the same tests performed on the SWT. After that, these results will be compared to check the accuracy of the models.

Models need some input parameters to solve the problem. These parameters are:

- **Simulink model**
  - $\Phi = 1.0035\,Wb$.
  - $L_e = 0.0328\,H$.
  - $R_e = 3\,\Omega$.
  - Pairs of poles = 10.
  - $C_{dc} = 1440\,\mu F$.
- **FEM model**
  - $L_e = 0.0328\,H$.
  - $R_e = 3\,\Omega$.
  - $C_{dc} = 1440\,\mu F$.

5.5.2.1 SWT No-load test comparison

First of all, the variation of v_{dc} and $v_{r,s,t}$ for different values of n will be compared. Fig. 5.40 presents how the values of $v_{r,s,t}$, obtained by the simulation models, are quite close to the real ones. Moreover, it also shows that the values of v_{dc} obtained with the simulink model are closer to the real ones than the values obtained with the FEM model. In any case, both models supply a quite acceptable accuracy.

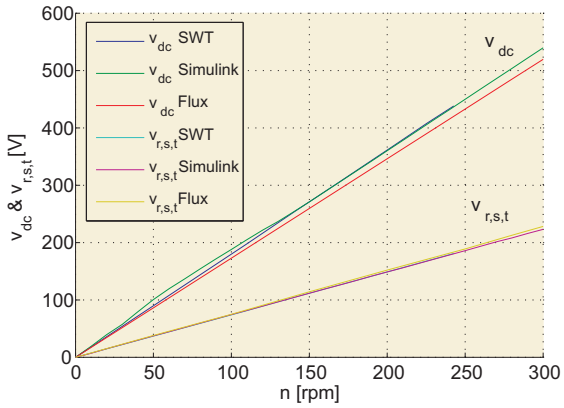

Figure 5.40: Comparison of $v_{dc}(n)$ and $v_{r,s,t}(n)$ in the No-load test.

Secondly, waveforms of v_{dc} and $v_{r,s,t}$, assuming a rotation speed of 150 rpm, will be compared. Time simulation for both models was sufficiently long so that the waveforms could stabilize. If waveforms obtained with Simulink model (Fig. 5.41) and with FEM model (Fig. 5.42) are compared with the real waveforms (Fig. 5.24), it can be observed that the values obtained are quite similar to the real ones.

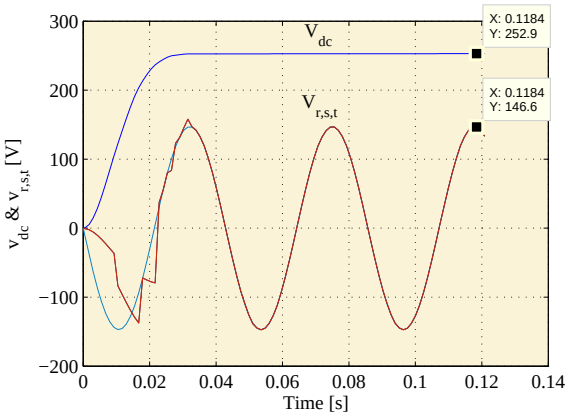

Figure 5.41: v_{dc} and $v_{r,s,t}$ waveforms achieved with Simulink in the No-load test at 150 rpm.

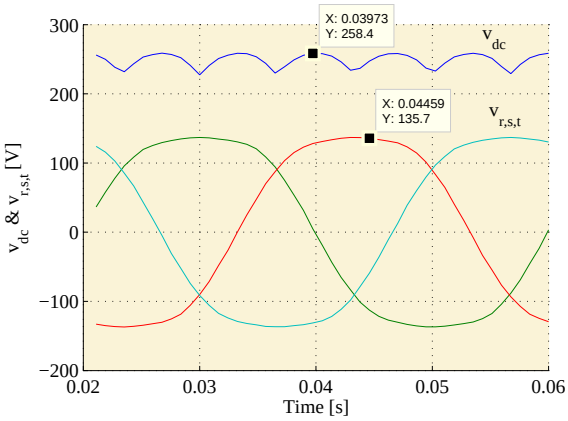

Figure 5.42: v_{dc} and $v_{r,s,t}$ waveforms achieved with FEM in the No-load test at 150 rpm.

Table 5.4 indicates this comparison and shows that the values achieved with the models, do not differ much. It should be noticed that the voltage obtained by simulation models in the No-load test, is 5% lower than the real voltage obtained on the SWT.

Table 5.4: Comparison of v_{dc} and $v_{r,s,t}$ obtained by means of FEM, Simulink and the SWT. Assuming a No-load test and $n = 150$ rpm.

Voltage	v [V]		
	SWT	Simulink	FEM
v_{dc}	269.9	252.9	258.4
$v_{r,s,t}$	151.3	146.6	135.7

5.5.2.2 SWT load test comparison, assuming a load of 31 Ω

Next, the results obtained with the models for a constant load of 31 Ω will be checked.

First of all, the voltage after the rectifier v_{dc} and the voltage after the PMSM $v_{r,s,t}$ will be compared (see Fig. 5.43). The current after the rectifier i_{dc} and the current after the PMSM $i_{r,s,t}$ will be also verified (see Fig. 5.44). It should be borne in mind that in this test, models fit better than in the case of the No-load test.

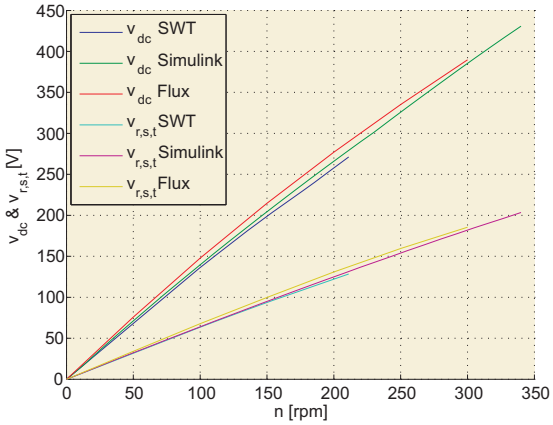

Figure 5.43: Comparison of $v_{dc}(n)$ and $v_{r,s,t}(n)$, assuming a load $R = 31\ \Omega$.

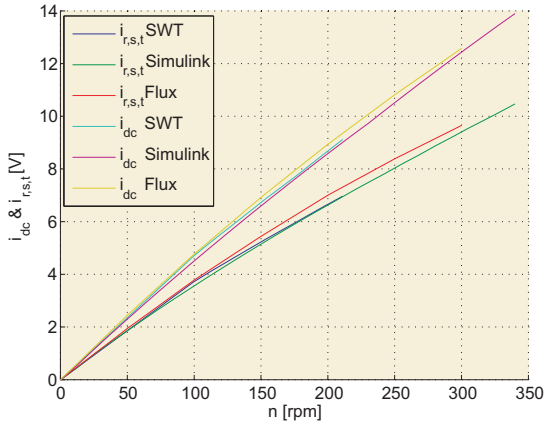

Figure 5.44: Comparison of $i_{dc}(n)$ and $i_{r,s,t}(n)$, assuming a load $R = 31\ \Omega$.

Secondly, the waveforms of v_{dc}, $v_{r,s,t}$, i_{dc} and $i_{r,s,t}$ for a rotor speed of 150 rpm will be analysed.

- Curves obtained by means of Simulink model (see Fig. 5.45).

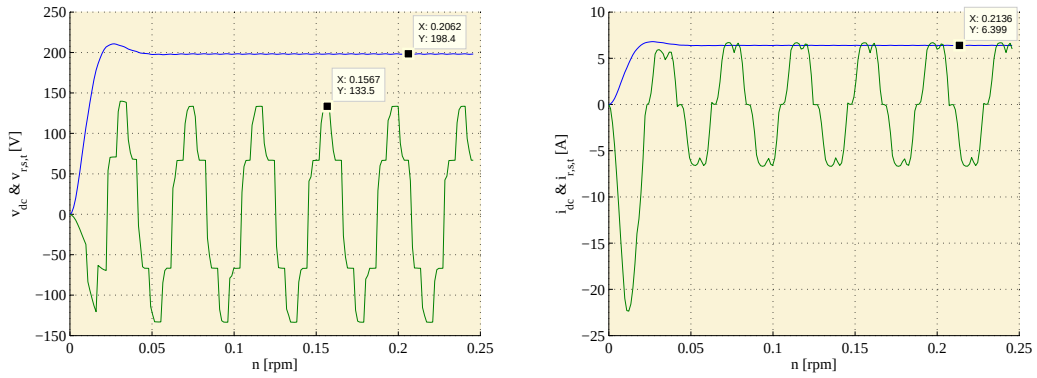

(a) v_{dc} vs. n and $v_{r,s,t}$ vs. n.

(b) i_{dc} vs. n and $i_{r,s,t}$ vs. n.

Figure 5.45: Voltage and current waveforms obtained by Simulink, assuming a load $R = 31\ \Omega$ and $n = 150$ rpm.

- Curves obtained by means of FEM model (see Fig. 5.46).

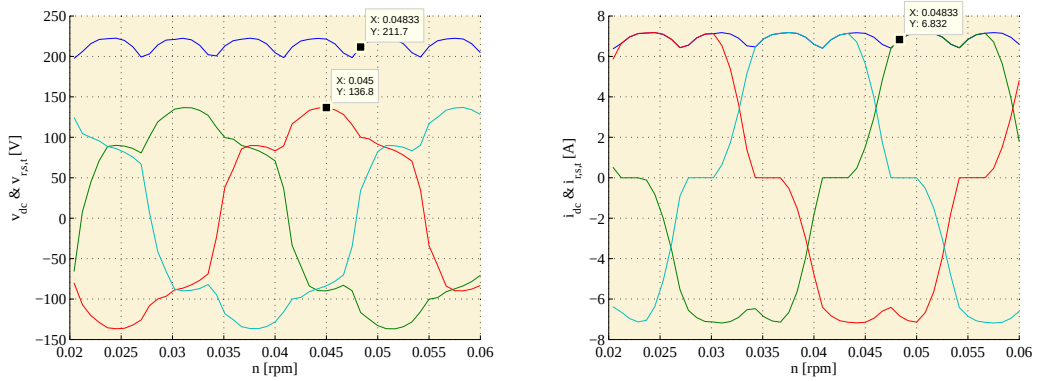

(a) v_{dc} vs. n and $v_{r,s,t}$ vs. n.

(b) i_{dc} vs. n and $i_{r,s,t}$ vs. n.

Figure 5.46: Voltage and current waveforms obtained by FEM model, assuming a load $R = 31\ \Omega$ and $n = 150$ rpm.

- Comparison of the real test for a constant load of 31 Ω, with the values obtained by means of the models (Fig. 5.27, Fig. 5.28, Fig. 5.45 and Fig. 5.46). This comparison can be seen in Table 5.5.

Table 5.5: Comparison of v_{dc}, $v_{r,s,t}$, and i_{dc} obtained by means of FEM, Simulink and the SWT. Assuming a load $R = 31\ \Omega$ and $n = 150$ rpm.

Values	v [V] and i [A]		
	SWT	Simulink	FEM
v_{dc}	201.5	198.4	211.7
$v_{r,s,t}$	133.1	133.5	136.8
i_{dc}	6.7	6.4	6.8

5.5.2.3 SWT load test comparison, assuming a load of 75 Ω

In this section, the results obtained with the models for a constant load of 75 Ω will be checked.

In the first place, the voltage after the rectifier v_{dc} and the voltage after the PMSM $v_{r,s,t}$ will be compared (see Fig. 5.47). The current after the rectifier i_{dc} and the current after the PMSM $i_{r,s,t}$ will be also verified (see Fig. 5.48).

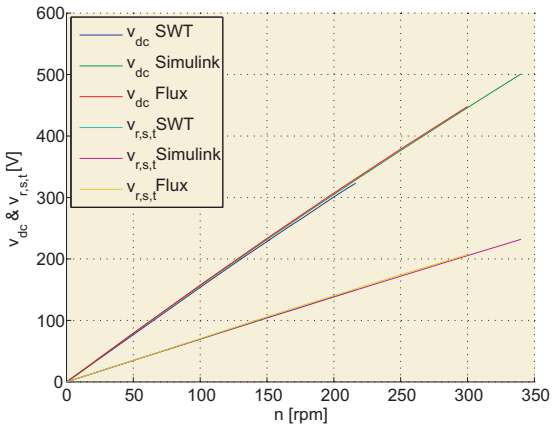

Figure 5.47: Comparison of $v_{dc}(n)$ and $v_{r,s,t}(n)$, assuming a load $R = 75\ \Omega$.

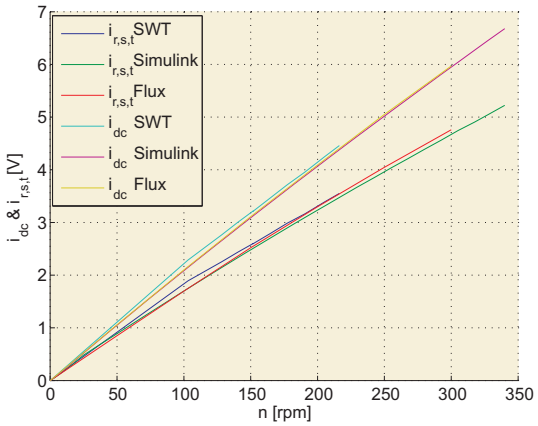

Figure 5.48: Comparison of $i_{dc}(n)$ and $i_{r,s,t}(n)$, assuming a load $R = 75\ \Omega$.

Next, waveforms of v_{dc}, $v_{r,s,t}$, i_{dc} and $i_{r,s,t}$ will be contrasted.

- Figures obtained by means of the Simulink model (see Fig. 5.49).

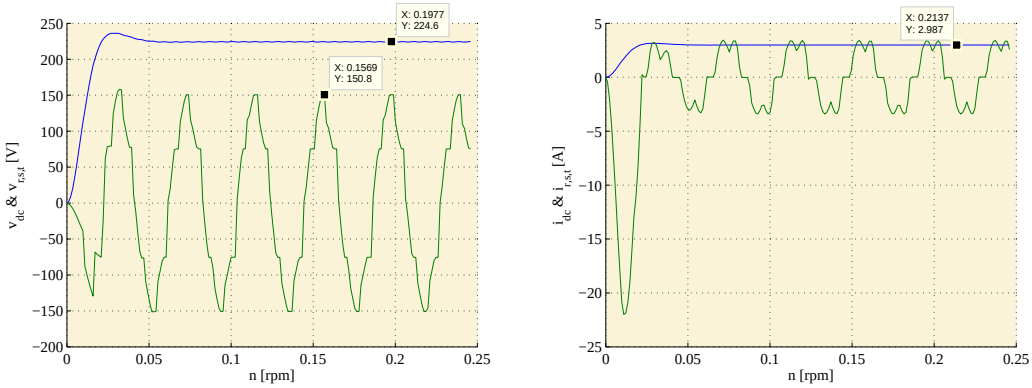

(a) v_{dc} vs. n and $v_{r,s,t}$ vs. n.

(b) i_{dc} vs. n and $i_{r,s,t}$ vs. n.

Figure 5.49: Voltage and current waveforms obtained by Simulink, assuming a load $R = 75\ \Omega$ and $n = 150$ rpm.

- Figures obtained by means of the FEM model (see Fig. 5.50).

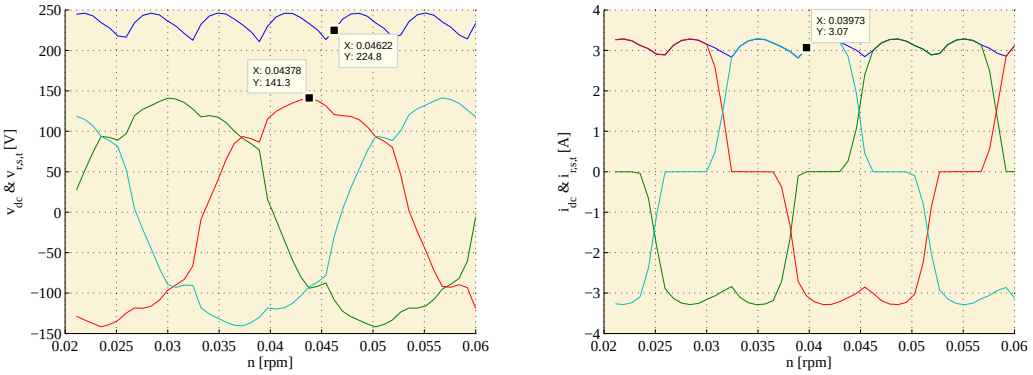

(a) v_{dc} vs. n and $v_{r,s,t}$ vs. n.

(b) i_{dc} vs. n and $i_{r,s,t}$ vs. n.

Figure 5.50: Voltage and current waveforms obtained by FEM model, assuming a load $R = 75\ \Omega$ and $n = 150$ rpm.

- Comparison of the real test for a constant load of 75 Ω, with the values obtained by means of the models (Fig. 5.32, Fig. 5.33, Fig. 5.49 and Fig. 5.50). This comparison can be seen in Table 5.6.

Table 5.6: Comparison of v_{dc}, $v_{r,s,t}$, and i_{dc} obtained by means of FEM, Simulink and the SWT. Assuming a load $R = 75\ \Omega$ and $n = 150$ rpm.

Values	v [V] and i [A]		
	SWT	Simulink	FEM
$v_{dc}[V]$	234.3	224.6	224.8
$v_{r,s,t}[V]$	150.4	150.8	141.3
$i_{dc}[A]$	3.05	2.98	3.07

5.5.2.4 SWT load test comparison, assuming a rated load test.

Below, the results obtained with the models for a rated load test will be checked:

- Comparison of v_{dc} and $v_{r,s,t}$ obtained by Simulink and FEM models, with the results got from the SWT, for different speed values (see Fig. 5.51).

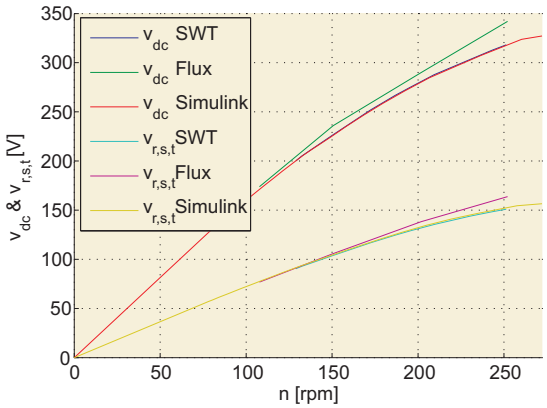

Figure 5.51: Comparison of $v_{dc}(n)$ and $v_{r,s,t}(n)$, assuming a rated load test.

- Comparison of i_{dc} and $i_{r,s,t}$ obtained by Simulink and FEM models, with the results got from the SWT, for different speed values (see Fig. 5.52).

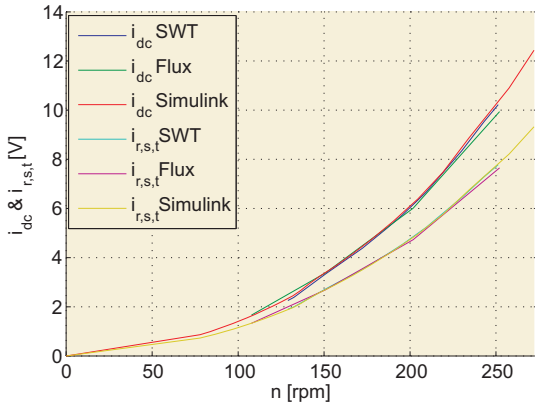

Figure 5.52: Comparison of $i_{dc}(n)$ and $i_{r,s,t}(n)$, assuming a rated load test.

- Comparison of the active power P_{pmsm} and the reactive power Q_{pmsm} calculated by Simulink model, with the results obtained from the SWT, for different speed values (see Fig. 5.53).

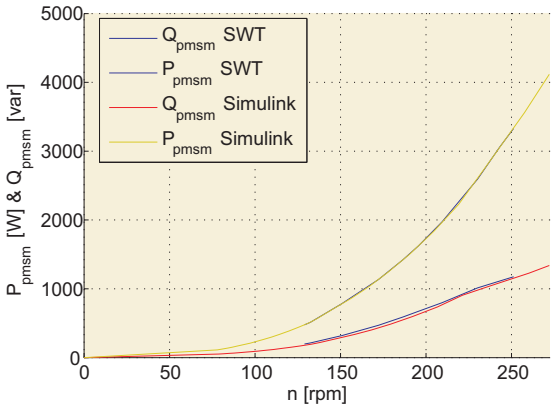

Figure 5.53: Comparison of $P_{pmsm}(n)$ and $Q_{pmsm}(n)$, assuming a rated load test.

- Waveforms of P_{dc} and P_{grid} obtained with Simulink model, for $n = 150$ rpm (see Fig. 5.54).

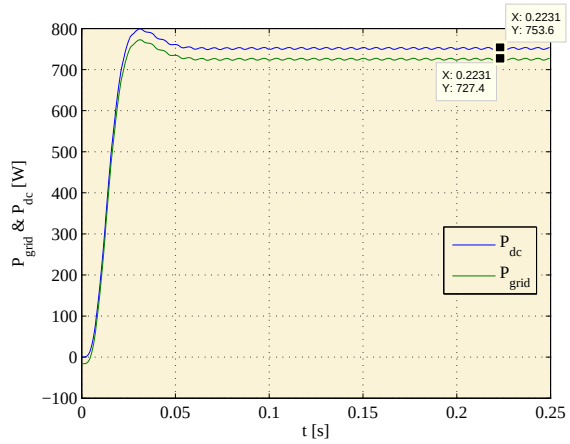

Figure 5.54: P_{dc} and P_{grid} waveforms obtained by Simulink, assuming a rated load test and $n = 150$ rpm.

- Waveforms of v_{dc}, $v_{r,s,t}$, i_{dc} and $i_{r,s,t}$ obtained with Simulink model, for $n = 150$ rpm (see Fig. 5.55).

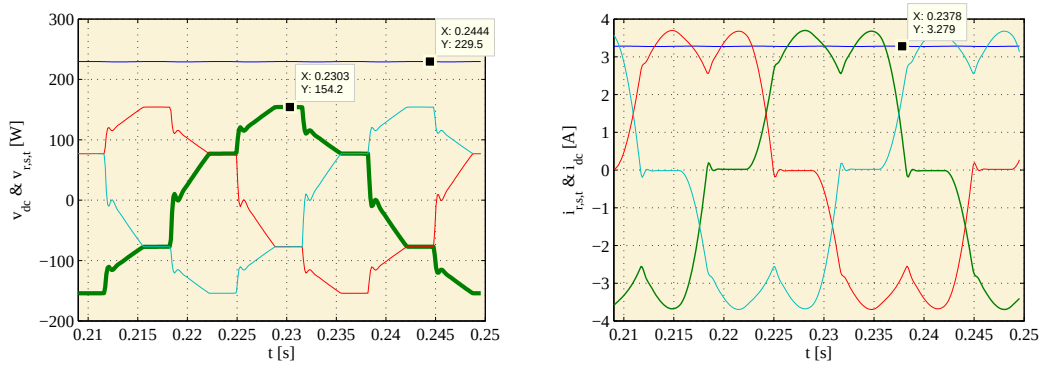

(a) v_{dc} vs. n and $v_{r,s,t}$ vs. n.

(b) i_{dc} vs. n and $i_{r,s,t}$ vs. n.

Figure 5.55: Voltage and current waveforms obtained by Simulink, assuming a rated load test and $n = 150$ rpm.

- Waveforms of v_{dc}, $v_{r,s,t}$, i_{dc} and $i_{r,s,t}$ obtained with FEM model, for $n = 150$ rpm (see Fig. 5.56).

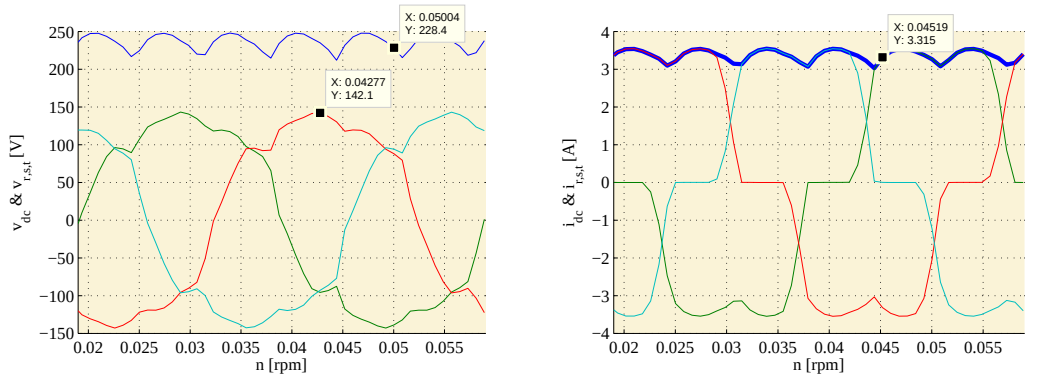

(a) v_{dc} vs. n and $v_{r,s,t}$ vs. n.

(b) i_{dc} vs. n and $i_{r,s,t}$ vs. n.

Figure 5.56: Voltage and current waveforms obtained by FEM model, assuming a rated load test and $n = 150$ rpm.

- Comparison of the real test, assuming a rated load test, with the values obtained by means of the models (Fig. 5.37, Fig. 5.38, Fig. 5.55 and Fig. 5.56).

Table 5.7: Comparison of v_{dc}, $v_{r,s,t}$, and i_{dc} obtained by means of FEM, Simulink and the SWT. Assuming a rated load test and $n = 150$ rpm.

Values	v [V] and i [A]		
	SWT	Simulink	FEM
v_{dc}	224.5	229.5	228.4
$v_{r,s,t}$	148.8	154.2	142.1
i_{dc}	3.416	3.27	3.31

Once, you have elaborated an accuracy model that allows you to predict the SWT performance, different modifications can be introduced in the model (for instance, connecting a capacitor bank). These changes allow you to carry out a study of the SWT, without having to test directly on the SWT. All this allows you:

- To protect the SWT from unnecessary damages.
- To save money. It is possible to try several settings, without requiring any investment.

The reason why two different models were used, is that each of them allows you to get certain parameters of the SWT.

On one hand, the Simulink model lets you define all electronic components in a fast and easy way. Moreover, it also enables you to connect several kinds of elements, such as: coils, capacitors, thyristors, etc. However, this model does not pay much attention to the internal operations of the electrical machine.

On the other hand, the FEM model focuses much more on the PMSM. This model is able to measure the internal machine losses, such as: copper losses, iron losses, magnet losses, etc. In addition, it is also able to compute the magnetic field in each part of the PMSM.

The next step will be to improve the efficiency of SWT.

5.5.3 Step 3: Obtain the Maximum Torque Point Tracker (MTPT)

The SWT rated characteristics will be used to calculate C_p, λ, and the Maximum Torque Point Tracker (MTPT) (see Section 5.5). Thus:

- C_p: Eq. (5.14) will be used to obtain the power coefficient C_p. Knowing the values $d = 4.2$ m, $N = 3$, $L/D = 30$ and $u_h = 11$ m/s, you will be able to get the Fig. 5.57(a) that relates the mechanical power P_w with λ or in other words, P_w with the SWT rotation speed n (see Eq. 5.13).

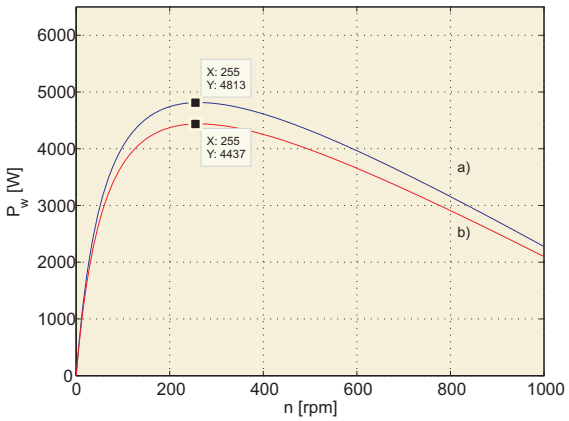

Figure 5.57: Mechanical power P_w vs. rotation speed n, assuming a $u_h = 11$ m/s: a) $C_p = 0.392$. b) $C_p = 0.36$.

Fig. 5.57(a) shows that the SWT can extract from the wind, a maximum mechanical power P_w of 4813 W, turning at $n = 255$ rpm and for a wind speed of $u_h = 11$ m/s. If these values are replaced in Eq. (5.11), you achieve:

$$C_p(\lambda,\beta) = \frac{P_w}{\left(\frac{1}{2}\frac{\pi\, d^2}{4}\,\rho\, u_1^3\right)} = \frac{4813}{\left(\frac{1}{2}\frac{\pi 4.2^2}{4}\cdot 1.3311^3\right)} \simeq 0.392 \tag{5.22}$$

If this value is compared with the rated one it can be appreciated a small discrepancy, which is due to the existence of several factors that the model has not taken into account. These factors were explained in Section 5.2. To take into account these factors, the value of C_p will have to be decreased a percentage. This percentage will be calculated as follows:

$$\Delta C_p = 100 - \frac{C_{p_{ideal}} - C_{p_{real}}}{C_{p_{ideal}}}\cdot 100 = 100 - \frac{0.392 - 0.36}{0.392}\cdot 100 \simeq 91.8\% \tag{5.23}$$

Applying this correction to the Eq. (5.15), you get:

$$P_w = \left(\frac{\Delta\, C_p}{100}\right)\left(\frac{1}{2}\,\frac{\pi\, d^2}{4}\,\rho\, u_1^3\right)\left(\frac{16}{27}\frac{\lambda}{\lambda + \frac{1.32+(\frac{\lambda-8}{20})^2}{N^{2/3}}} - 0.57\frac{\lambda^2}{\frac{L}{D}(\lambda + \frac{1}{2N})}\right) \tag{5.24}$$

If $\Delta C_p = 91.8\%$ is substituted in Eq. (5.24), the Fig. 5.57(b) is obtained. In this figure it can be seen that the real mechanical power P_w is close to 4437 W.

It should be noted, as discussed previously, that reaching the *Betz limit* was impossible because of some restrictive parameters. In the example this can be seen, because the theoretical maximum value is 0.593 and the real one is 0.36. In this way, the SWT can only extract the 36% from the wind energy.

- λ: For its calculation, Eq. (5.13) will be used.

$$\lambda = \frac{Speed\,of\,rotor\,tip}{Wind\,speed} = \frac{\frac{\omega d}{2}}{u_h} = \frac{\frac{255 \cdot 2 \cdot \pi \cdot 4.2}{2 \cdot 60}}{11} \simeq 5.1 \tag{5.25}$$

- Maximum Torque Point Tracker (MTPT).

  To obtain the MTPT, the Eq. (5.24) will be used. In this equation, the reduction of the mechanical power P_w has been considered because the parameter ΔC_p has been added. Using that equation and taking into account that, λ is a function of the SWT diameter and the wind speed, the Fig. 5.58(a) can be obtained.

  In this figure, you can see highlighted the relationship $P_{w_{max}}(n)$ that produces, for different wind speeds, the maximum mechanical power. As mentioned before, all these points have the property that P_w is maximum and consequently C_p is maximum as well and close to 0.36. Therefore, all these points will have a constant value of λ.

  All these maximum points can be represented in a new curve, Fig. 5.58(b). This figure is known as the Maximum Power Point Tracker (MPPT).

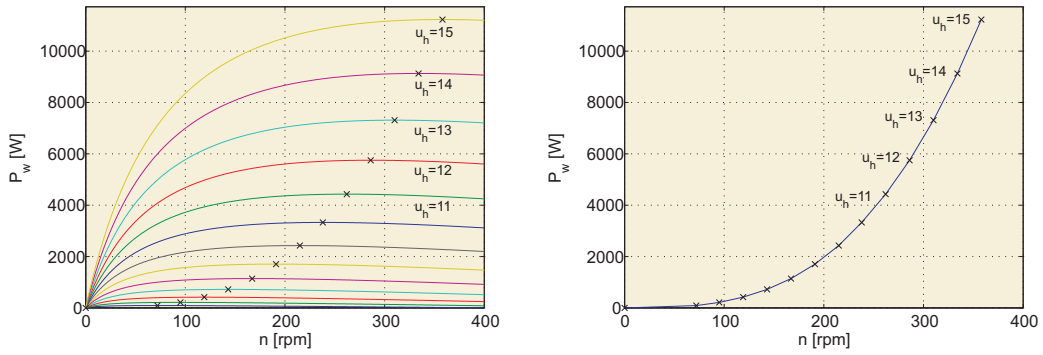

(a) P_w vs. n, for different wind speeds u_h.

(b) $P_{w_{max}}$ vs. n, for several wind speeds u_h.

Figure 5.58: MPPT, assuming $L/D = 30$ and $C_p = 0.36$.

Considering the Eq. (4.1), the optimal relationship $T_w(n)$ can also be obtained. It will be known as the Maximum Torque Point Tracker (MTPT) (see Fig. 5.59). It can be seen that for a rotor speed of 250 rpm the mechanical torque is close to 150 Nm.

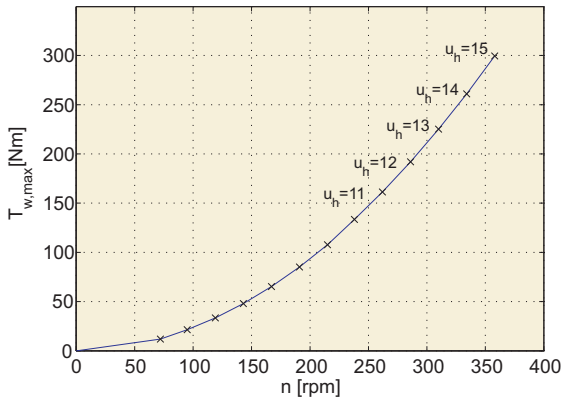

Figure 5.59: MTPT, assuming a $L/D = 30$ and $C_p = 0.36$.

Note that the MTPT must remain unchanged for every value of the variable resistor R. Therefore, MTPT in 3D can be represented as a parallel surface to axis R, Fig. 5.59. This figure will become more interesting later, when the SWT operating surfaces are calculated.

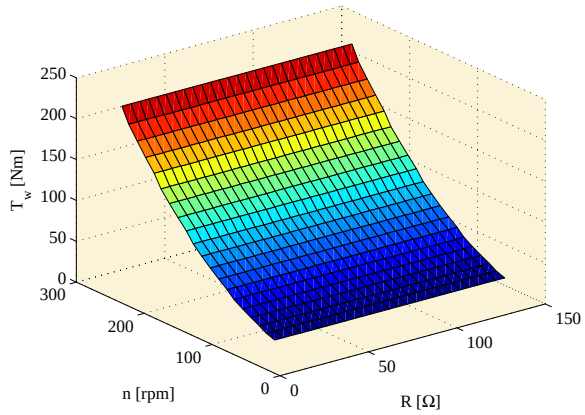

Figure 5.60: MTPT in 3D, assuming a $L/D = 30$ and $C_p = 0.36$.

Table 5.8 shows the values of the relationship $T_w(n)$ for several wind speeds, assuming a value of $C = 0$.

Table 5.8: Results of steps 3 and 5. Without capacitor bank.

Step 3			Step 5		
u_h	n	T_w	R	P_{grid}	v_{dc}
11.9	276.9	194.5	20	4346.1	299.2
10.1	233.2	138.8	30	2804.7	293.5
9.2	213.3	115.4	35	2170.3	278.8
8.4	194.9	97.7	40	1702.6	264.1
7.4	172.2	74.6	50	1171.0	245.1
6.0	139.2	50.2	65	644.0	208.3
5.0	116.0	33.9	85	361.2	180.1
4.1	95.0	23.3	105	197.2	150.9
3.1	72.7	13.0	150	75.1	118.5

5.5.4 Step 4: Calculate a range of capacities [C_i-C_k]

Once the magnetizing effect produced by capacitors, when they are connected to the outlet of the PMSM, is known (see Section 5.3); we will be able to study the effect produced by different capacitors in a specific SWT.

Using Simulink model, the relationship C [μF], R [Ω] and P_{grid} [W] was calculated for different rotation speeds, such as: 50, 100, 150, 200 and 250 rpm (see Fig. 5.61).

From Fig. 5.61 it can be concluded that each rotation speed n will have its own optimal capacity C. This conclusion can also be reached if you take into account that the capacitive impedance X_{cap} depends on the frequency. That is to say, it depends on the rotation speed n, therefore a constant capacity C will be able to provide various values of X_{cap} and consequently different magnetizing effects. The Eq. (5.26) shows this dependence.

$$X_{cap} = \frac{1}{2\,\pi\,f\,C} \tag{5.26}$$

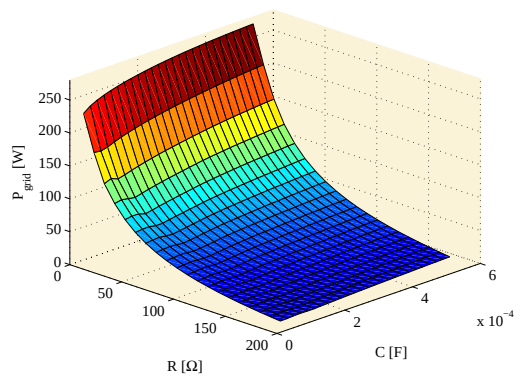

(a) 50 rpm.

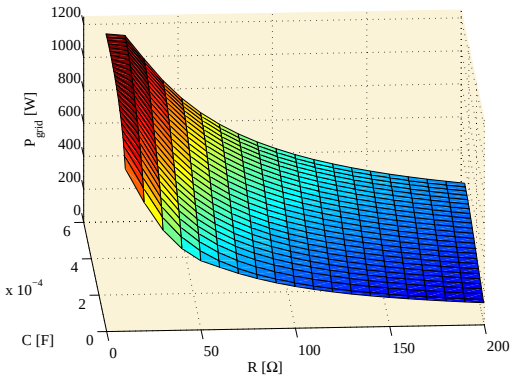

(b) 100 rpm.

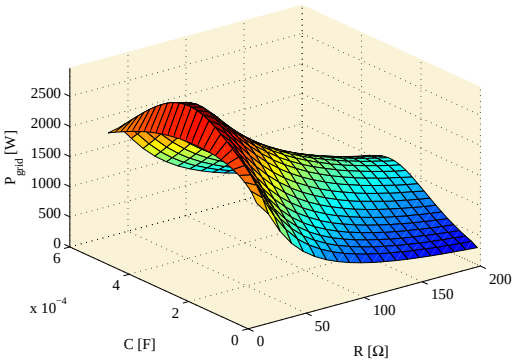

(c) 150 rpm.

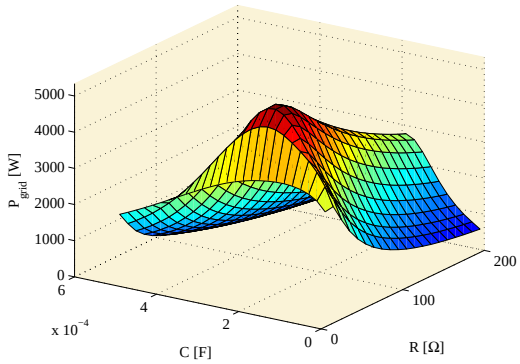

(d) 200 rpm.

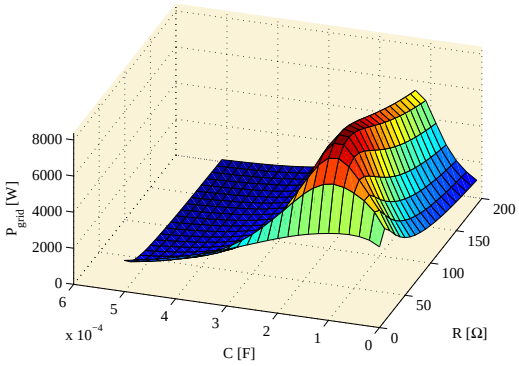

(e) 250 rpm.

Figure 5.61: P_{grid} vs. R and C, for different rotation speeds.

If the rated case is studied (Fig. 5.61(e)), it can be seen how by increasing the capacity C for each value of R, the power injected to the grid P_{grid} increases up to a

maximum value C_{max}, from which P_{grid} decreases. Thus, the value C_{max} that maximizes the P_{grid} is obtained.

However, the value of C_{max} must be controlled because it could also increase the phase current $i_{r,s,t}$ into the PMSM windings and thereby cause damage. Therefore, taking into account that the winding wire diameter is 0.8 mm, the maximum allowed current will be approximately 11 A.

Once the value of the maximum current i_r is known, the capacity range [C_i-C_k] can be obtained by means of drawing a perpendicular surface to the axis $i_{r,s,t}$ (see Fig. 5.62).

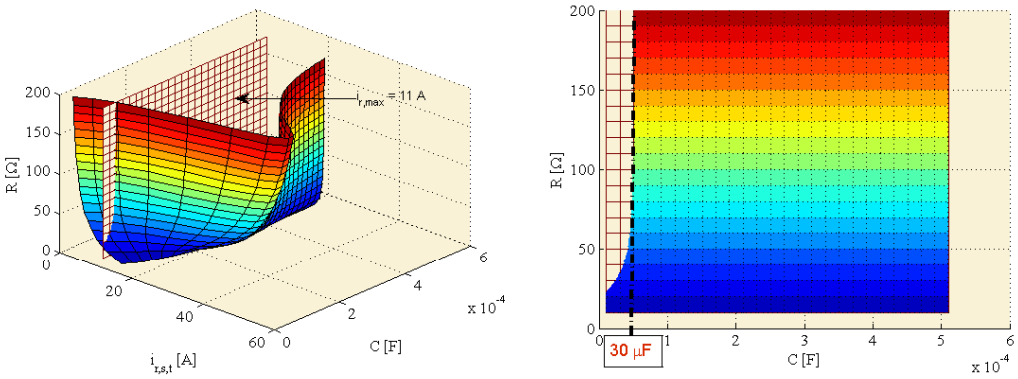

(a) $i_{r,s,t}$ vs. R and C.

(b) Variable resistor R vs. capacity C, assuming $i_{r,s,t} = 11$ A.

Figure 5.62: $i_{r,s,t}$ vs. R and C, not exceeding the restriction of $i_{r,s,t} \leq 11$ A and assuming n=250 rpm.

Thus, it is calculated that the capacity C will be between $C_i = 0$ and $C_k = 30$ μF, for every value of R. The tested capacities will be: 0, 4, 6, 8, 10, 12, 14, 16, 20, and 24 μF.

In the end, Fig. 5.63(a) shows the relationships $P_{grid}(R, C)$ and $P_w(R, C)$ for a rotation speed n=250 rpm. In this figure you can perfectly appreciate some details, such as:

- Initially, if you increase the capacity C the grid power P_{grid} increases. But when C reaches a limit value, then P_{grid} begins to decrease. Therefore, there will be a capacity value that maximizes P_{grid}.

- If you increase the variable resistor R then P_{grid} also increases. But when R reaches a limit value then, P_{grid} starts to decrease.
- The difference, between both surfaces in the power axis, matches with the SWT total losses. These total losses are the addition of the: mechanical losses, PMSM losses, rectifier losses and inverter losses.

In addition, Fig. 5.63(b) illustrates the relationships $P_{pmsm}(R, C)$ and $P_w(R, C)$ for a rotation speed n=250 rpm. In this figure the difference, in the power axis between both surfaces, matches with the internal losses of the PMSM. Comparing this last figure with Fig. 5.63(a), you are able to see that there is practically no difference between them. In conclusion, the predominant losses in the system (PMSM + Rectifier + Inverter) are the PMSM losses.

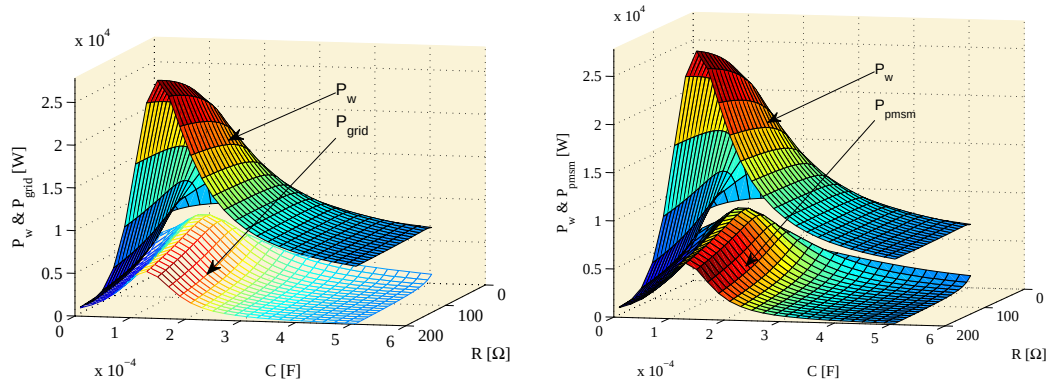

(a) P_w vs. R and C and P_{grid} vs. R and C. (b) P_w vs. R and C and P_{pmsm} vs. R and C.

Figure 5.63: Analysis of existing losses in the SWT for different values of C and R, assuming n=250 rpm.

5.5.5 Step 5: Obtain MPCCs for several values of C

Using Simulink, simulations will be done varying n and R, for values of C between 0 and 30 μF. It should be borne in mind that the more values of C you test, the more accurate the results will be.

In addition, the simulink model needs other ranges to solve the problem. These ranges are:

- n varying from 0 to 400 rpm.

- u_h varying from 0 to 15 m/s.
- R varying from 20 to 150 Ω.

For each value of C, you will have to develop the next steps:

- Step 5.1: Calculate the SWT operating surface $T_w(R, n)$.

  The operating surfaces that the Simulink model is able to calculate are:

  - Relationship $T_w(R, n)$.
  - Relationship $P_w(R, n)$.
  - Relationship $i_{r,s,t}(R, n)$.
  - Relationship $v_{r,s,t}(R, n)$.
  - Relationship $P_{r,s,t}(R, n)$.
  - Relationship $Q_{r,s,t}(R, n)$.
  - Relationship $S_{r,s,t}(R, n)$.
  - Relationship $P_{pmsm}(R, n)$.
  - Relationship $Q_{pmsm}(R, n)$.
  - Relationship $S_{pmsm}(R, n)$.
  - Relationship $i_{dc}(R, n)$.
  - Relationship $v_{dc}(R, n)$.
  - Relationship $P_{dc}(R, n)$.
  - Relationship $i_{grid}(R, n)$.
  - Relationship $v_{grid}(R, n)$.
  - Relationship $P_{grid}(R, n)$.

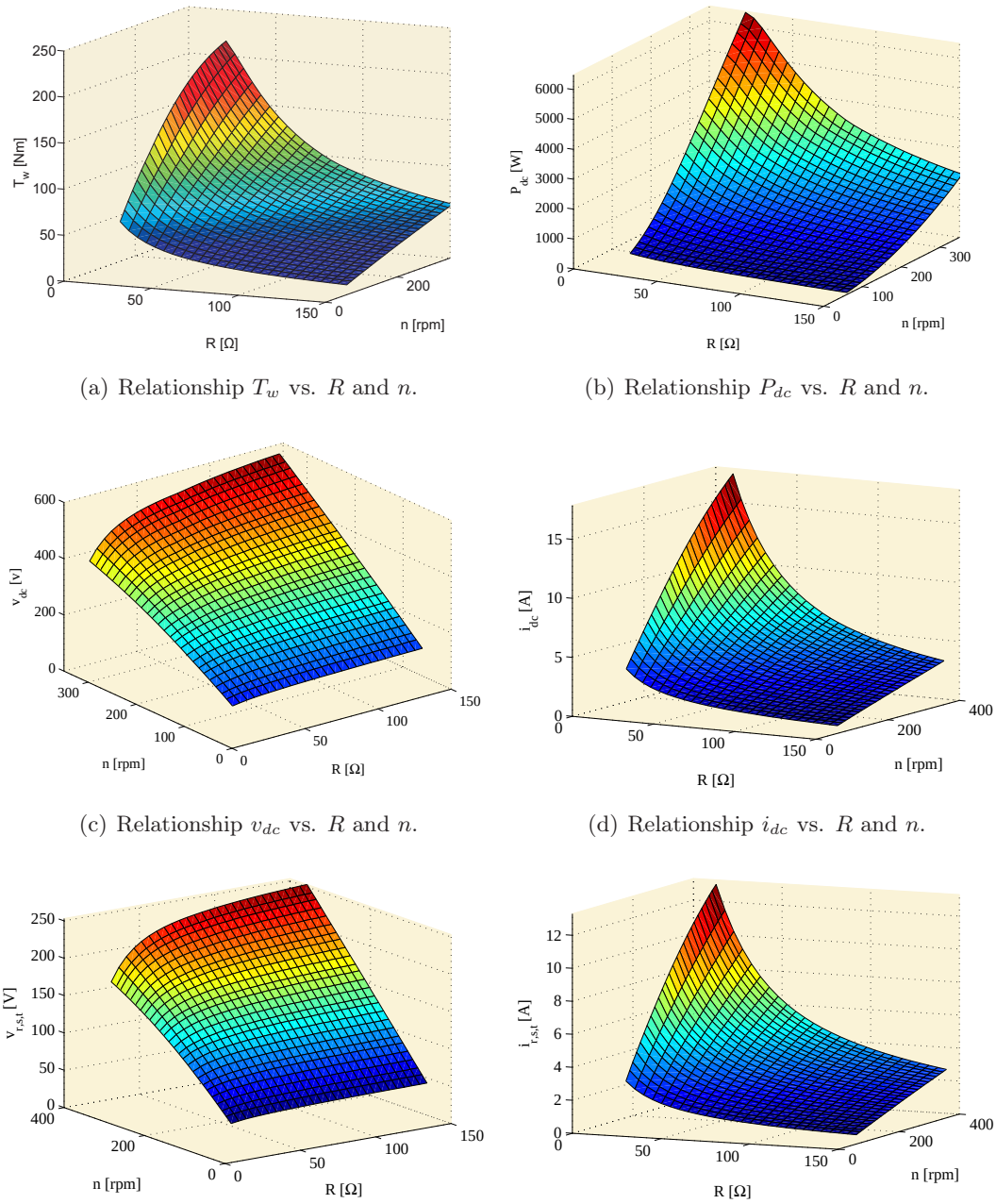

(a) Relationship T_w vs. R and n.

(b) Relationship P_{dc} vs. R and n.

(c) Relationship v_{dc} vs. R and n.

(d) Relationship i_{dc} vs. R and n.

(e) Relationship $v_{r,s,t}$ vs. R and n.

(f) Relationship $i_{r,s,t}$ vs. R and n.

Figure 5.64: SWT operating surfaces as a function of R and n.

Fig. 5.64 shows some of these SWT operating surfaces.

After that, you have to obtain the intersection between the surface $T_w(R, n)$

(Fig. 5.64(a)) and the MTPT (Fig. 5.14). Thus, you can get the relationship $R(n)$ that allows you to extract the maximum mechanical power from wind (see Fig. 5.65).

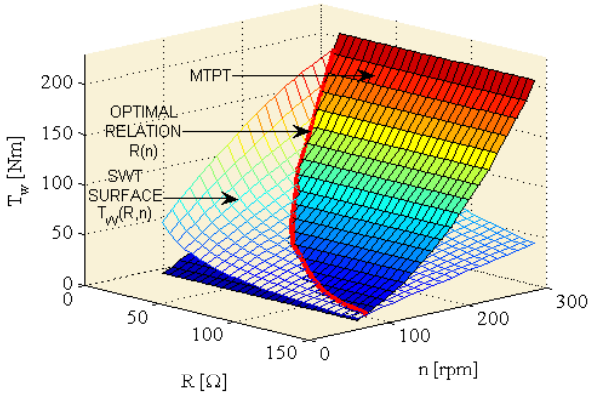

(a) 3D intersection.

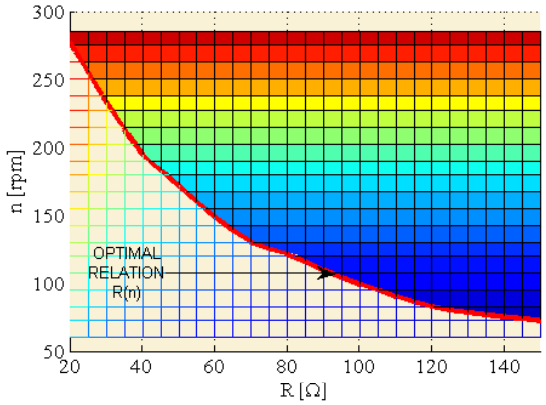

(b) Optimal relationship $R(n)$.

Figure 5.65: Intersection between the MTPT and the SWT operating surface $T_w(R, n)$.

- Step 5.2: Project the optimal relationship $R(n)$ perpendicular to the R-n plane (Fig. 5.66).

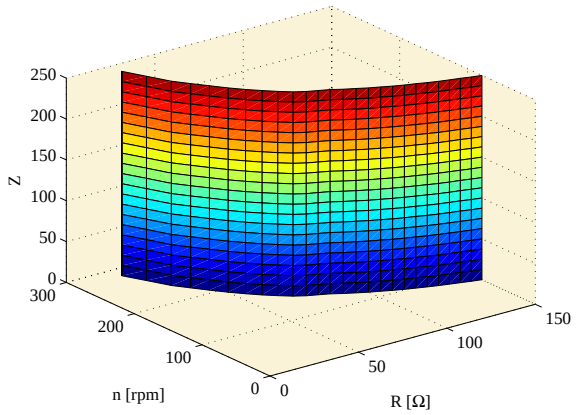

Figure 5.66: Optimal relationship $R(n)$ projected perpendicular to the R-n plane.

Table 5.8 shows the values of the relationship $R(n)$ for several wind speeds, assuming a value of $C = 0$.

- Step 5.3: Determine by Simulink the SWT operating surfaces $P_{grid}(R, n)$ and $v_{dc}(R, n)$.

  Now that the optimal relationship $R(n)$ (Fig. 5.66) is known, you can calculate the rest of the optimal parameters, such as:

  - Power, current and voltage in the PMSM.
  - Power, current and voltage in the rectifier.
  - Power, current and voltage in the grid.

  To get all the optimal parameters, you only have to obtain the intersection of the SWT operating surfaces (Fig. 5.64) with the surface obtained in Step 5.2.

  Fig. 5.67 shows the optimal relationship $v_{dc}(n)$.

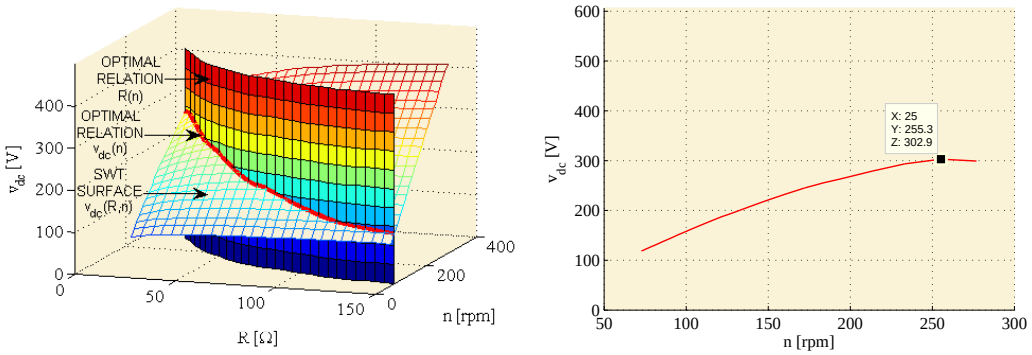

(a) 3D intersection.

(b) Optimal relationship $v_{dc}(n)$.

Figure 5.67: Intersection between the optimal relationship $R(n)$ and the SWT operating surface $v_{dc}(R, n)$.

Fig. 5.68 shows the optimal relationship $P_{dc}(n)$.

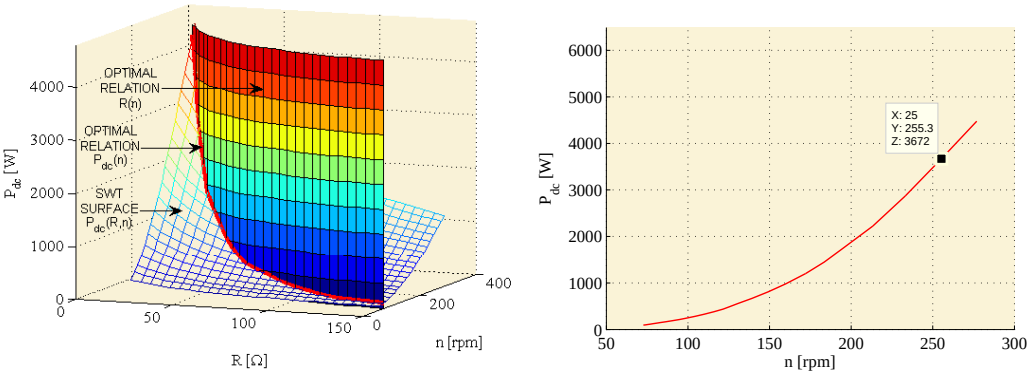

(a) 3D intersection.

(b) Optimal relationship $P_{dc}(n)$.

Figure 5.68: Intersection between the optimal relationship $R(n)$ and the SWT operating surface $P_{dc}(R, n)$.

Finally, if you obtain the intersection between the rest of the SWT operating surfaces and Fig. 5.66, you will find out the values of i_{dc}, P_{pmsm}, $v_{r,s,t}$, $i_{r,s,t}$, and P_w when the SWT is working under the optimal relationship $R(n)$.

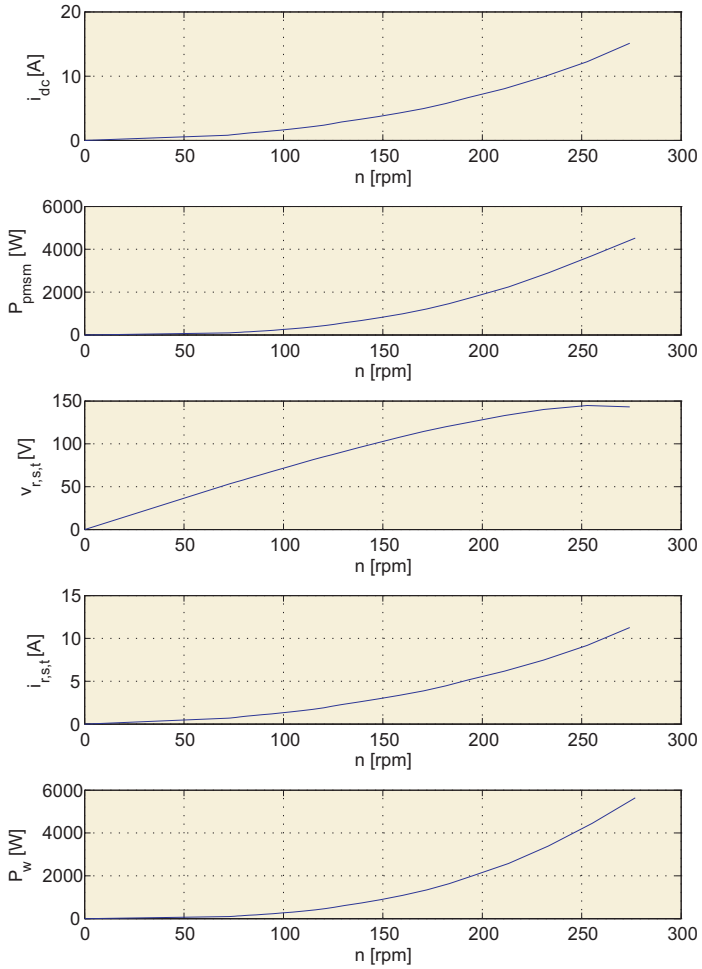

Figure 5.69: Optimal relationships: $i_{dc}(n)$, $P_{pmsm}(n)$, $v_{r,s,t}(n)$, $i_{r,s,t}(n)$ and $P_w(n)$.

The last step to get the relationship $P_{grid}(R, n)$ will be to estimate the inverter efficiency η_{inv} by means of several tests. After calculating η_{inv}, it will be used to obtain the grid power P_{grid} according to:

$$P_{grid} = \eta_{inv} P_{dc} \tag{5.27}$$

$$P_{grid} = P_{dc} - \Delta P_{inv} \tag{5.28}$$

To estimate the inverter losses ΔP_{inv} several tests with various load curves were performed. Each one of these load curves have the characteristic that they were made for a constant value of R. To obtain these load curves, the following parameters were used:

- Variable resistor R: 20, 25, 27, 29, 31, 33, 35, 40, 45, 50, 60 and 75 Ω.
- DC voltage v_{dc}: between 0 and 350 V.
- Rotation speed n: between 0 and 260 rpm.

These values were chosen using the experience of previous tests. In this way, the SWT was working within its rated operating conditions and it was not subjected to unnecessary overloads. The following formulas were used to calculate the load curves:

$$P_{dc} = v_{dc} i_{dc} \tag{5.29}$$

$$P_{dc} = \frac{v_{dc}^2}{R} \tag{5.30}$$

These formulas give the relationship P_{dc} vs. v_{dc}, but what is really needed is the relationship P_{grid} vs. v_{dc}. In this case, it is supposed that $P_{dc} = P_{grid}$ because in this first step, we only need some load curves to estimate the inverter efficiency. The only restriction to consider is that the system is working without being overloaded to avoid damaging the equipment.

Below, Fig. 5.70 shows the load curves that were used. This curves will help us to estimate the inverter losses ΔP_{inv}.

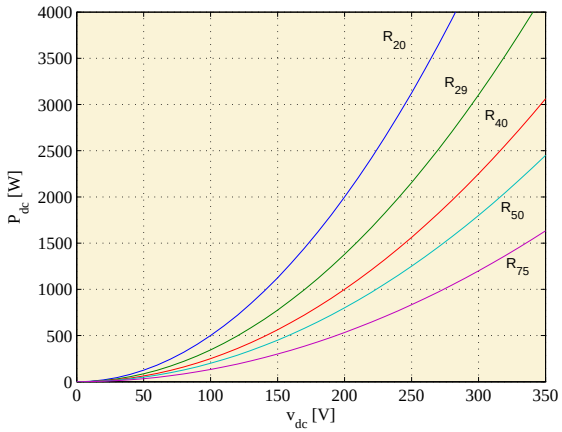

Figure 5.70: Load curves used to measure the inverter losses.

After doing the tests for all load curves, the results will be plotted on a graph (Fig. 5.71). This figure shows a cloud of points that is the relationship between the rectifier current i_{dc} and the inverter losses ΔP_{inv}. As discussed further, the losses in the inverter and in the rectifier are small if they are compared with the losses in the PMSM. Therefore, you can approximate the inverter losses with the trend line of that cloud of points, which has the following equation:

$$\Delta P_{inv} = 16.06\, e^{0.1491\, i_{dc}} \tag{5.31}$$

The Eq. (5.31) can be seen highlighted in Fig. 5.71. In this way, if this equation is replaced into the Eq. (5.28), the grid power P_{grid} can be easily obtained.

$$P_{grid} = P_{dc} - 16.06\, e^{0.1491\, i_{dc}} \tag{5.32}$$

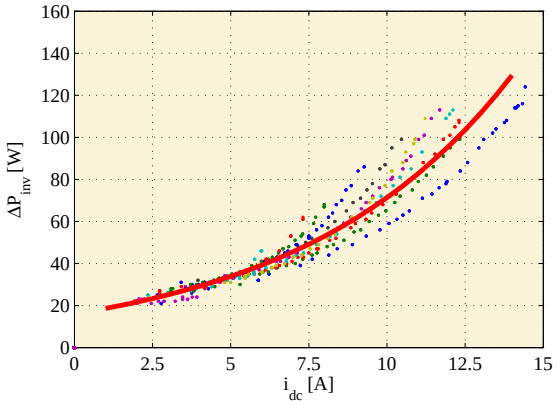

Figure 5.71: Inverter losses ΔP_{inv} vs. rectifier DC current i_{dc}.

Thus, if the rectifier current and power are known, then the SWT operating surface $P_{grid}(R, n)$ can be calculated. To know the optimal relationship $P_{grid}(n)$, you only have to obtain the intersection of the SWT surfaces $P_{grid}(R, n)$ with the surface obtained in Step 5.2.

Fig. 5.72 shows the optimal relationship $P_{grid}(n)$.

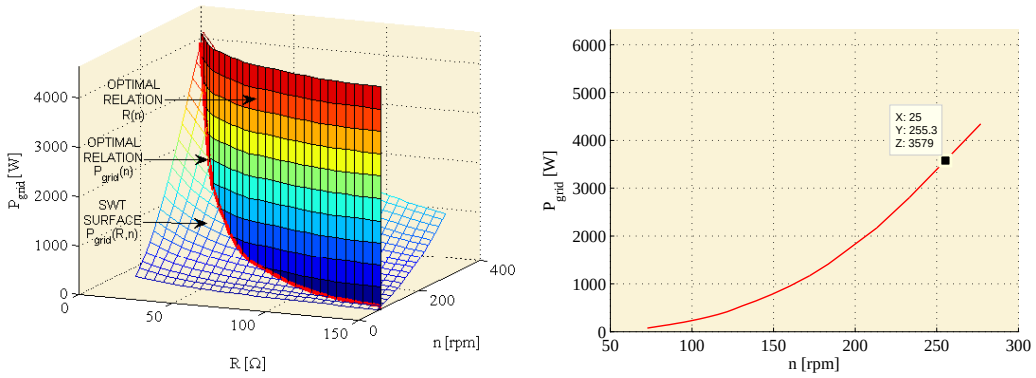

(a) 3D intersection.

(b) Optimal relationship $P_{grid}(n)$.

Figure 5.72: Intersection between the optimal relationship $R(n)$ and the SWT operating surface $P_{grid}(R, n)$.

- Step 5.4: Obtain P_{grid} vs. v_{dc}, also known as the Maximum Power Characteristic Curve (MPCC).

  Finally, joining the relationships $P_{grid}(n)$ and v_{dc}(n), you can easily get the optimal relationship $P_{grid}(v_{dc})$, assuming a value of $C = 0$ (see Fig. 5.73).

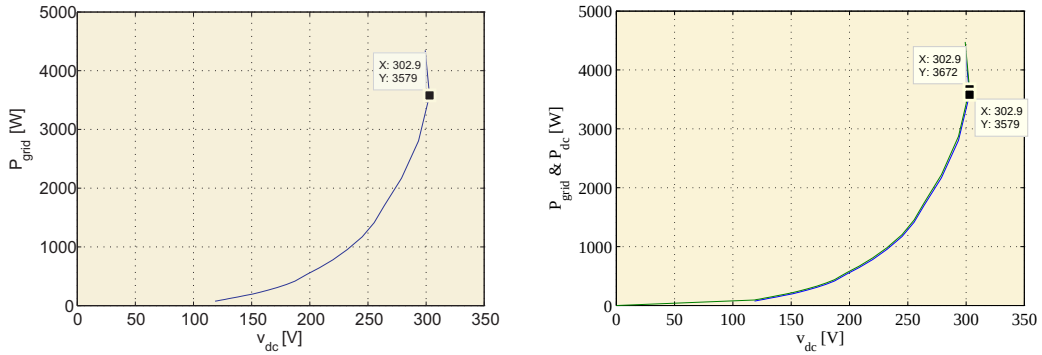

(a) MPCC, assuming a value of $C = 0$.

(b) P_{grid} vs. v_{dc} and P_{dc} vs. v_{dc}.

Figure 5.73: Comparison between $P_{grid}(v_{dc})$ and $P_{dc}(v_{dc})$, assuming $C = 0$.

In Fig. 5.73(b) it is clear that the difference between $P_{dc}(v_{dc})$ and $P_{grid}(v_{dc})$ is very small because of the high inverter efficiency.

Table 5.8 shows the values of the relationship $P_{grid}(v_{dc})$ for several wind speeds, assuming a value of $C = 0$.

On the one hand, this MPCC is important if the SWT is connected directly to the grid, since this curve allows us to extract the maximum wind power for different rotation speeds of the SWT.

On the other hand, if the SWT is connected to a storage battery, the MPCC will be imposed. Thus, for all SWT rotation speeds the variable resistor will be practically constant. The most common connection type for SWT is to work with storage batteries. That is the reason why some tests, that have been carried out in Section 5.5.1, have been performed with a constant load R.

Finally, by repeating these four steps (from 5.1 to 5.4) for each value of C, you will be able to obtain the rest of the MPCCs. They can be seen in Fig. 5.74.

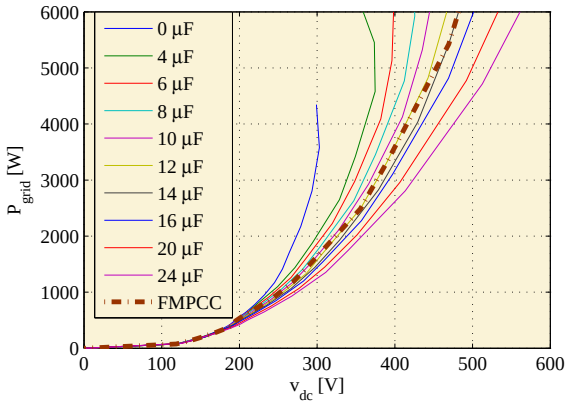

Figure 5.74: MPCCs obtained with different capacitor banks.

Once the MPCC associated with each capacity is known, a comparison of the grid power P_{grid} for different wind speeds u_h (from 4 to 12 m/s) and for each value of the capacity C, can be established (see Table 5.9).

In this table, maximum grid powers obtained for each wind speed u_h are highlighted. The column titled Ideal, means that the system always has connected the capacity that produces the maximum grid power P_{grid}, for each wind speed. Therefore, its values will coincide with highlighted ones.

Table 5.9: Energy improvement achieved by connecting capacitor banks (delta connection).

$u_h[m/s]$	$P_{grid}[W]$							
	$0\mu F$	$4\mu F$	$6\mu F$	$8\mu F$	$10\mu F$	$12\mu F$	$14\mu F$	Ideal
5.0	360.5	363.0	361.6	360.4	358.7	358.6	359.7	363.0
6.0	643.2	644.3	645.3	650.3	648.5	647.1	650.1	650.3
7.0	995.5	1005.9	1010.7	1008.7	1013.9	1010.6	1007.5	1013.9
8.0	1464.9	1491.8	1503.0	1496.8	1503.4	1500.1	1492.7	1503.4
9.0	2054.6	2124.5	2122.2	2141.5	2120.5	2142.3	2135.1	2142.3
10.0	2763.9	2851.5	2888.0	2877.2	2899.1	2899.7	2870.2	2899.7
11.0	3572.0	3766.3	3784.5	3817.8	3807.9	3845.4	3804.2	3845.4
12.0	4401.3	4731.4	4834.4	4822.8	4895.3	4855.0	4921.1	4921.1

Thus, using the Eq. (5.17), the values of Table 5.9 and a P_{rated}=3500 W, the power densities of Fig. 5.75 for different wind classes are obtained. In this figure, the increase in power density that occurs when the ideal capacities are connected can be seen. It should be noted that the higher the WC is, the higher the efficiency increment is.

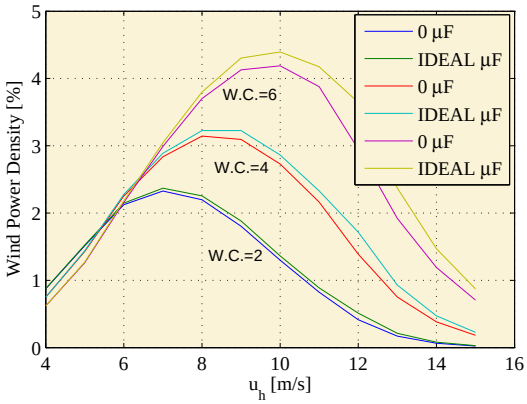

Figure 5.75: Power density in the SWT for WCs 2, 4 and 6.

In the same way that we have obtained the MPCCs for different capacitor banks, we can also obtain the relationship $P_{grid}(u_h)$ for each capacity C (see Fig. 5.76).

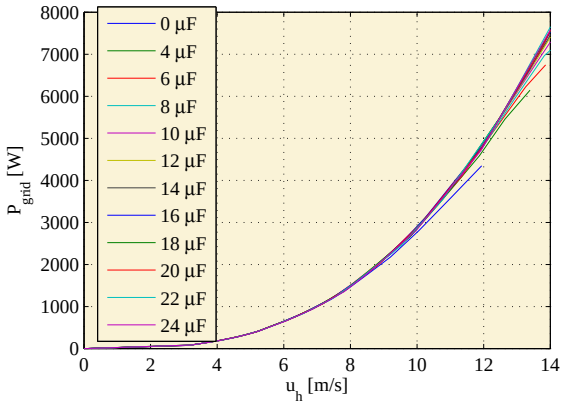

Figure 5.76: P_{grid} vs. u_h, for several capacitor banks.

Initially, if you pay attention to Fig. 5.76 you cannot appreciate the difference between using one capacity or another. Then, this figure will be studied around specific speeds, such as: 4, 5, 6, 7, 8, 9, 10, 11 and 12 m/s. As you can see in Fig. 5.77 and Fig. 5.78, each wind speed u_h has a capacity C that maximizes the grid power P_{grid}. Thus:

- Fig. 5.77(a): For a wind speed of 4 m/s the capacity that maximizes the grid power P_{grid} is 4μF.
- Fig. 5.77(b): For a wind speed of 5 m/s the capacity that maximizes the grid power P_{grid} is 4μF.
- Fig. 5.77(c): For a wind speed of 6 m/s the capacity that maximizes the grid power P_{grid} is 8μF.
- Fig. 5.77(d): For a wind speed of 7 m/s the capacity that maximizes the grid power P_{grid} is 10μF.
- Fig. 5.77(e): For a wind speed of 8 m/s the capacity that maximizes the grid power P_{grid} is 10μF.
- Fig. 5.77(f): For a wind speed of 9 m/s the capacity that maximizes the grid power P_{grid} is 12μF.
- Fig. 5.78(a): For a wind speed of 10 m/s the capacity that maximizes the grid power P_{grid} is 12μF.

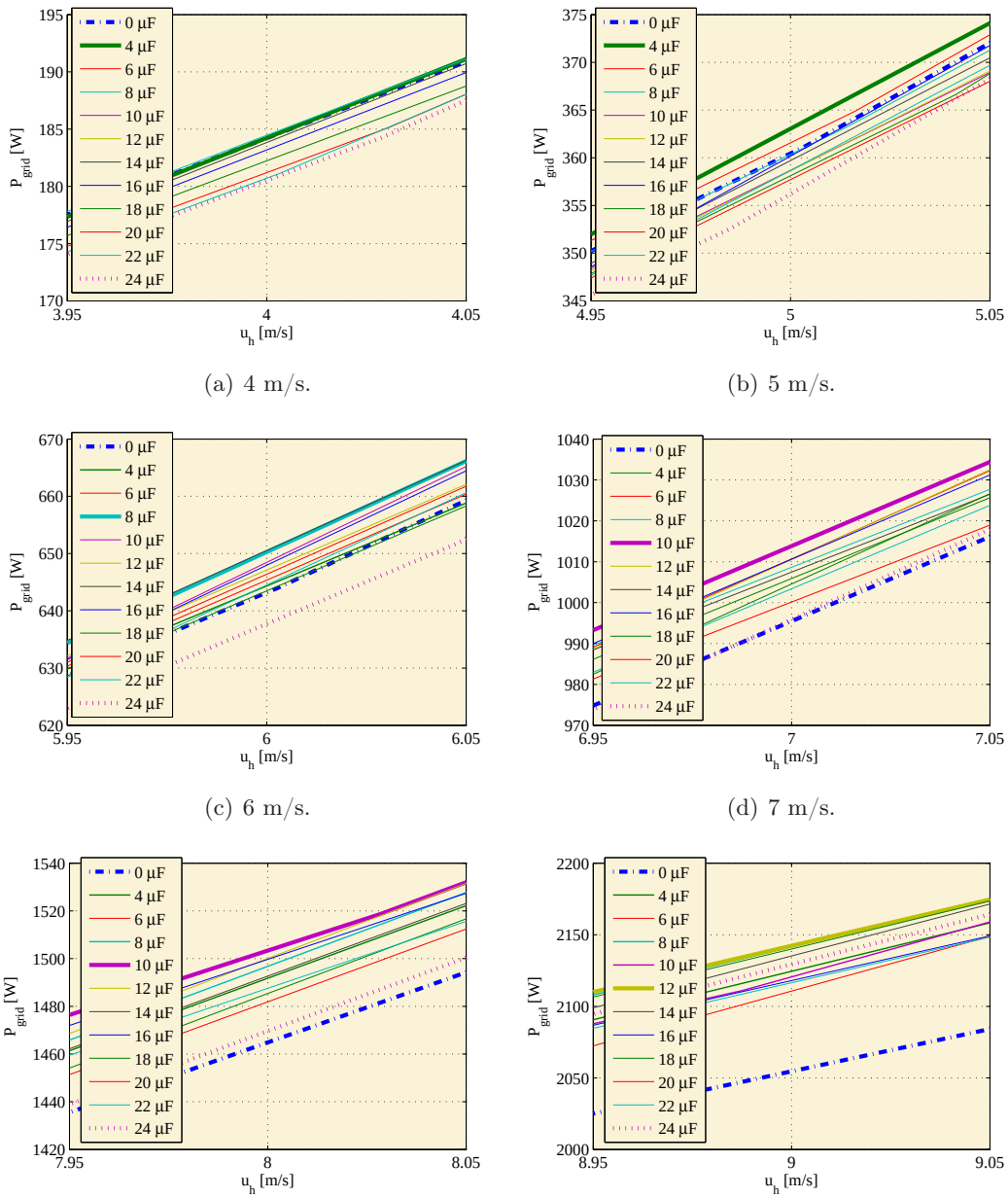

(a) 4 m/s.

(b) 5 m/s.

(c) 6 m/s.

(d) 7 m/s.

(e) 8 m/s.

(f) 9 m/s.

Figure 5.77: Optimal capacitor banks, for wind speeds between 4 and 9 m/s.

– Fig. 5.78(b): For a wind speed of 11 m/s the capacity that maximizes the grid power P_{grid} is 12μF.

– Fig. 5.78(c): For a wind speed of 12 m/s the capacity that maximizes the

grid power P_{grid} is 14μF.

In Fig. 5.77 and Fig. 5.78 you only have the capacity values up to 24 μF. This is because for higher capacity values, the grid power P_{grid} does not increase (assuming u_h from 4 to 12 m/s).

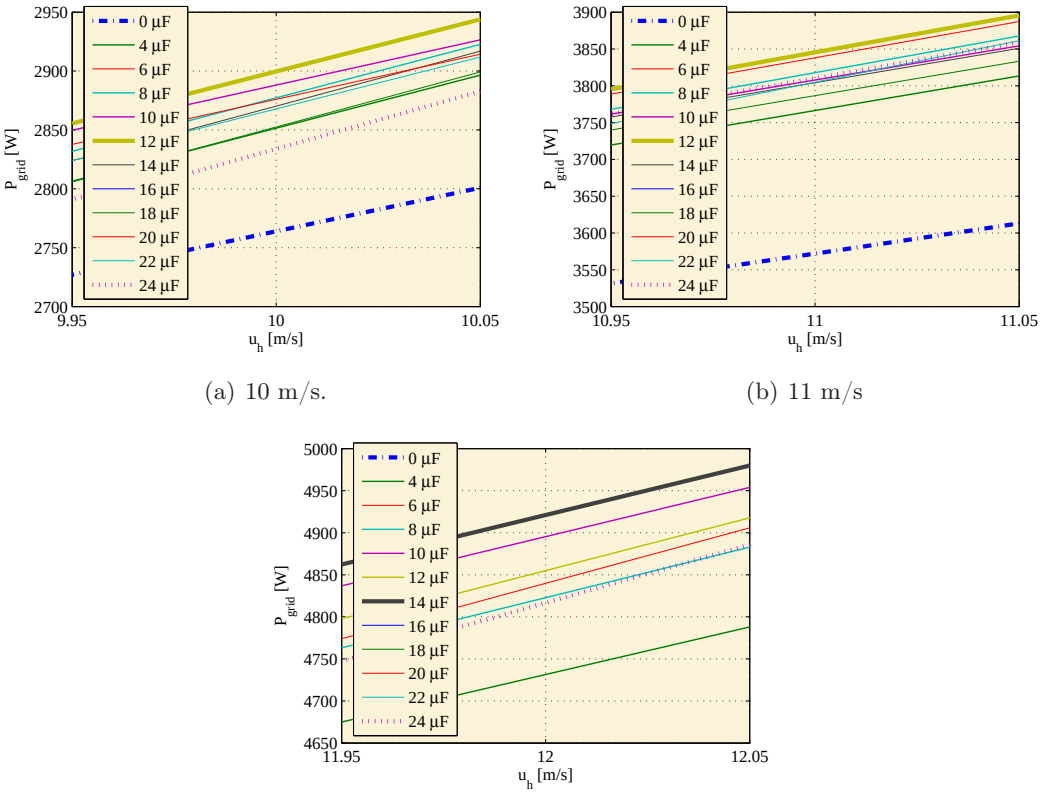

(a) 10 m/s.

(b) 11 m/s

(c) 12 m/s.

Figure 5.78: Optimal capacitor banks, for wind speeds between 10 and 12 m/s.

5.5.6 Step 6: Analyse the results and perform an economic study

Now, using the well-known Weibull distribution (see Eq. (5.16)), an economic study will be made.

Table 5.10 shows the energy $P_d(u_h)$ (see Eq. (5.17)) which is injected into the grid, for different wind speeds u_h and capacities C (assuming WC=2 and a height of 10 m).

Table 5.10: Annual benefits produced by placing different capacitors at a location with WC=2, height = 10m.

$u_h[m/s]$	$P_d(u_h)$ [KWh]							
	$0\mu F$	$4\mu F$	$6\mu F$	$8\mu F$	$10\mu F$	$12\mu F$	$14\mu F$	Ideal
4	257.2	257.3	257.7	257.6	257.9	257.5	256.7	257.3
5	441.1	444.3	442.5	441.0	438.9	438.9	440.2	444.3
6	622.5	623.6	624.6	629.3	627.6	626.3	629.6	629.3
7	696.4	703.6	707.0	705.6	709.2	706.9	704.7	709.2
8	682.1	694.7	701.8	697.0	700.1	698.5	695.1	700.1
9	589.7	609.7	609.1	614.6	608.6	614.9	612.8	614.9
10	454.4	468.8	474.8	473.0	474.8	476.7	471.8	476.7
11	313.4	330.5	332.1	335.0	334.1	337.4	333.8	337.4
12	174.2	207.0	211.5	211.0	214.1	212.4	215.3	215.3
13	81.3	96.5	98.6	98.4	99.9	99.0	100.4	100.4
14	35.5	42.2	43.1	43.0	43.6	43.3	43.9	43.9
15	14.6	17.3	17.7	17.6	17.9	17.7	18.0	18.0
h_e	1246.4	1284.4	1291.5	1292.3	1293.4	1294.1	1292.1	1299.0
E_{tot}	4362.3	4495.4	4520.4	4523.1	4526.7	4529.4	4522.3	4546.6
$\Delta\eta \Rightarrow$		3.05	3.62	3.68	3.77	3.83	3.67	4.22
$\Delta € \Rightarrow$		23.11	27.46	27.92	28.55	29.03	27.78	32.01

This table also shows the values of the next parameters:

- Using Eq. (5.18), you can obtain the annual total energy E_{tot} that can be extracted from the SWT.
- Using Eq. (5.19), you can calculate an indicative parameter h_e which helps you to determine the increment, in hours per year, for which the SWT shaft will supply power into the grid.
- $\Delta\eta$ (Eq. (5.20)) represents the increment in annual total energy injected into the grid E_{tot} for different capacitor banks, comparing it with the case without capacitor bank.
- $\Delta €$ (Eq. (5.21)) represents the annual profit that would be obtained by using different capacitor banks, comparing it with the case without capacitor banks.

As Table 5.10 shows, the value of C that produces the highest benefit is 12 μF (4529 [kWh] and 29.03 [Δ€]). Taking into account that every capacitor costs about 10 €, it is easy to understand that in the first year the costs are covered. So, from the second year on, the capacitor bank would begin to achieve profits.

Analysing the system performance for the rest of the WCs (at a height of 10 m), the results shown in Table 5.11 are obtained. This table shows that for WC values equal to or higher than 3, the investment can be recovered during the first year of use. It can be also seen that for each WC the value of the optimal capacity varies. Hence, it is necessary to know the location of the SWT, in order to choose the capacitor bank that achieves the maximum efficiency.

Table 5.11: Annual benefits produced by placing different capacitors for all WCs and a height of 10 m.

WCs (u_m)	Δ€ (Height = 10 m)						
	$4\mu F$	$6\mu F$	$8\mu F$	$10\mu F$	$12\mu F$	$14\mu F$	Ideal
1 (4.4 m/s)	9.0	10.8	11.1	11.2	11.1	10.5	13.1
2 (5.1 m/s)	23.1	27.5	27.9	28.6	29.0	27.8	32.0
3 (5.6 m/s)	39.4	46.3	46.9	48.5	49.2	47.8	53.3
4 (6.0 m/s)	55.9	65.3	66.0	68.7	69.4	68.2	74.6
5 (6.4 m/s)	74.8	86.9	87.8	91.8	92.4	91.7	99.0
6 (7.0 m/s)	105.9	122.5	123.4	129.8	130.0	130.3	138.8
7 (9.4 m/s)	217.4	249.6	249.9	265.9	262.6	269.6	280.0

The last column of Table 5.11 represents the case where the optimal capacity, for each wind speed, is connected. To achieve it, you could connect:

- Groups of capacitor banks in parallel that work in an automated way. Depending on the type of machine and the variation of the optimal capacity with wind speed, more or less capacitor banks will have to be connected. This method would be viable for those SWTs that work in a wide range of wind speeds and where the optimal capacities vary significantly. Otherwise, the connection of more than one capacitor bank could make this solution expensive. This solution would also be feasible for SWTs with higher rated power.

- A *Static Var Compensator* (SVC) that provides, at every moment, the optimal capacity by means of power electronics. Apparently this would be the optimal solution but it should be noted that the SVC would add additional costs and losses that have not been taken into account in the development of Table 5.11.

If instead of placing the SWT at a height of 10 m, it were placed at 50 m, the average wind speeds would increase (see Table 5.1). In this way, a greater profit would be achieved (see Table 5.12).

Table 5.12: Annual benefits produced by placing different capacitors for all WCs and a height of 50 m.

WCs (u_m)	Δ€ (Height = 50 m)						
	$4\mu F$	$6\mu F$	$8\mu F$	$10\mu F$	$12\mu F$	$14\mu F$	Ideal
1 (5.6 m/s)	39.4	46.3	46.9	48.5	49.2	47.8	53.3
2 (6.4 m/s)	74.8	86.9	87.8	91.8	92.4	91.7	99.0
3 (7.0 m/s)	105.9	122.5	123.4	129.8	130.0	130.3	138.8
4 (7.5 m/s)	132.5	152.9	153.7	162.3	161.8	163.4	172.6
5 (8.0 m/s)	15.1	182.1	182.9	193.6	192.4	195.5	205.2
6 (8.8 m/s)	194.7	223.8	224.3	238.2	235.8	241.2	251.5
7 (11.9 m/s)	267.0	305.7	305.3	326.3	320.2	331.9	341.7

Table 5.13: Efficiency increase produced by placing different capacitors for all WCs and a height of 10 m.

WC	$\Delta\eta$ [%] (Height = 10 m)				
	$6\mu F$	$8\mu F$	$10\mu F$	$12\mu F$	$14\mu F$
1	2.21	2.25	2.25	2.26	2.13
2	3.62	3.68	3.77	3.83	3.67
3	4.76	4.83	4.99	5.06	4.92
4	5.67	5.74	5.97	6.03	5.93
5	6.54	6.61	6.91	6.95	6.90
6	7.73	7.79	8.19	8.20	8.22
7	10.96	10.97	11.68	11.53	11.84

Finally, Table 5.13 shows the efficiency increase produced when using different capacitor banks and WCs. For WC=2 and height=10 m, the efficiency increment was

3.83%.

5.5.7 Step 7: Obtain the Final Maximum Power Characteristic Curve (FMPCC).

To obtain the FMPCC, you only have to take the results of Fig. 5.74 and select the part of every MPCC that produces the maximum grid power P_{grid}. In Fig. 5.74 the FMPCC is highlighted.

5.5.8 Comparison between real and Simulink results, for a test with $C = 12\ \mu$F

In Fig. 4.30, you can see the electric diagram that was followed to make the test.

Once the simulated results were obtained, a real test was undertaken to check them. The test consisted of connecting a capacitor bank of 12 μF (delta connection) to the SWT.

Fig. 5.79 compares the theoretic relationship $P_{pmsm}(n)$ with the experimental one. You can see that the results are quite accurate.

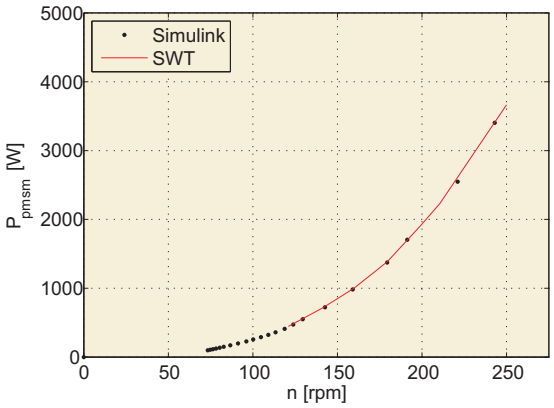

Figure 5.79: Simulated and experimental results (C=12 μF).

6

Conclusions

The increasing development of small-wind energy has made it necessary to study new methods that improve their efficiency. This paper presents a methodology to increase the SWT efficiency by using a capacitor bank. This methodology will use a Simulink model to simulate the system.

The results obtained with the Simulink model can be considered suitable because they show a high degree of match with the performance of the real machine. As an example, the efficiency increases predicted by the simulations were the same as those obtained in the real tests. Given the accuracy of the Simulink model, all modifications can be extrapolated to the SWT.

It has been shown that connecting different capacitor banks to the system modifies SWT performance and the MPCC. The power obtained from the SWT increases as a result of connecting capacitor banks, and is only limited by the maximum current that can flow through the PMSM windings. In our research we found that connecting a capacitor bank of 12μF increases the SWT efficiency by 3.83%. Thus, in PMSM design, added shunt capacity could be a new parameter to bear in mind.

It must be taken into account that it is necessary to know the location of the SWT, and the associated average wind speed, in order to connect the optimal capacitor bank.

The methodology described in this work could be used by electrical machine manufacturers to reduce the PMSM size because a new electrical machine with a capacitor bank would include the following modifications in order to obtain the same power: less copper (the capacitor bank decreases the current that flows through the PMSM), smaller magnet size (magnetizing effect of the capacitors) and fewer magnetic plates.

If these modifications are included in SWT design, manufacturing costs would decrease substantially, and even more so in the case of higher WCs.

References

[1] A. Pullen and S. Sawyer. **Annual Market Update 2010. Global Wind Report. Global Wind Energy Council**. In *Grafik and Ilustration*, pages 1–72, 2010. xv, xxi, 4, 5, 6, 8

[2] **Small Wind Turbine Global Market Study**. 2010. 10

[3] **Small Wind Industry Strategy**. 2010. 15

[4] W. Li, G. Joos, and J. Belanger. **Real-Time Simulation of a Wind Turbine Generator Coupled With a Battery Supercapacitor Energy Storage System**. *Industrial Electronics, IEEE Transactions on*, **57**(4):1137–1145, April 2010. 17

[5] Y. Fan, K.T. Chau, and M. Cheng. **A New Three-Phase Doubly Salient Permanent Magnet Machine for Wind Power Generation**. *Industry Applications, IEEE Transactions on*, **42**(1):53–60, Jan.-Feb. 2006. 17

[6] E. Spooner and A.C. Williamson. **Direct Coupled, Permanent Magnet Generators for Wind Turbine Applications**. *Electric Power Applications, IEE Proceedings* -, **143**(1):1–8, Jan 1996. 17

[7] F. Pitzalis, N. Corino, M. Ottella, P. Perlo, and P. Guglielmi. **Study of High Efficiency Small Diameter Annular Wind Turbines by Means of CAE Techniques**. In *Industry Applications Conference, 2007. 42nd IAS Annual Meeting. Conference Record of the 2007 IEEE*, pages 706–713, Sept. 2007. 17

[8] F.M. Rodrigo, L.C.H. de Lucas, S.P. Gomez, and J.M.G. de la Fuente. **Analysis of the Efficiency Improvement in Small Wind Turbines when**

Speed Is Controlled. In *Industrial Electronics, 2007. ISIE 2007. IEEE International Symposium on*, pages 437–442, June 2007. 17

[9] D.S. Oliveira, G.J.M. de Sousa, A.R. Rangel, D.L. Queiroz, E.F. de Oliveira, L.P.C. dos Santos, L.F.A. Fontenele, and P.A.M. Bezerra. **Low Cost and High Efficiency Static Converter for Small Wind Systems**. In *Power Electronics Conference, 2009. COBEP '09. Brazilian*, pages 972–977, 2009. 17

[10] **Matlab-Simulink. User's manual (2008)**. July 2008. 19, 24, 59

[11] **Flux. User's manual (2010)**. July 2008. 24, 32

[12] **Windspot 3.5 KW, Sonkyo Energy. Data sheets (2010)**. July 2008. 23

[13] **Rectifier Ginlong. Data sheets (2010)**. July 2008. 23

[14] K. Yamazaki and N. Fukushima. **Iron-Loss Modeling for Rotating Machines: Comparison Between Bertotti's Three-Term Expression and 3-D Eddy-Current Analysis**. *Magnetics, IEEE Transactions on*, **46**(8):3121–3124, Aug. 2010. 24

[15] **UNE-EN 60034-2-1, Rotating electrical machines. Part 2-1: Standard methods for determining losses and efficiency from tests (excluding machines for traction vehicles), 2009.** 28

[16] **UNE-EN 60085, Electrical insulation. Thermal evaluation and designation, 2008.** 29

[17] L. Sun, H. Li, and B. Xu. **Precise Determination of Permanent Magnet Synchronous Motor Parameters Based on Parameter Identification Technique**. In *Electrical Machines and Systems, 2003. ICEMS 2003. Sixth International Conference on*, **1**, pages 34–36 vol.1, Nov. 2003. 30

[18] M. Kesraoui, N. Korichi, and A. Belkadi. **Maximum Power Point Tracker of Wind Energy Conversion System**. *Renewable Energy*, **36**:2655–2662, (2011). 59

[19] N. Milivojevic, I. Stamenkovic, and N. Schofield. **Power and Energy Analysis of Commercial Small Wind Turbine systems**. In *Industrial Technology (ICIT), 2010 IEEE International Conference on* pages 1739–1744, March 2010. 59, 83

[20] E.F. Fuchs, A.J. Vandenput, J. Holl, and J.C. White. **Design Analysis of Capacitor-Start, Capacitor-Run Single-Phase Induction Motors**. *Energy Conversion, IEEE Transactions on*, **5**(2):327–336, Jun 1990. 59

[21] C. Umans S. Fitzgerald, A.E. Kingsley. **Electric Machinery**. In *Mc Graw Hill*, 2003. 59, 72

[22] M. Sathyajith. **Wind Energy. Fundamentals, Resource Analysis and Economics**. In *Springer*, pages 1–167, 2006. 60, 83

[23] S. Rodríguez, J.L. Arnalte and J.C. Burgos. **Sistemas Eléctricos de Producción de Energía Elétrica**. In *Editorial Rueda S.L.*, pages 1–450, 2003. xvi, 61, 62, 65

[24] G.A.M. van Kuik. **The Lanchester Betz Joukowsky limit**. *Wind Energy*, **10**(3). 63

[25] R.E. Wilson and B.S Lissaman. **Aerodynamic Performance of Wind Turbines**. In *University of Stuttgart*, pages 1–167, 1976. 67

[26] Z. Yu and A. Tuzuner. **Wind Speed Modeling and Energy Production Simulation with Weibull Sampling**. In *Power and Energy Society General Meeting - Conversion and Delivery of Electrical Energy in the 21st Century, 2008 IEEE*, pages 1 –6, July 2008. 83

[27] D.L. Elliot, C.G. Holladay, W.R. Barchet , H.P. Foote and W.F. Sandusky **Wind Energy Resource Atlas of the United States**. In *Golden, CO: U.S. Department of Energy Pacific Northwest (1986)*. xxi, 83, 84